Observations and Modeling of the Boundary Layer Accompanying a Tropical Squall Line

by
Melville E. Nicholls and Richard H. Johnson

Department of Atmospheric Science
Colorado State University
Fort Collins, Colorado

Colorado State University

Department of Atmospheric Science

Paper No. 366

OBSERVATIONS AND MODELING OF THE BOUNDARY LAYER ACCOMPANYING A TROPICAL SQUALL LINE

by

Melville E. Nicholls
and
Richard H. Johnson

Research supported by the
National Science Foundation
Division of Atmospheric Sciences
under grants
ATM-8015347 and ATM-8206808

Department of Atmospheric Science
Colorado State University
Fort Collins, Colorado 80523

April 1983

Atmospheric Science Paper No. 366

ABSTRACT

A composite analysis has been recently made of the boundary layer associated with the squall line that moved through the GATE ship array on the 12 September 1974, (Johnson and Nicholls, 1982). This observational study has motivated a modeling investigation of the recovery of the squall boundary layer wake which is reported on here. The zero-order model of the growth of an unstable boundary layer as modified by Lilly (1968), and the general structure entrainment model developed by Deardorff (1979) are used to simulate the wake recovery and to make more explicit the factors influencing the evolution of the mixed layer. A procedure is developed for obtaining the fully three dimensional mixed layer structure by formulating the model equations relative to the squall system in natural coordinates.

The results of this study show that the most important controls on inhibiting boundary layer growth in the wake of this squall line are a significant downward vertical velocity at the top of the mixed layer and an associated increase in stability of the overlying air. The surface buoyancy flux also has an important influence on mixed layer growth and the results indicate that horizontal advection should not be neglected if mixed layer specific humidity and dry static energy are to be predicted. The asymmetrical structure of the mixed layer height is well simulated by both models with lengthy recovery times occurring in regions of significant subsidence and relatively small surface buoyancy fluxes.

An unusual profile of specific humidity in the wake of the squall line is identified and an explanation proposed for its occurrence and

subsequent development. The specific humidity and dry static energy in the mixed layer seem to be predicted fairly well. The model results indicate that diabatic heating due to rainfall evaporation and radiation is important for sustaining the cool region within the squall wake. The results of this investigation may contribute, in addition to a better understanding of the physics and dynamics of tropical squall wake recovery, to an improved basis for the parameterization of convective effects in large scale numerical weather prediction models.

ACKNOWLEDGEMENTS

The authors thank Drs. Duane Stevens and Wayne Schubert for valuable comments and discussion. We have also benefited from discussions with Mr. Francis Crum and Mr. Gregory Tripoli. Mr. Tripoli provided the algorithm we have used to compute precipitation evaporation. Special thanks are extended to Ms. Machel Sandfort for typing the manuscript.

This research has been supported by the Division of Atmospheric Sciences, National Science Foundation under Grants ATM-8015347 and ATM-8206808.

TABLE OF CONTENTS

1. INTRODUCTION

Downdrafts associated with deep convective systems significantly modify the boundary layer, leading to substantially increased fluxes of sensible and latent heat over the tropical oceans. Within the tropical eastern Atlantic region during GATE (GARP Atlantic Tropical Experiment), downdraft-modified boundary layers or "wakes" accompanying precipitation systems were found on the average to cover about 30% of the total area (Gaynor and Mandics, 1978; Gaynor and Ropelewski, 1979). It is important to understand the effects of deep convective systems on the boundary layer so they might be parameterized in large scale models. If modeling of these mesoscale systems themselves is to be attempted, the proper treatment of the boundary layer may be an important consideration since it could have a significant effect on the dynamics of these systems.

This paper reports on a modeling study of mixed layer recovery following the passage of the squall line that moved through the GATE array on the 12 September 1974. Results of the observational study have already been reported by Johnson and Nicholls (1982) (hereafter referred to as JN), some of which will be repeated here (with some minor modifications) as well as some additional observations. JN was motivated by the work of Gamache and Houze (1982) who have obtained, by a rawinsonde compositing procedure, a remarkably coherent description of the three dimensional structure of this squall line. They selected a 9-hour

period during which the radar structure of the squall was approximately in steady state and composited GATE ship array soundings relative to the center of the squall radar echo. Likewise we have used the same composite procedure but confined our investigation to the boundary layer accompanying the squall.

The 12 September squall line seems to be characteristic of a particular type of squall line that is fairly commonly found off the coast of West Africa at about 15°N, although much more frequently over land. It has been shown by Aspliden et al. (1976) and Payne and McGarry (1977), that the development of squall lines over West Africa is related to the passage of large-scale wave disturbances that occur in association with the 700 mb east African jet. The preferred location for squall development is in advance (1/4 to 1/8 of a wavelength ahead) of the wave trough axis at 700 mb between 10° and 15°N. The squall lines that develop move westward at an average speed of 16 m s^{-1}. They seem to be more intense over land than over the ocean presumably due to stronger surface heating and, in fact, often decay rapidly as they move over the cooler sea surface. This type of system is quite suitable for the study of boundary layer recovery since it often has quite a long lifetime. Gamache and Houze (1982) have determined that for about a 9 hour period the 12 September squall was in approximatly in steady state with a fairly symmetrical line arc structure (the gust front). To its rear a strongly suppressed wake occurred free of convective scale clouds. Turbulence produced by surface friction is apparently small within the squall wake (except in the vicinity of the gust front); however, the importance of shear production in the interfacial layer is not known with certainty. A crude estimate indicates it is probably negligible in

some regions behind the squall line where wind shear is small, but in other regions, in particular close to the squall front, it appears to be significant. A necessary requirement for the applicability of the models used in this study is that buoyant production dominates.

For these squall lines the feedback of the suppressed mixed layer on the dynamics of the system is probably small. The gust front moves at a high speed and the strong convergence along it is responsible for deep convection (although the initiation of convection often occurs ahead of it as noted by Houze, 1977). Convective cells reach their maximum intensity some 20-40 km behind the gust front; at this stage they have developed strong convective scale evaporatively driven downdrafts which maintain the gust front and also cut off the low level source of convectively unstable air. Strong convective activity is thus inhibited leading to a fairly narrow line (~ 50 km wide) of deep convective cells which give way to weaker mesoscale ascent in the anvil and descent beneath this. A schematic cross-section of the squall structure is shown in Fig. 1 (from Zipser, 1977). This study focuses on the recovery of the mixed layer behind the region of convective scale downdrafts. The development of the mixed layer in this region obviously has no effect on the behavior of the gust front but is important in determining the time scale for which strong convection is inhibited after the passage of the squall line. In some systems such as a comparatively slow moving cloud cluster or a tropical storm the development of the downdraft modified boundary layer may have a significant feedback on the dynamics of the systems themselves.

Two models have been used in this study to explore the factors controlling mixed layer development following the passage of the squall

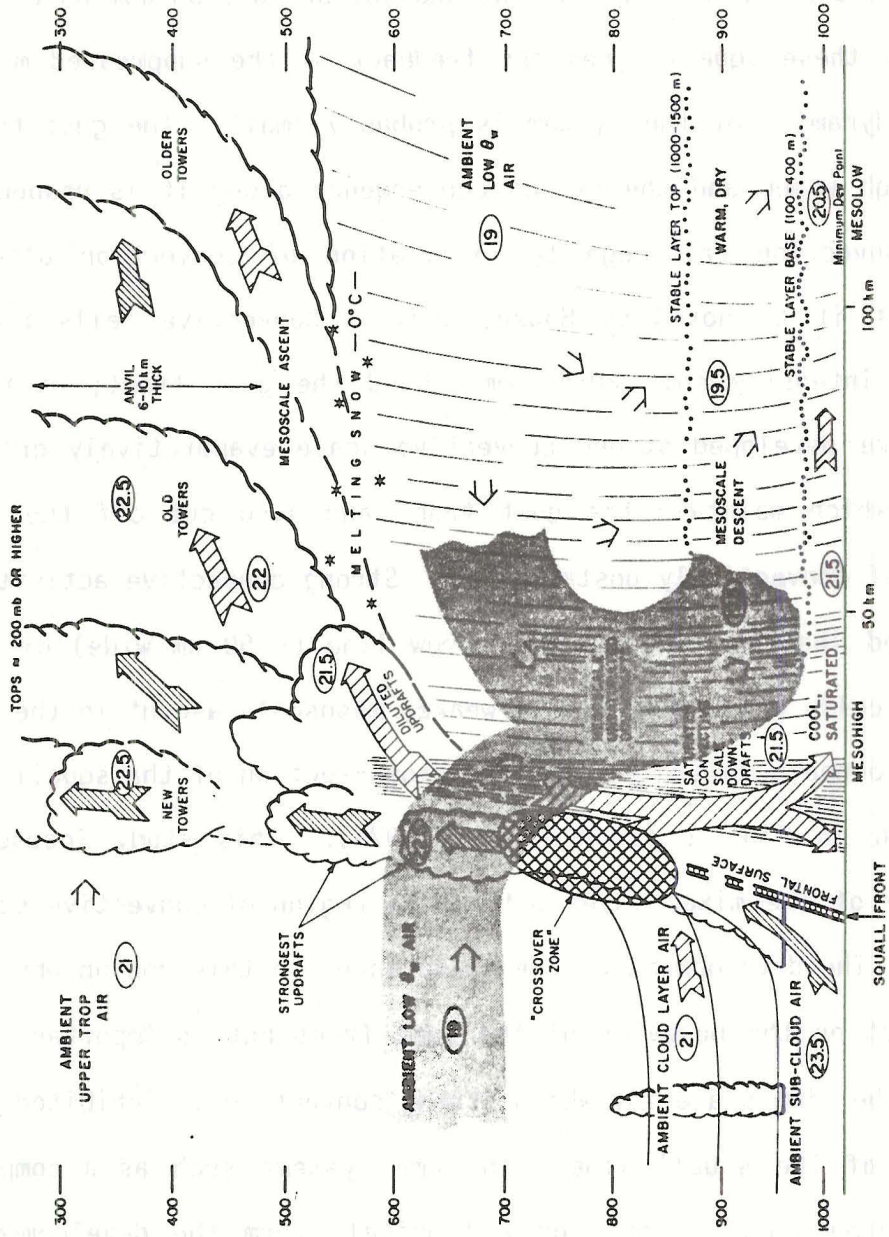

Fig. 1. Schematic cross section through a class of squall system (redrafted from Zipser, 1977). All flow is relative to the squall line which is moving from right to left. Circled numbers are typical values of θ_w in °C.

line: a zero-order jump model in which there are discontinuities in the thermodynamic fields at the top of the mixed layer, and the general structure entrainment model (hereafter referred to as the GSEM), which more realistically includes a finite depth transition layer. Previous modeling studies of mixed layer recovery following the passage of a squall have been made by Zipser (1977), and Fitzjarrald and Garstang (1981), using the zero-order jump model. Both of these had to make fairly crude estimates of the vertical velocity at the top of the mixed layer. Zipser's results showed that mesoscale sinking behind the squall line could account for the shallow mixed layers. Fitzjarrald and Garstang obtained qualitative agreement with the observations of mixed layer height, temperature and humidity, but did not use observed time varying fields of important quantities such as surface fluxes, lapse rates and horizontal velocity.

2. COMPOSITE DATA AND ANALYSIS PROCEDURES

The primary data used in this study are from the GATE A/B and C-scale rawinsonde archive obtained from the World Data Center A, Asheville, NC. The observations are from an array of fifteen ships, eleven of which are shown in Fig. 2. The four that are not shown in this figure, but which are used to some extent in the subsequent analyses, complete an outer hexagonal array, the A/B-scale array. A detailed discussion of the vertical resolution of the data is given in JN.

During the period of our composite analysis (0900-1800 GMT, 12 September 1974), soundings at 3-hourly intervals were obtained from most of the 15 ships. Hourly positions of the leading edge of the squall radar echo (taken from the paper of Gamache and Houze (1982)) are shown in Fig. 2 for the period 0900 to 2100 GMT. During this time the squall line moved southwestward across the region at an average speed of 13.5 m s^{-1}. Estimated center positions of the squall line at each hour are indicated by crosses. The reader is referred to Gamache and Houze (1982) for details regarding the composite analysis and compositing procedures.

Two components of the squall radar echo have been identified by Gamache and Houze using ship-based weather radars: (1) the squall line itself and (2) the post-squall anvil region. The former feature refers to the cumulonimbus convection on the leading edge of the squall system.

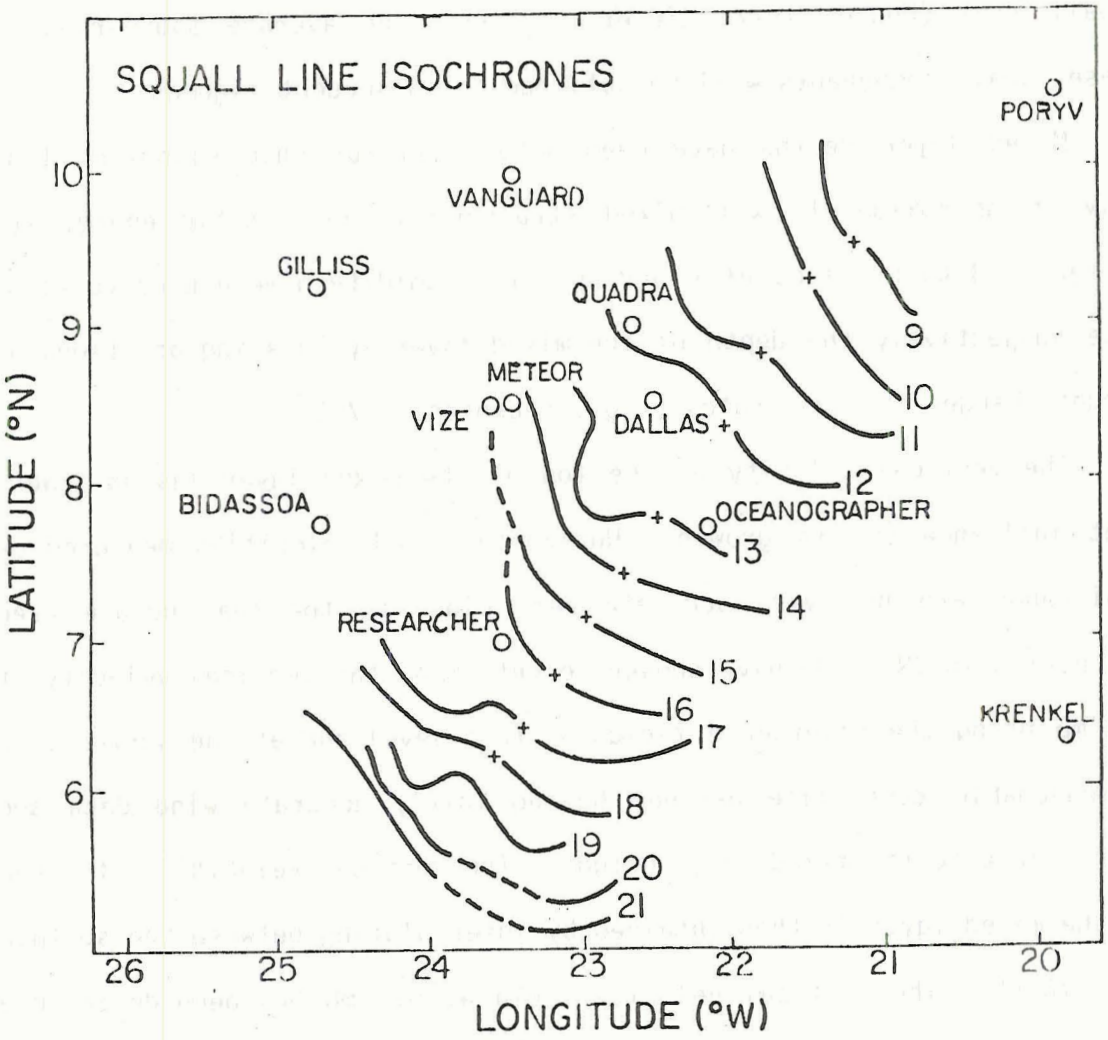

Fig. 2. Isochrone analysis of leading edge of squall line for the period 0900-2100 GMT 12 September 1974 (redrafted from Gamache and Houze, 1982). Crosses mark the center position of the squall. Ship positions are indicated.

The squall line has a movement that is at times characterized by discrete propagation that takes the form of new growth of convective cells out in advance of old ones, while old ones to the rear weaken (Houze, 1977). The post-squall anvil region refers to the nearly continuous stratiform cloud system of mesoscale (~ 200 km) dimension trailing the squall line (Houze, 1977; Zipser, 1977a). The average boundaries of these squall components will be outlined in subsequent figures.

Mixed layer depths have been determined for ship soundings that show an approximately well-mixed structure in dry static energy $s(\equiv c_p T+gz)$. Both profiles of s and specific humidity q were used to estimate subjectively the depth of the mixed layer by locating positions of abrupt changes in lapse rates (e.g., Esbensen, 1975).

The vertical velocity at the top of the mixed layer has an important influence on its growth. Horizontal wind velocities measured by rawinsonde are not very accurate very close to the sea surface (see discussion in JN). We have chosen to determine the vertical velocity at 970 mb using the divergence fields at this level and at the surface, as a reasonable compromise between having fairly accurate wind data and being close to the mixed layer height. The vertical velocity at the top of the mixed layer is then obtained by interpolating between the surface and 970 mb. The vertical velocity field at 970 mb has been determined from the continuity equation. Hence

$$\omega(970\ \text{mb}) = \omega_{sfc} - \int_{P_{sfc}}^{970\ \text{mb}} \nabla_H \cdot \underset{\sim}{v} dp \cong \langle \nabla_H \cdot \underset{\sim}{v} \rangle \Delta p$$

where the angled brackets refer to the average between p_{sfc} and 970 mb. It can be shown from the composite analysis of the pressure field in JN

that it is a good approximation to let ω_{sfc} be zero. Wind vectors were plotted at the surface and at 970 mb and a subjective streamline and isotach analysis carried out. Divergences were calculated at these levels using a 60 km grid, and then averaged so as to obtain ω(970 mb).

Surface sensible and latent heat fluxes S_o and LE_o, respectively, have been determined using ship boom data from the Gillis, Dallas, Researcher and Oceanographer and the bulk aerodynamic relationships

$$S_o = \bar{\rho} C_p C_h \bar{U}_{10} (\bar{\theta}_o - \bar{\theta}_{10}) \tag{2.1}$$

$$E_o = \bar{\rho} C_e \bar{U}_{10} (\bar{q}_o - \bar{q}_{10}) \tag{2.2}$$

where $\bar{\rho}$ is the mean density, C_p specific heat, C_h the bulk transfer coefficient for sensible heat, C_e the bulk transfer coefficient for water vapor, E_o the surface evaporation, and $\bar{U}_{10}$ the mean wind speed at 10 m. The subscripts o and 10 refer to values at the ocean surface and 10 m respectively, and overbar to a time average (10 minute means are used in our analyses). The recommended values for C_h and C_e for both undisturbed and disturbed conditions are $1.6 \pm 0.5 \times 10^{-3}$ and $1.4 \pm 0.4 \times 10^{-3}$, respectively (U.S. GATE Workshop, 1977). A correction term that reflects the dependence of C_p on specific humidity has been added to ( ) in some recent studies (e.g., Reinking and Barnes, 1981) based on an analysis by Brook (1978). More recently, however, Frank and Emmitt (1981) and Businger (1982) have argued that Brook's correction is in error and, therefore, we have neglected it. The surface buoyancy flux is formulated in terms of the virtual static energy

$$s_v = s(1+0.61q). \tag{2.3}$$

From this equation it can be shown (e.g. Arakawa and Schubert, 1974) that the surface flux of virtual static energy $F_{sv} = (w's_v')_o$ is given by

$$F_{sv} = S_o + 0.61\ \bar{s}\ E_o. \tag{2.4}$$

3. COMPOSITE RESULTS

3.a Mixed Layer Depth

A subjective analysis of the mixed layer depths for the composite squall is shown in Fig. 3. It can be seen there as an extensive area behind the squall line where the mixed layer is very shallow. There is a significant asymmetry in the mixed layer structure about a centerline perpendicular to the squall line. Another noticeable feature of the composite mixed layer analysis is a region of shallow mixed layers in advance of approximately perpendicular to the squall. This feature is most likely associated with a line of cumulonimbus convection that existed preceding the squall (Zipser, 1977a,b; Gamache and Houze, 1982).

3.b Wind Fields

The surface and 970 mb flow fields are shown in Figs. 4 and 5. They differ slightly from JN since some attention there was given to soundings at 2100 in regions of sparse data, although the squall system was only reasonably approximated by steady state between 0900-1800. These are felt to be unreliable and have been neglected here. The surface analysis shows (1) a confluence line perpendicular to and in advance of the squall line, (2) a convergence line coincident with the leading edge of the squall and (3) a strong diffluence center beneath the mesoscale anvil cloud. The vertical velocity field at 970 mb (375 m) is shown in Fig. 6. It shows a region of strong mesoscale subsidence behind the squall line, offset somewhat from the surface diffluence

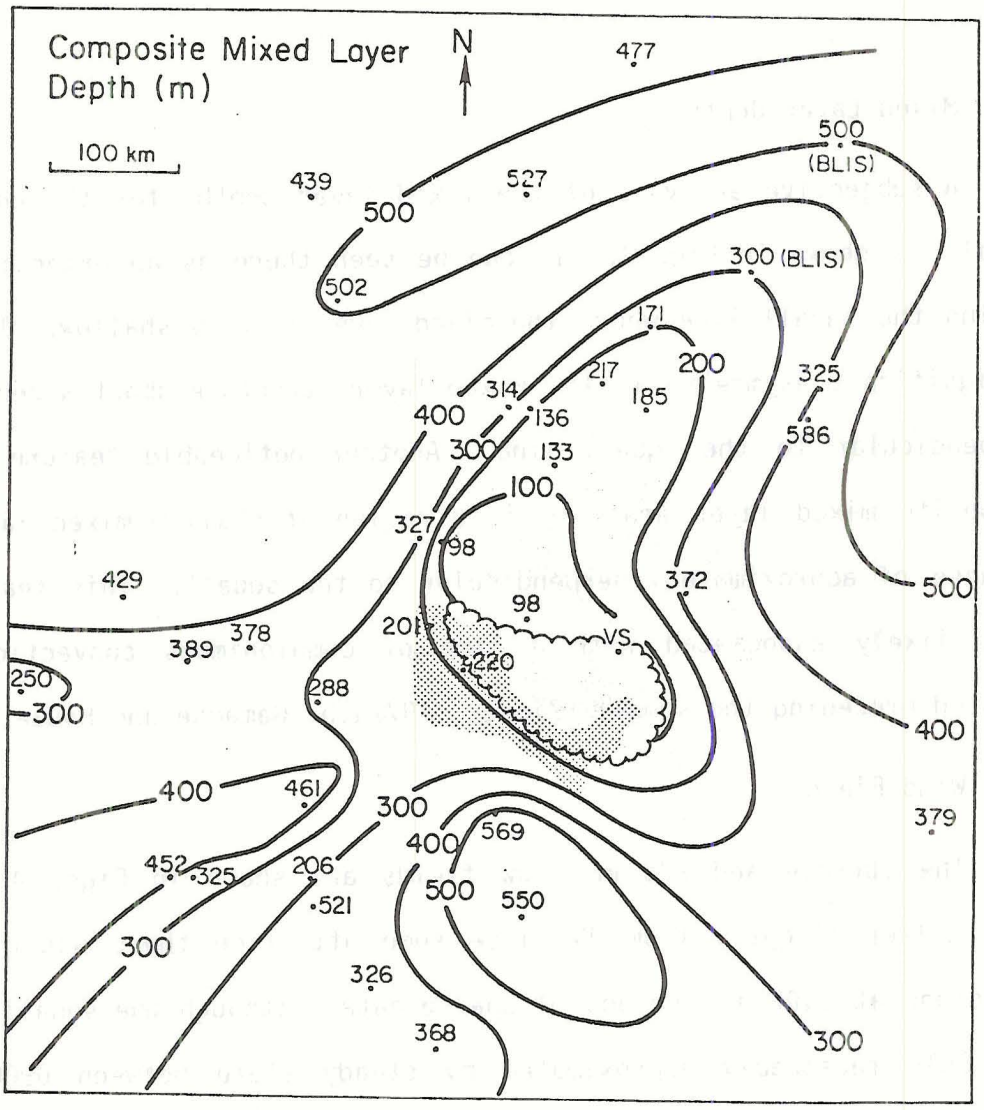

Fig. 3. Composite mixed layer depth (m) (redrafted from Johnson and Nicholls, 1982). Actual depths at sounding positions are indicated; VS denotes a very stable lapse rate in the lowest several 100 m at indicated sounding position. Scalloped curve encloses estimated area of very stable boundary layer. Dark and light shaded regions denote squall-line (convective echo) and anvil stratiform echo) regions, respectively. BLIS observations are from tethersonde instrumentation aboard the Dallas.

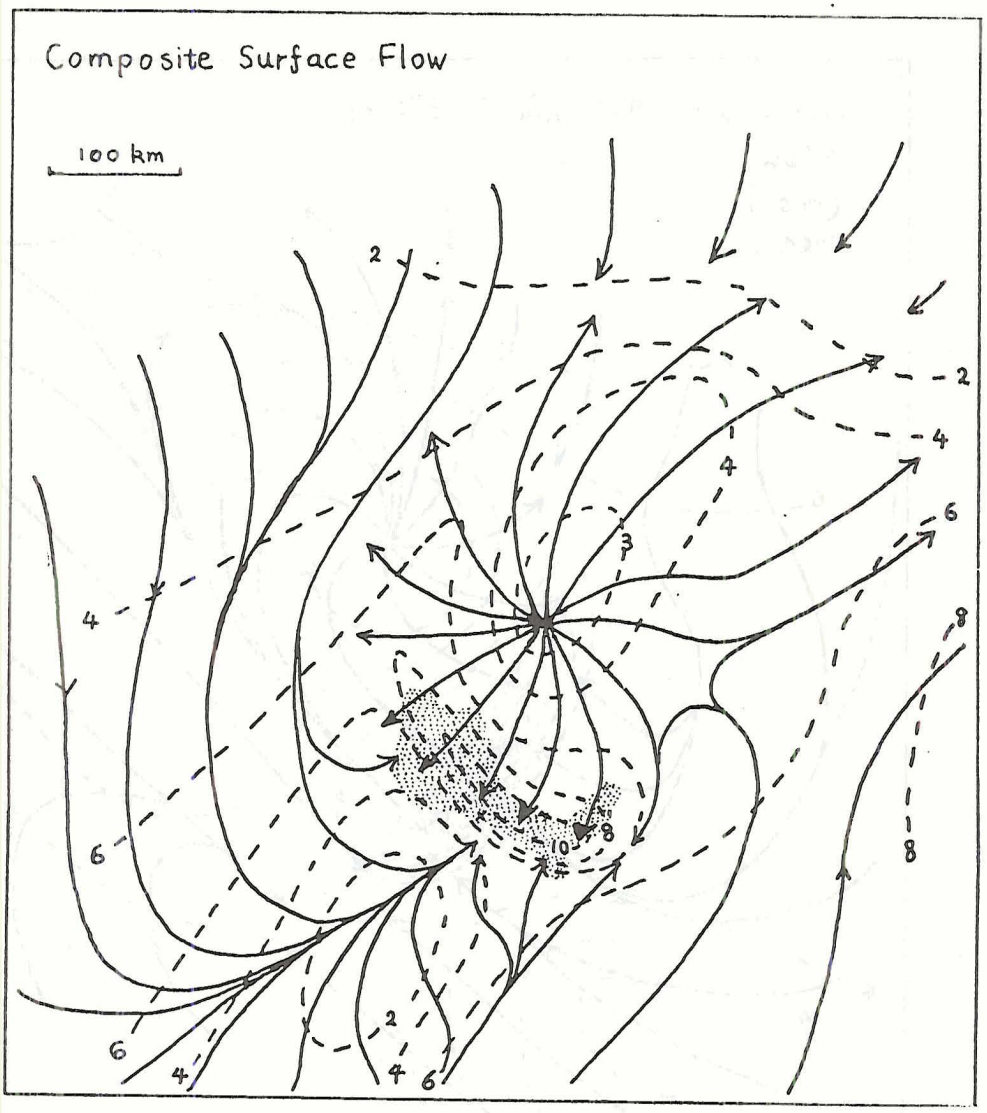

Fig. 4. Composite surface streamline flow. Dashed lines are isotachs ($m\ s^{-1}$).

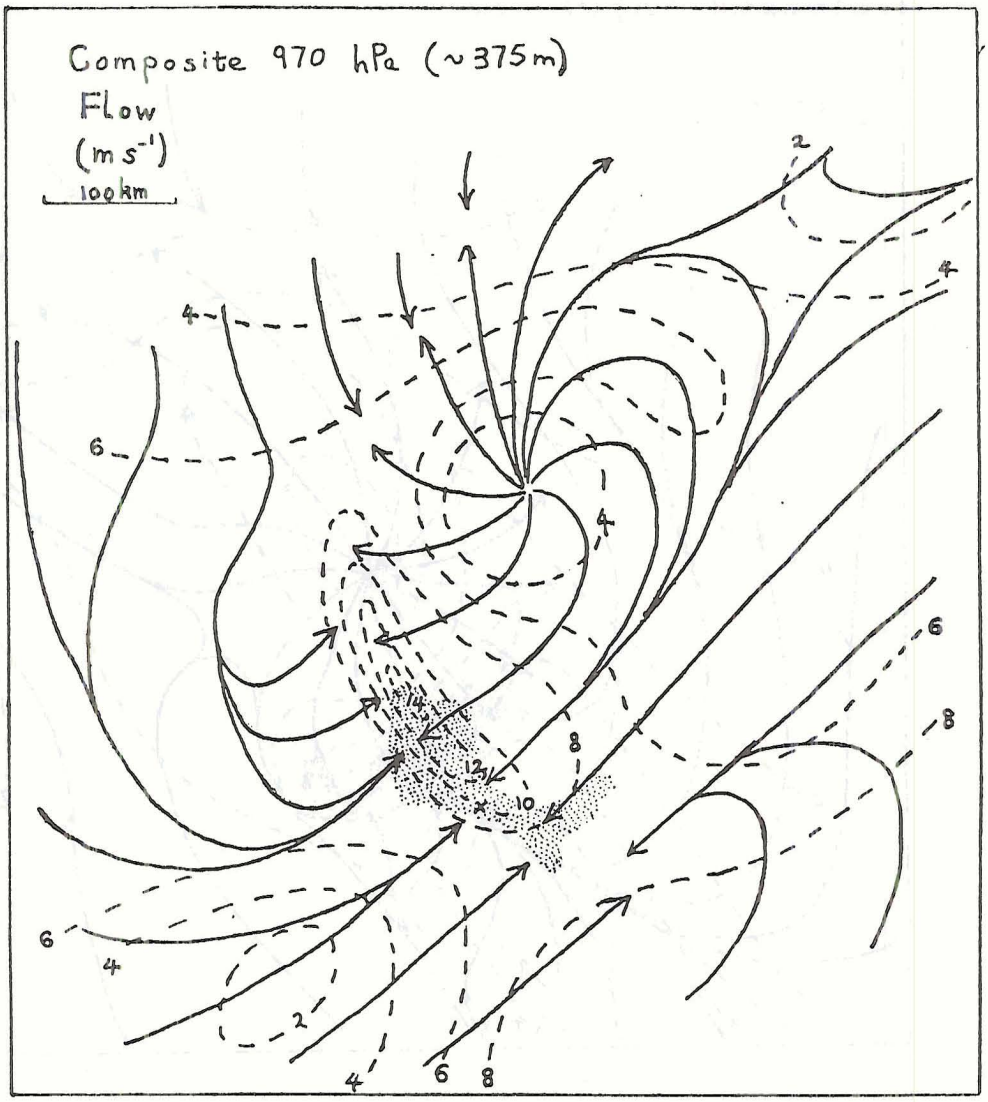

Fig. 5. Composite flow at 970 hPa (~ 375 m). Dashed lines are isotachs.

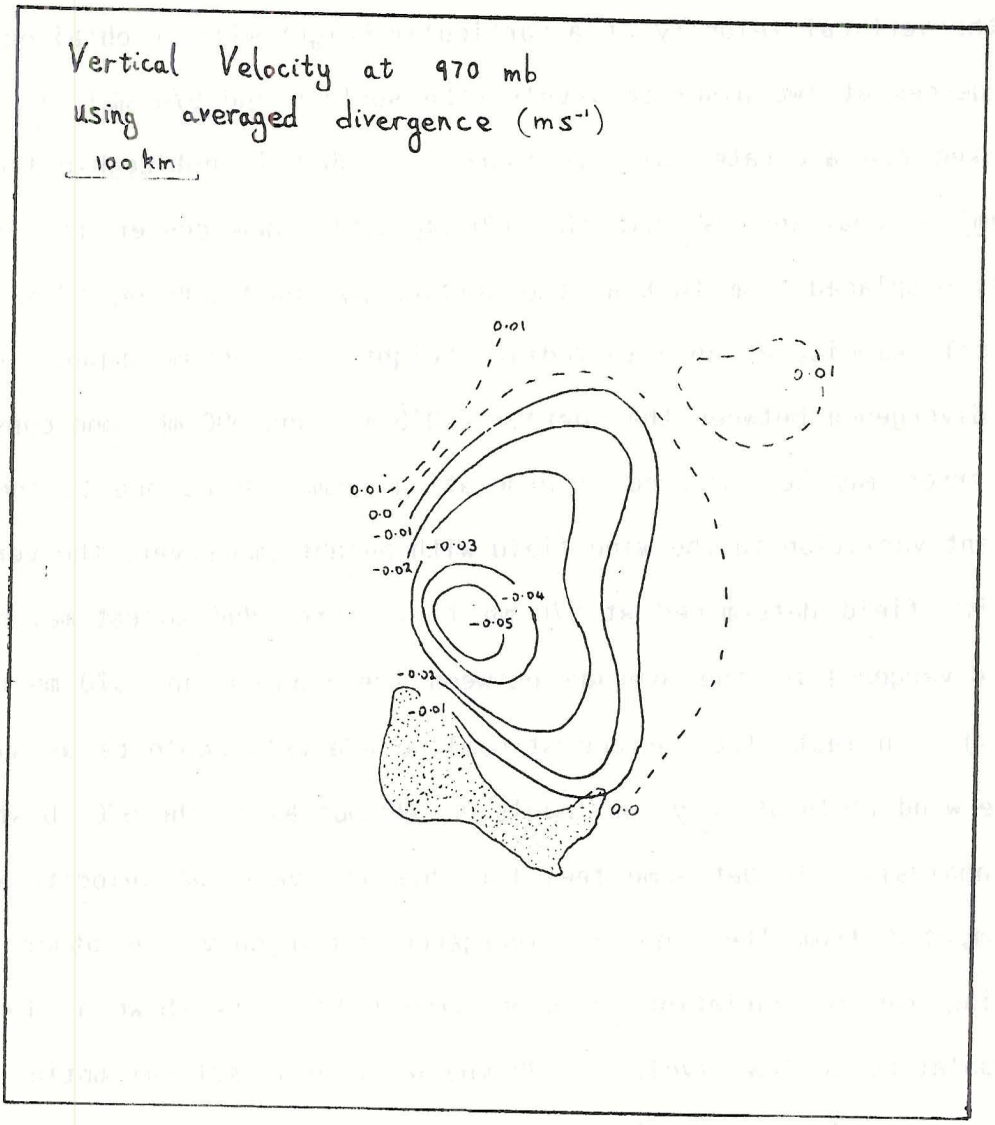

Fig. 6. Vertical velocity field at 970 mb (m s^{-1}), determined by averaging the surface and 970 mb divergences.

center due to the increase in wind speed that occurs towards the squall front. Well behind the squall line weak upward vertical motion is diagnosed. Since the vertical motion at the top of the mixed layer turns out to be an extremely important factor in determining its growth, and the vertical velocity at a particular height will be obtained using divergences at two discrete levels (the surface and 970 mb), it should be asked how accurate this procedure is. What is noticeable from the streamline analyses is that the 970 mb diffluence center is significantly displaced from that at the surface by about 100 km. The actual vertical velocity at an intermediate height, say 990 mb depends on the mean divergence between the surface (1010 mb) and 990 mb, and considerable error may be incurred interpolating from 970 mb due to the significant variation in the wind field with height (moreover, the vertical velocity field determined at 970 mb is in error due to estimating the mean divergence by the average between the surface and 970 mb divergences). In fact, the surface streamline analysis could be as similar to the wind field at very low levels (> 990 mb) as is the 970 mb streamline analysis. To get some feel for this the vertical velocity at 970 mb computed from the surface divergence field only, in other words allowing for no variation of wind with height, is shown in Fig. 7. Interpolating to low levels (> 990 mb) with this vertical motion field may be as good as using the former. There are evidently some differences between these two fields; in particular, the maximum vertical velocity computed using the surface divergence only, is stronger. Since for modeling purposes we need the vertical velocity between 1000 mb and about 950 mb, it seems reasonable to interpolate from the vertical velocity at 970 mb calculated using the average divergence between the surface and this level, but the degree of approximation should be noted.

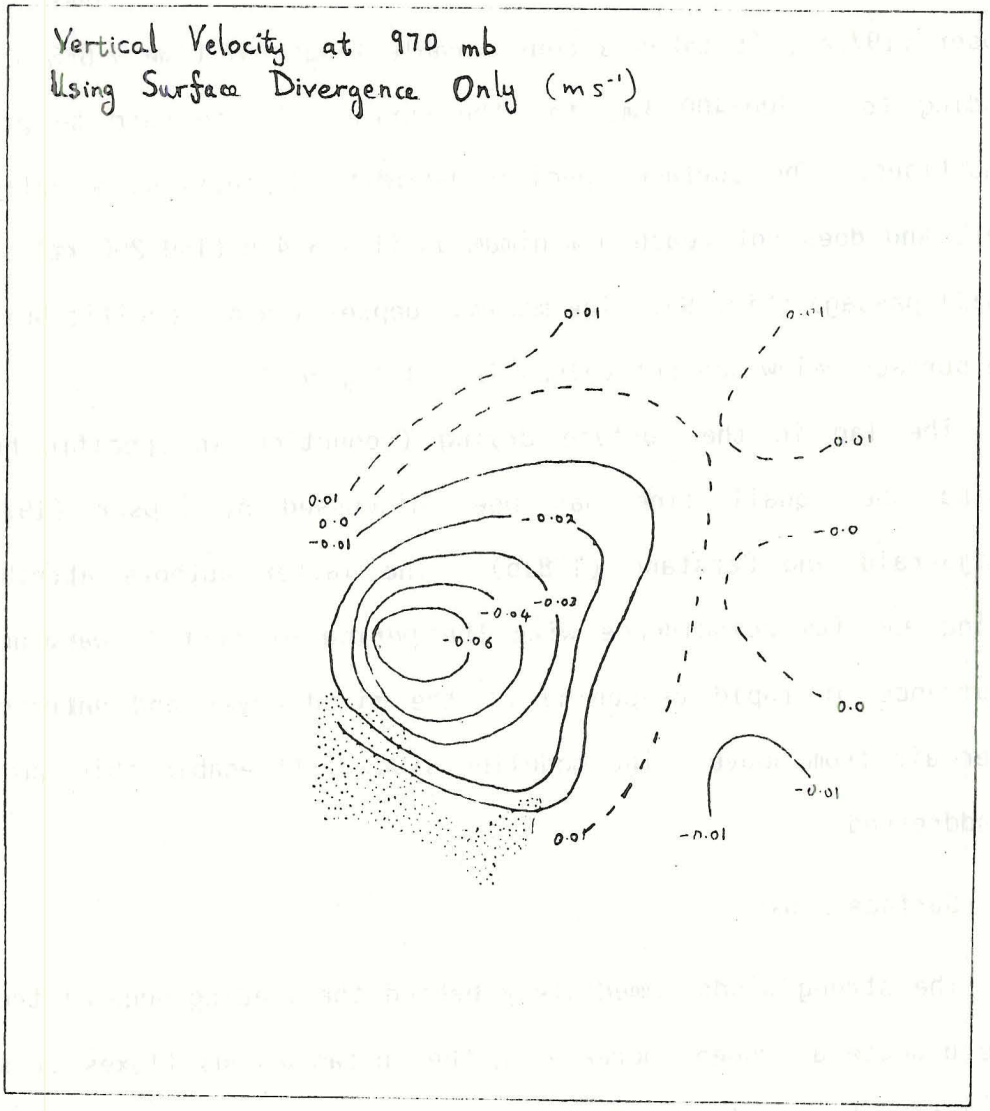

Fig. 7. Vertical velocity field at 970 mb (m s^{-1}), determined using the surface divergences.

3.c Surface Temperature and Specific Humidity Fields

Accompanying the passage of the squall is a sudden drop in the temperature of ~ 4°C with the coolest surface air ~ 50 km behind the leading edge of the squall (Fig. 8). As discussed by Houze (1977) and Zipser (1977a), it takes a considerable length of time ~ 6-8 h (corresponding to ~ 300-400 km) for the surface air to warm to pre-squall conditions. The surface specific humidity depression is delayed however, and does not reach a minimum until ~ 3-4 h (150-200 km) after the squall passage (Fig. 9). The maximum depression of specific humidity at the surface below ambient values is ~ 3-4 g kg^{-1}.

The lag in the surface drying (reduction in specific humidity) behind the squall line has been discussed by Zipser (1977a) and Fitzjarrald and Garstang (1981b). The latter authors attribute the drying and its coincidence with the period of surface warming to the occurrence of rapid deepening of the mixed layer and entrainment of drier air from above. The modeling study will enable this question to be addressed.

3.d Surface Fluxes

The strong winds immediately behind the leading edge of the squall line produce a sudden increase in the instantaneous fluxes of sensible and latent heat. The composite analysis of surface latent heat flux is shown in Fig. 10. The enhancement of the latent heat flux over the majority of the wake area can largely be attributed to significant surface drying (Fig. 9).

The virtual static energy flux is shown in Fig. 11. It is primarily the surface cooling by convective downdrafts that contributes to

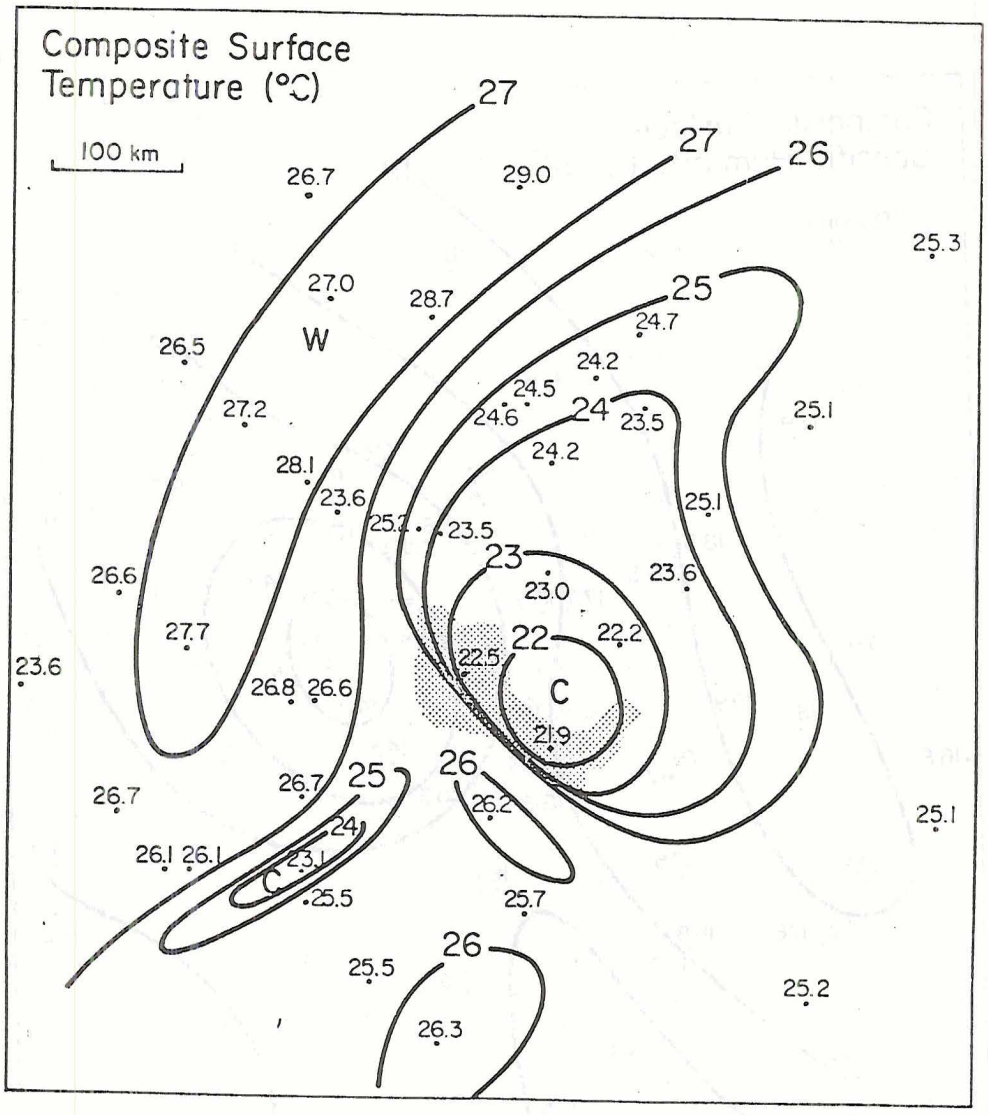

Fig. 8. Composite surface temperature at ship deck or ~ 10 m level (°C). (redrafted from Johnson and Nicholls, 1982)

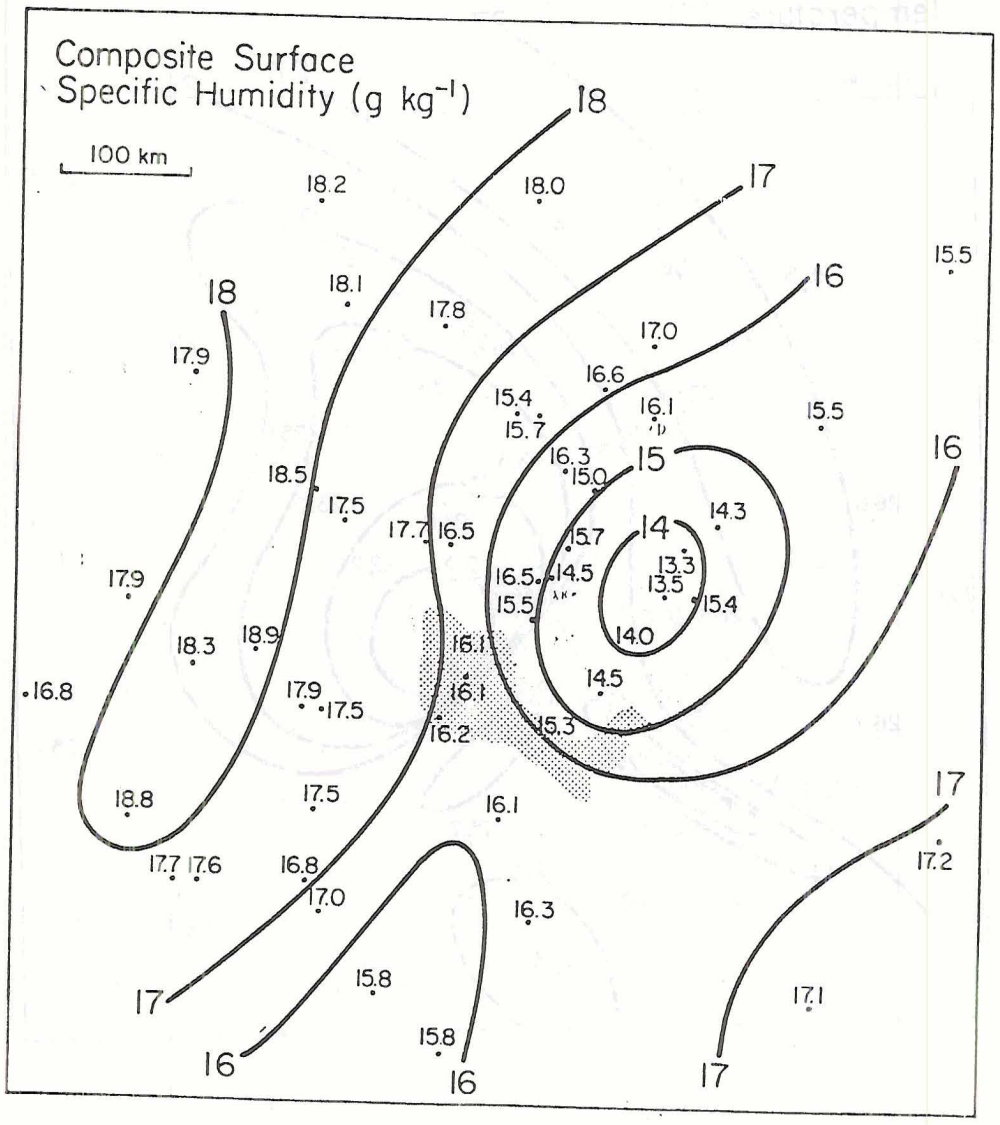

Fig. 9. Composite surface specific humidity (g kg^{-1}). (redrafted from Johnson and Nicholls, 1982)

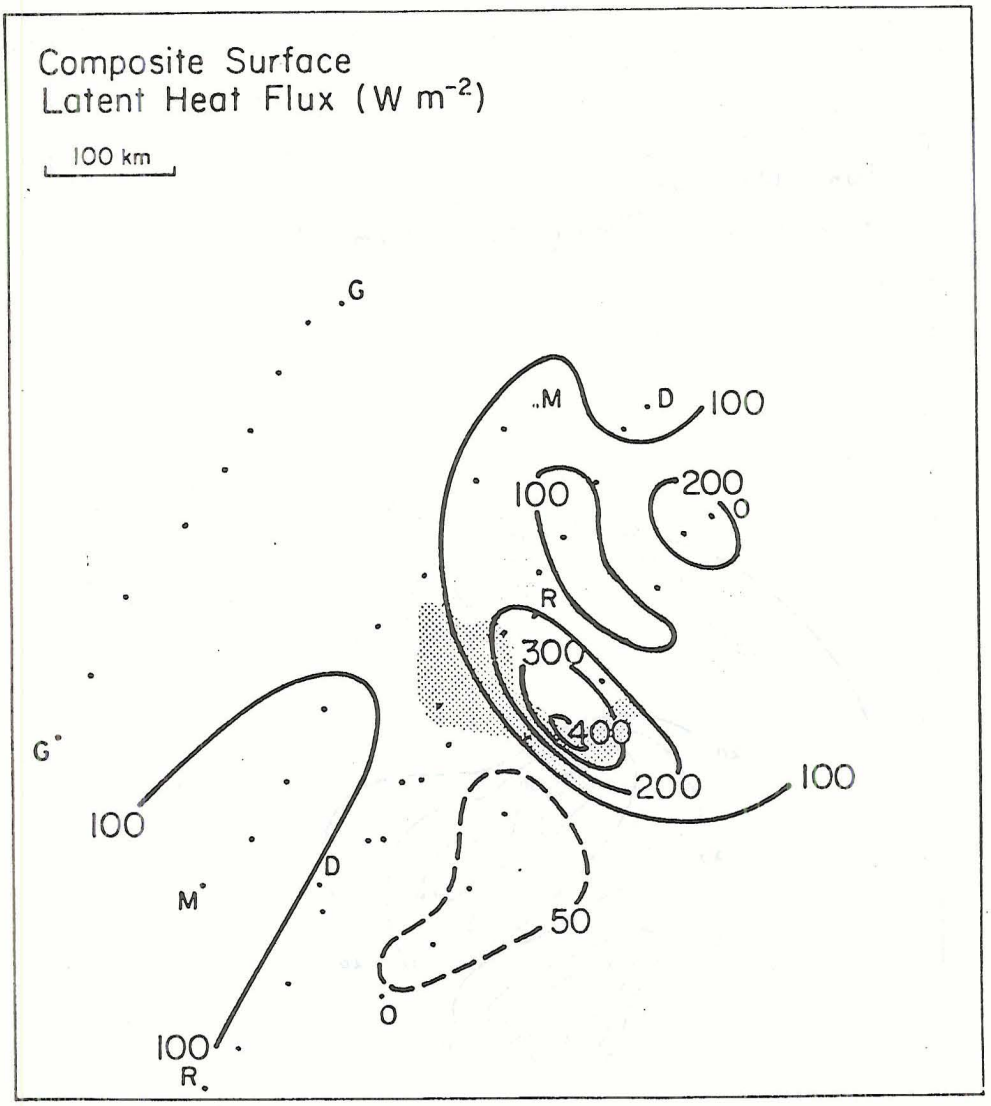

Fig. 10. Composite surface latent heat flux (W m^{-2}) (redrafted from Johnson and Nicholls, 1982). Hourly positions of Gillis (G), Meteor (M), Dallas (D), Researcher (R), and Oceanographer (O) are indicated by dots.

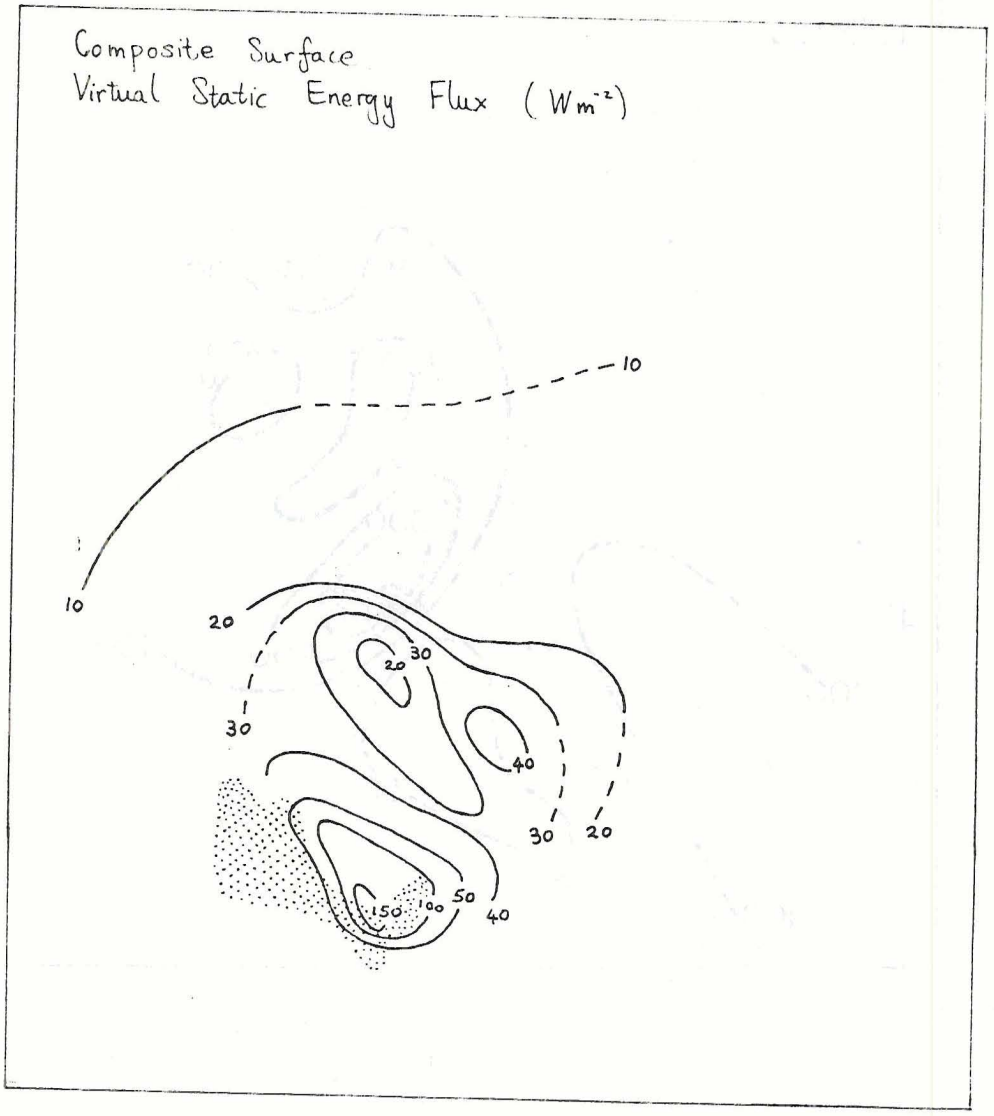

Fig. 11. Composite surface virtual static energy flux (W m^{-2}).

enhanced virtual static energy flux over most of the anvil region. Maximum values of both virtual static energy and latent heat fluxes occur on the south east side of the squall system and a relative minimum occurs near the center of maximum surface divergence where winds are very light.

3.e Lapse Rates Above the Transition Layer

Above the mixed layer top there exists a transition layer (or interfacial layer) about 100 m thick which normally has a very stable lapse rate of dry static energy. The growth and thermodynamic structure of an entraining mixed layer is highly sensitive to the type of air above the transition layer. Hence special attention is being given to the development of the dry static energy and specific humidity profiles. Some profiles of dry static energy and specific humidity found behind the squall line are shown in Figs. 12 to 16. The ships Oceanographer, Researcher, Dallas and Meteor are denoted by O,R,D, and M respectively, and the time of the sounding (GMT) is given in parenthesis. Figs. 12 and 13 all show a mixed layer structure except for the O(1513) sounding which was taken close to the squall front (just outside the convective region); apparently in this region mixed layers, if they exist at all have depths smaller than that resolvable by the sounding data ($\lesssim$ 50 m). Figs. 14 and 15 show profiles of specific humidity; note that most of these profiles have an unusual structure, with a minimum in specific humidity occurring some distance above the surface capped by a relative maxima. Fig. 16 shows two soundings taken about 3 hrs later than the period during which the squall system could be considered to be in a steady state; again an unusual specific humidity profile is observed.

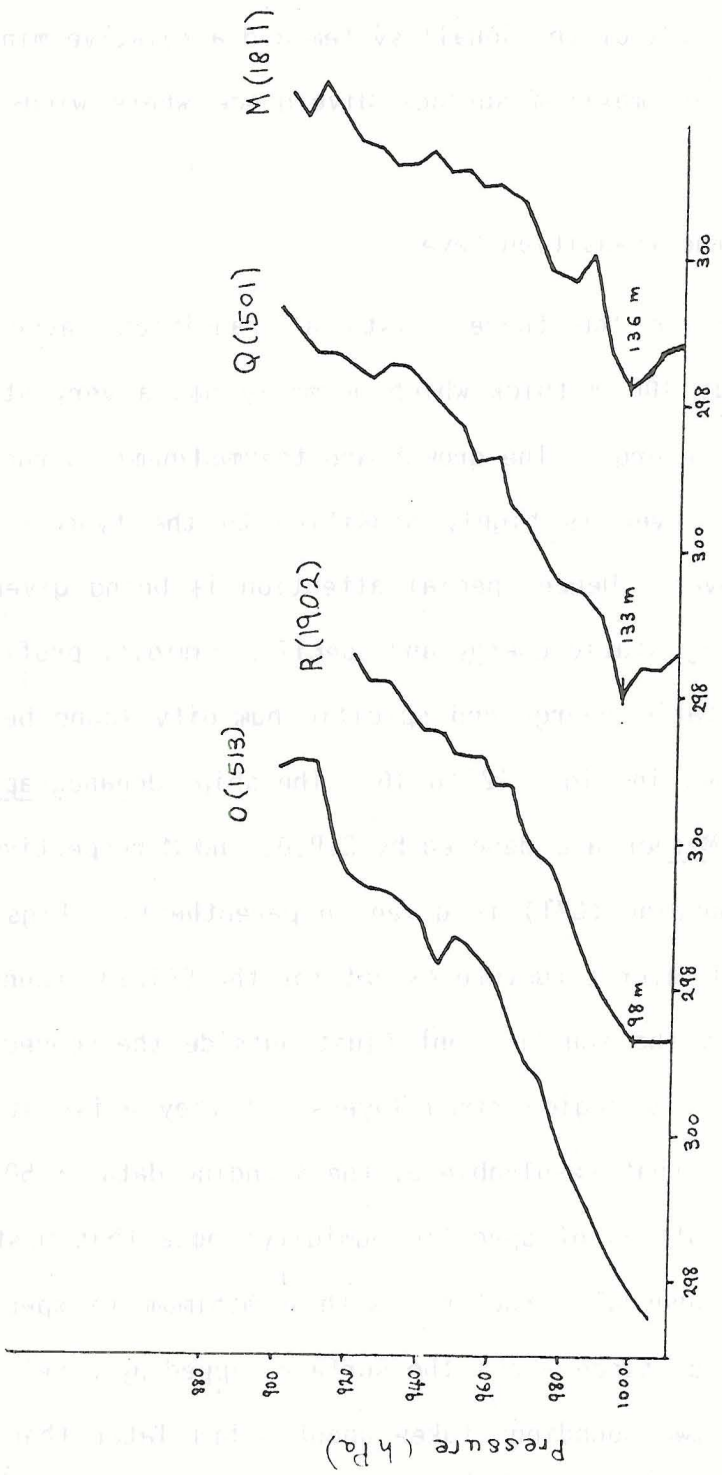

Fig. 12. Profiles of dry static energy within the squall wake. The soundings shown are positioned fairly close to the squall line (convective echo) region. Mixed layer depths (m) are indicated. The ship and time of sounding are given.

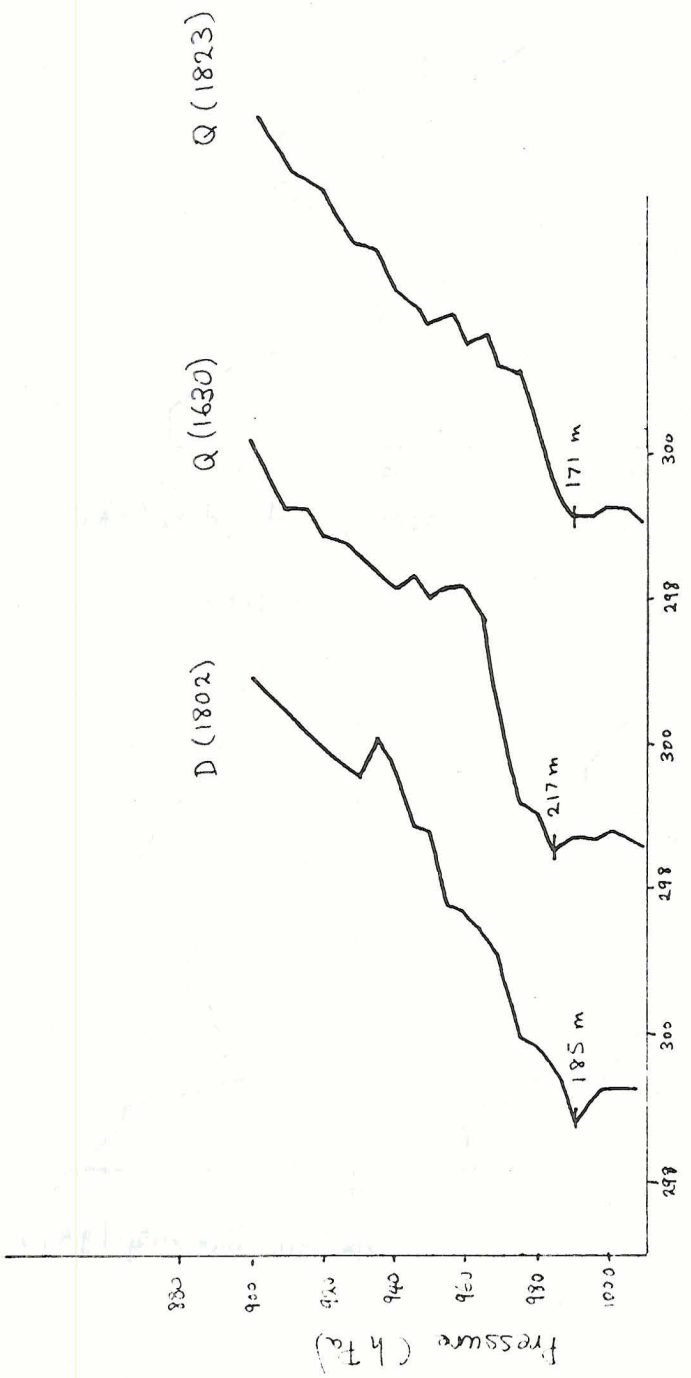

Fig. 13. As in Fig. 12 except for soundings which are positioned further behind the squall line (convective echo) region.

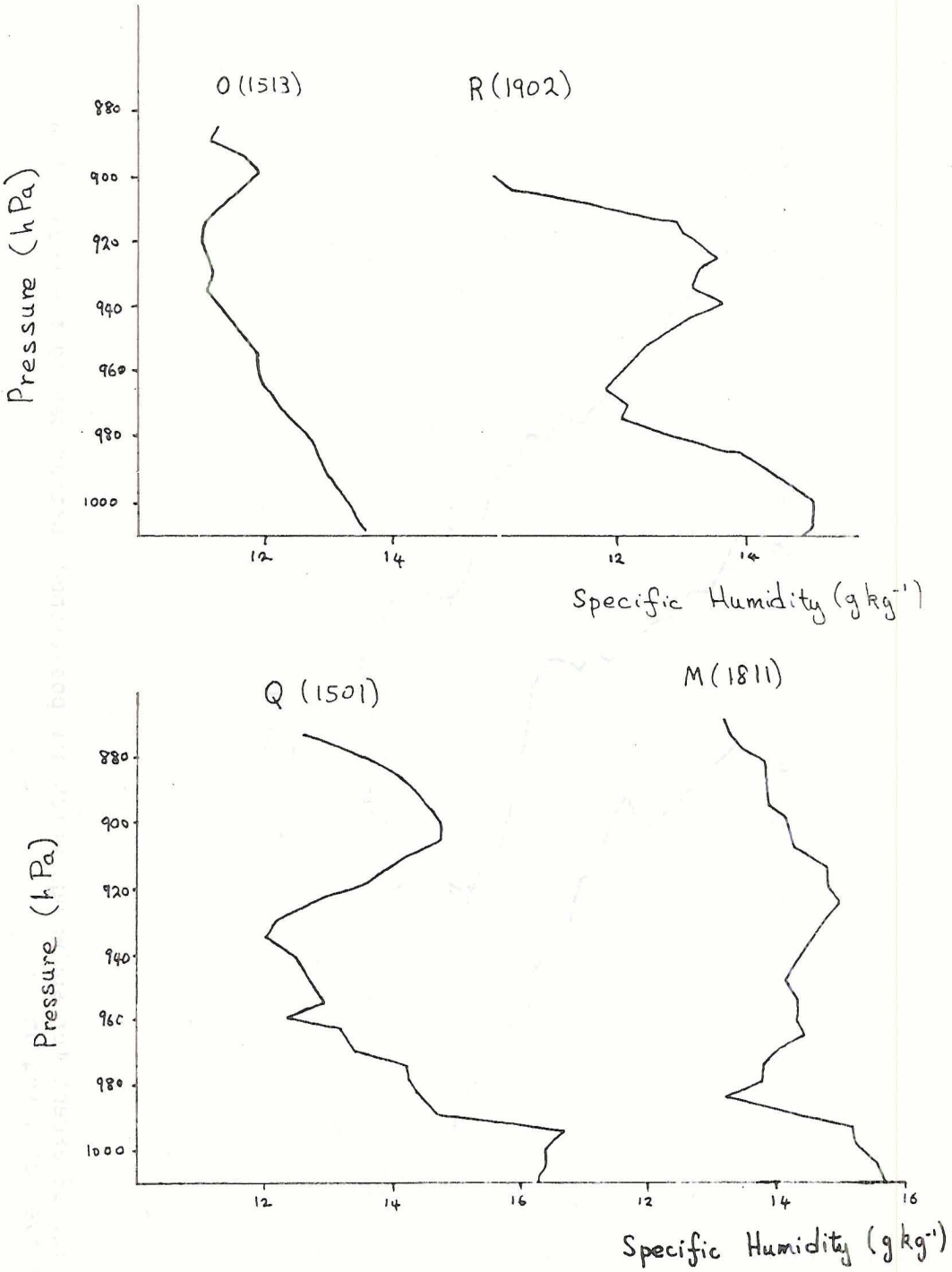

Fig. 14. Profiles of specific humidity for the same soundings as in Fig. 12.

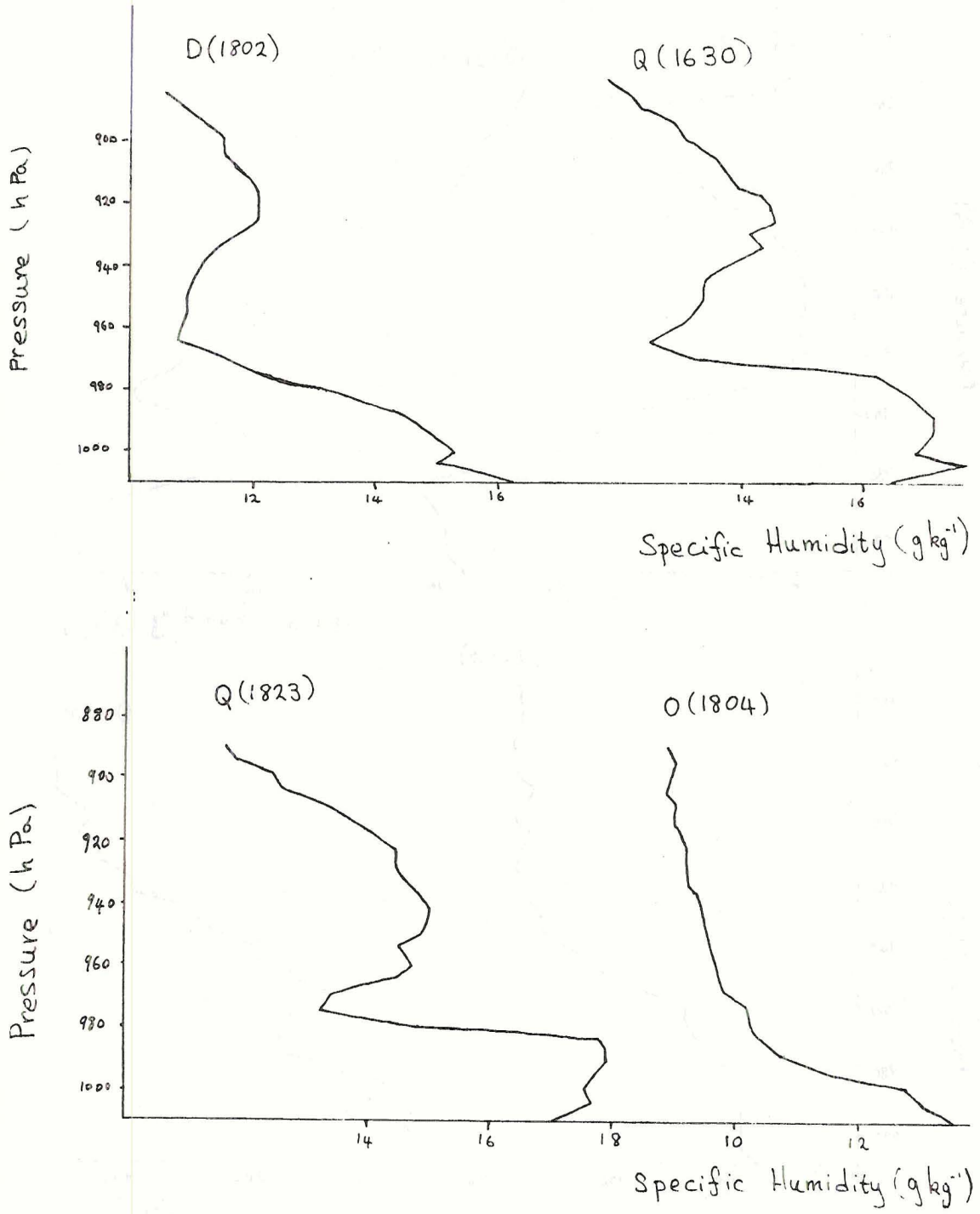

Fig. 15. Profiles of specific humidity for the same soundings as in Fig. 13. The profile for Oceanographer, 1804 GMT is also shown.

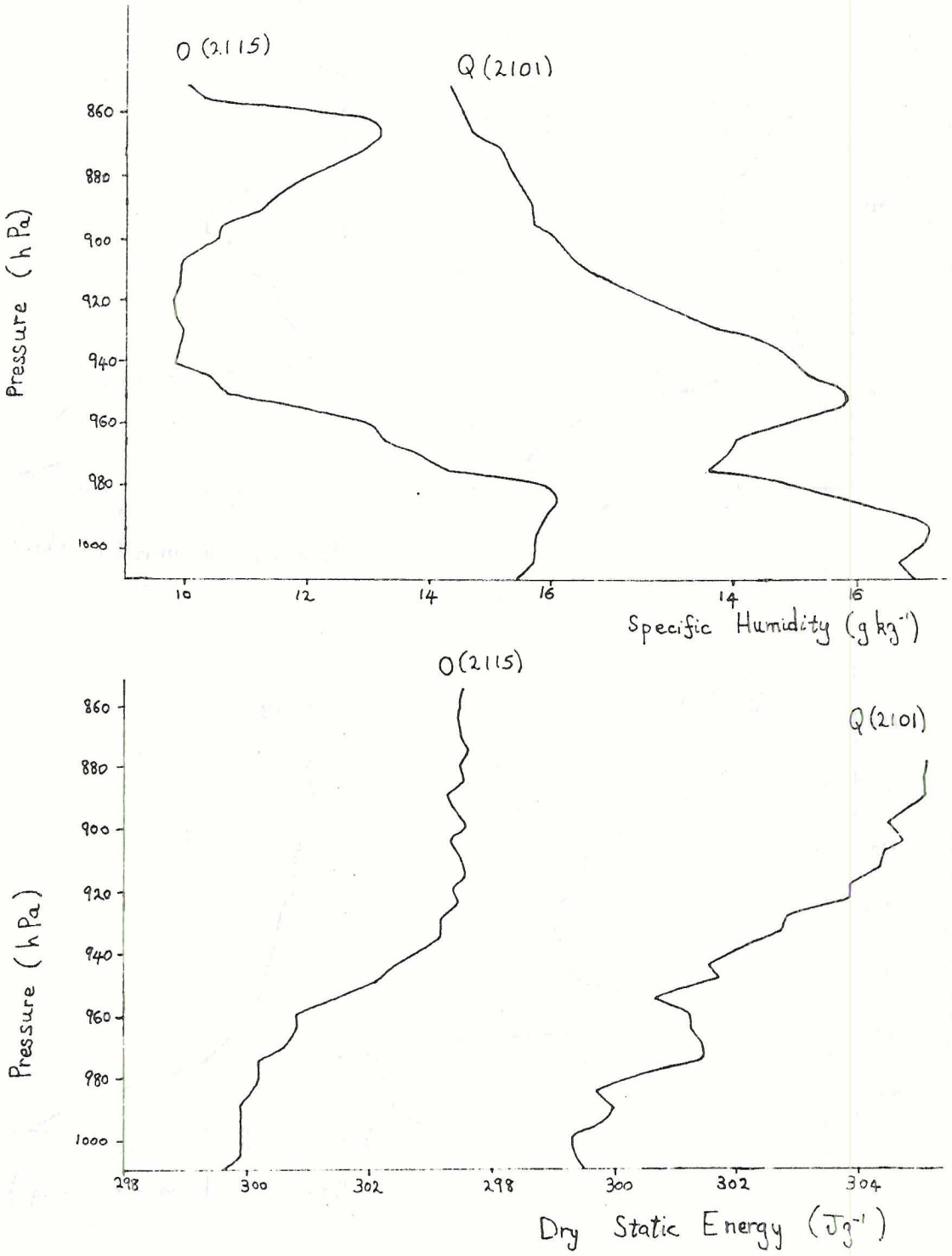

Fig. 16. Profiles of specific humidity and dry static energy for two soundings taken after the time for which the squall system could be considered to be in steady state.

It can be seen from these profiles that it is difficult to estimate transition layer depth but that it appears to be about 100 m. (Fitzjarrald and Garstang, (1981a) using an extensive set of GATE boundary layer profiles obtained a median transition layer thickness of 100 m and a mean of 183 m.)

Fig. 17 shows the composite analysis of the gradient of the dry static energy (ds/dz) above the transition layer. There is a significant increase in stability above the transition layer that occurs in the wake of the squall line. Fig. 18 shows the composite analysis of the gradient of specific humidity (dq/dz) above the transition layer. The ship positions and time of soundings are indicated and can be matched to the profiles of Figs. 14 and 15. This analysis is somewhat speculative and partly based on the following hypothetical model of the development of the lapse rate: Convective downdrafts occur in cores or cells and result in air originally at about 3 km or above being brought down to the surface (Betts, 1976). Idealized schematic profiles of the modification of the dry static energy and specific humidity from ambient values ahead of the squall line to values just behind the region of strong convective downdrafts are shown in Fig. 19, A and B. The dry static energy and specific humidity profiles in B should be compared with the O(1513) sounding (Figs. 12 and 14). Just after the squall passage the mixed layer is absent or extremely small. The formation of the relative maxima in specific humidity at 1 km or higher from the surface is hypothesized to occur due to dry air (in the sense that q is less) from the convective downdrafts spreading out beneath moister air in between downdraft cores. Although rainfall evaporation is large in the convective downdraft air, it is conceivable that it arrives at the

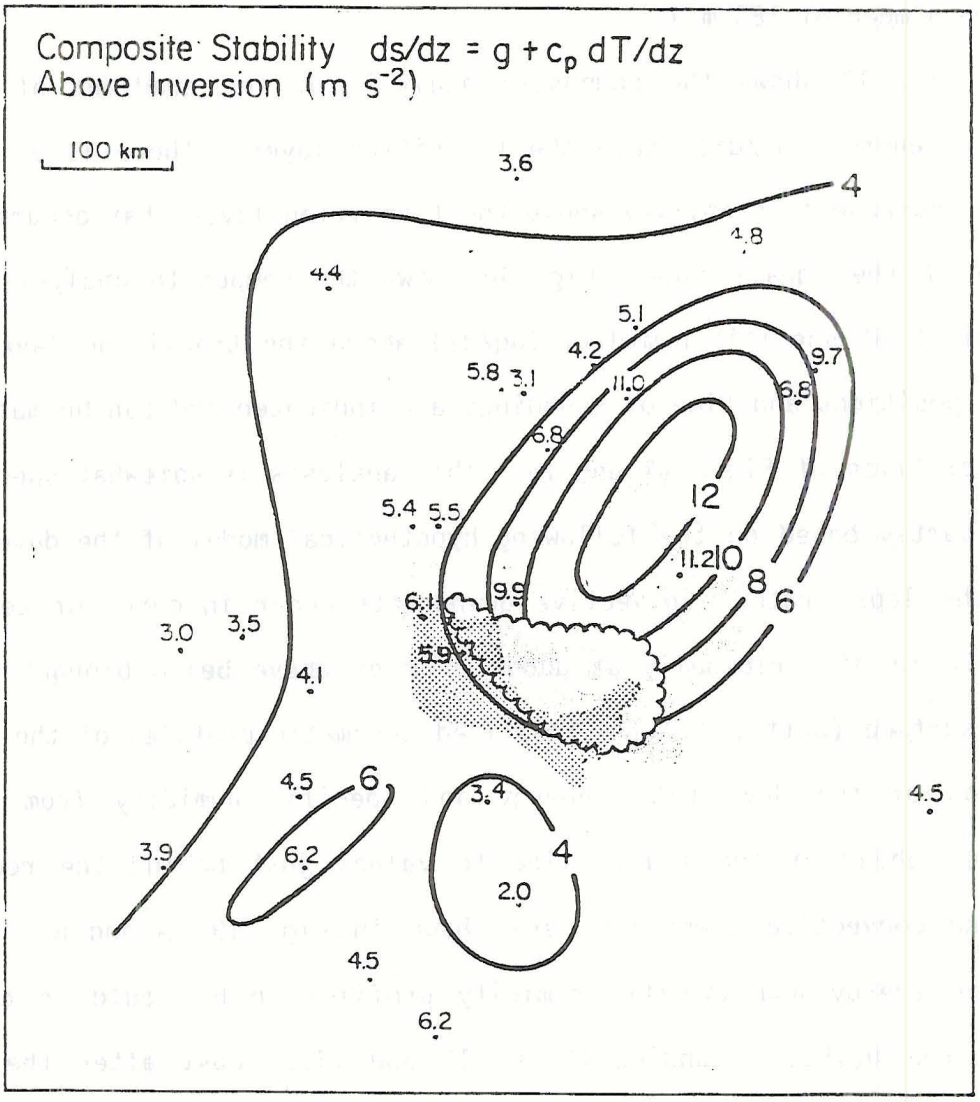

Fig. 17. Composite stability atop the mixed layer inversion (m s^{-2}) (redrafted from Johnson and Nicholls, 1982). Scalloped curve enclosed estimated area of very stable boundary layer as in Fig. 3.

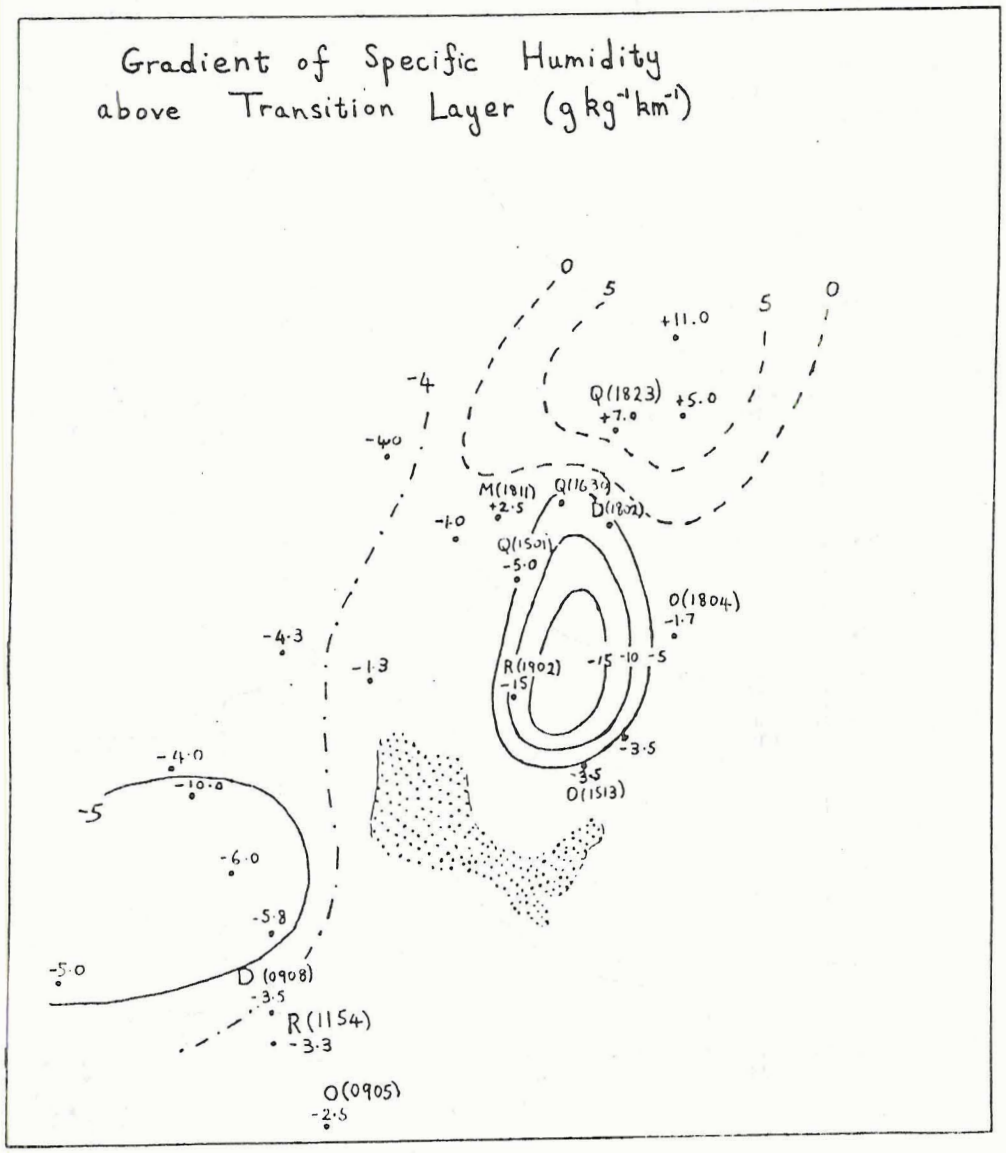

Fig. 18. Composite lapse rate of specific humidity atop the mixed layer inversion. The ship and time of some of the soundings are indicated and can be matched with those of Figs. 12 and 13.

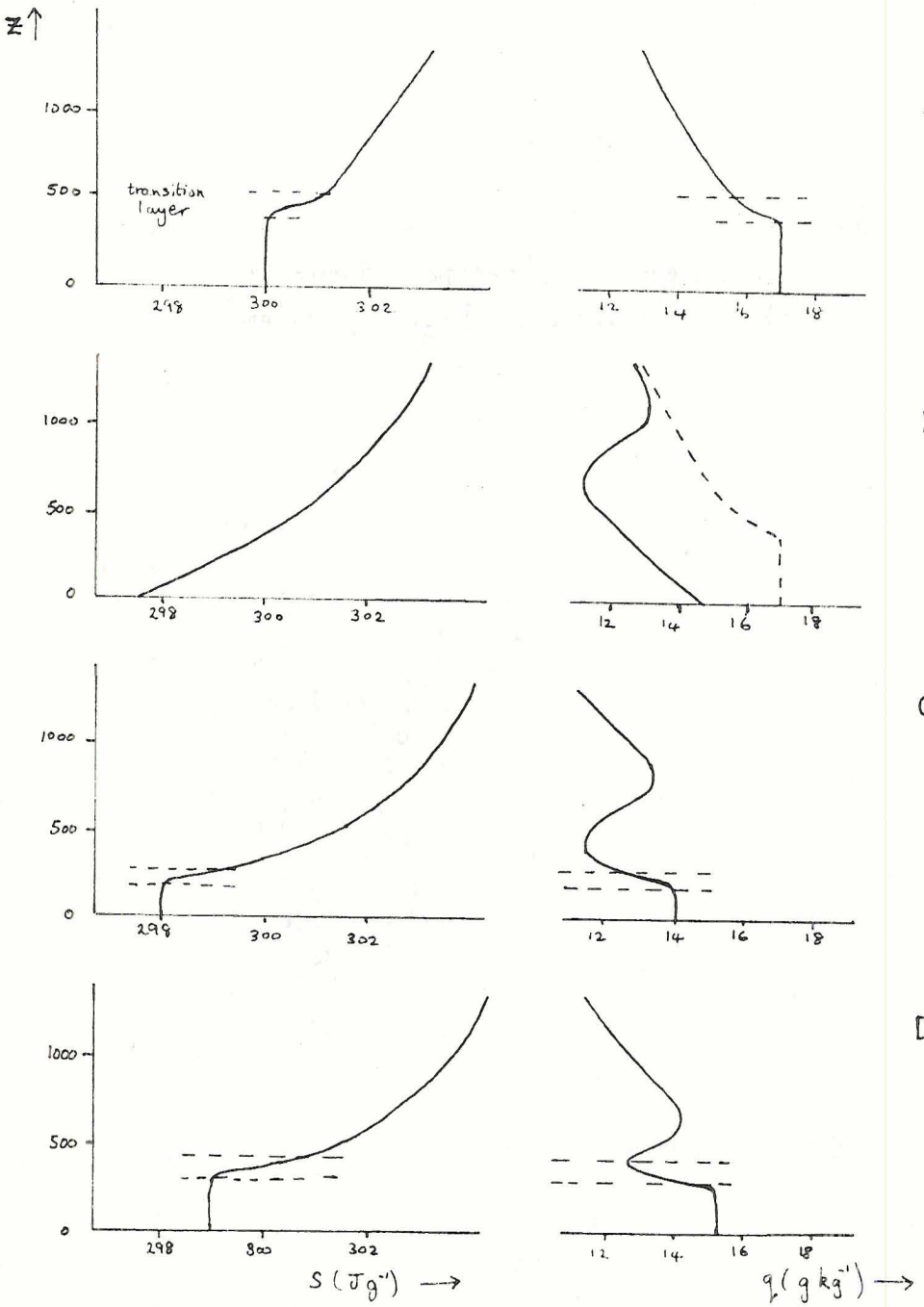

Fig. 19. Idealized schematic profiles showing the modification of dry static energy and specific humidity that occurs with the passage of the squall system. (A) Shows thermodynamic structure of air ahead of squall line. (B) Just outside the region of convective scale downdrafts (~50-100 km behind leading edge of squall line). (C) Middle of squall wake (~ 100-250 km behind leading edge). (D) Rear of squall wake (> 250 km behind leading edge).

surface with a lower q than the surrounding air (it could still be nearly saturated due to its low temperature). Fig. 20 shows moist static energy ($h = c_pT + gz + Lq$) profiles for three soundings ahead of the squall line and three soundings within the squall wake. There is a considerable decrease in the low level moist static energy after the passage of the squall line. Also noticeable in the soundings within the squall wake, in particular for R(1902) and Q(1501) is a minimum in moist static energy just above the surface capped by a relative maxima, very similar to the specific humidity profiles (see Fig. 14). These profiles are consistent with the idea that air from convective downdraft cores spreads out at the surface beneath air which has not originated from such a high level. The depth of this convectively produced downdraft outflow seems to be between 500 m to 1000 m.

Another possible factor contributing to the unusual specific humidity profile could be rainfall evaporation underneath the anvil being a significant function of height. However, this could not account for the shape of the moist static energy profile. (Note that low level moist static energy can be increased by sensible and latent heat exchanges at the sea-air interface.) Rainfall evaporation combined with the effect of vertical wind shear could also play a part. Gamache and Houze's (1982a) 850 mb streamline analysis shows that the wind speed relative to the squall is less at this level than it is at the surface. If we followed an air parcel starting at 850 mb compared to one at the surface, relative to the squall, we would expect it to descend in the mesoscale downdraft (see Fig. 6) and since it is moving slower relative to the squall line than air closer to the surface, to remain within the rainfall region for longer and thus might increase its moisture content over that of the air directly beneath it.

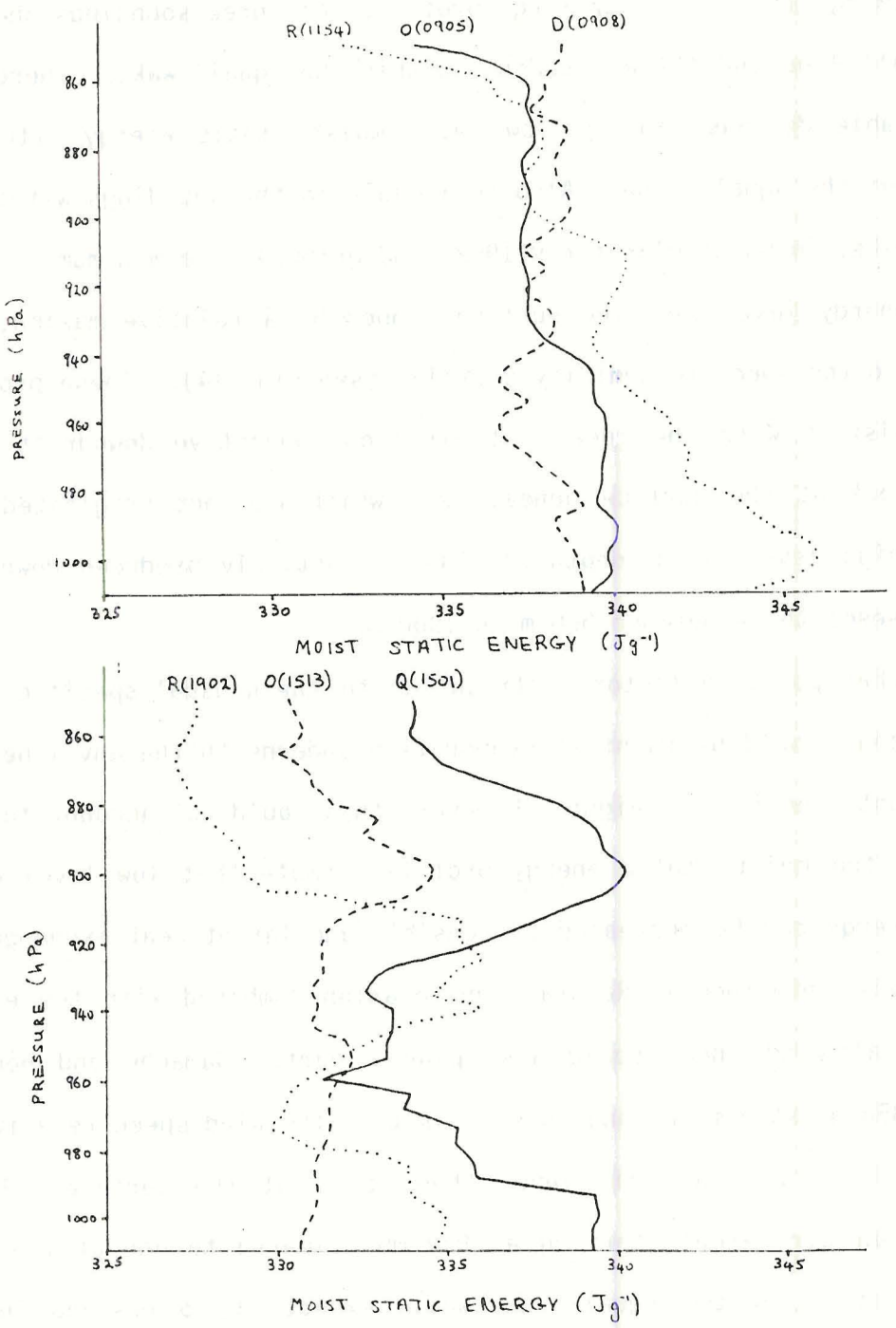

Fig. 20. Moist static energy profiles for three soundings ahead of the squall line and three soundings within the squall wake. The ship and time of sounding can be matched to those of Fig. 18.

To understand how profile B might develop as we follow the air parcel trajectory, it helps to consider the equations to be derived in Chapter 5 for the gradients of virtual static energy and specific humidity in the stable air above the transition layer. (These equations were used by Carson, 1973.) For the case of constant divergence (with height)

$$\frac{d_H \Gamma_{Sv}}{dt} = - \Gamma_{Sv} \frac{\bar{w}(z)}{z} \tag{3.1}$$

$$\frac{d_H \Gamma_q}{dt} = - \Gamma_q \frac{\bar{w}(z)}{z} \tag{3.2}$$

where Γ_{Sv} (= ds_v/dz) is the gradient of virtual static energy and Γ_q (= dq/dz) is the gradient of specific humidity (note that gradients are the negative of the lapse rates). These equations indicate that subsidence will act to increase the magnitude of the gradient and that this rate of change is proportional to the gradient. If we were to follow the trajectory relative to the squall line of a column of air with profiles B some 50-100 km we might qualitatively expect the new profiles to look like those in Fig. 19C. Subsidence has brought the relative maxima in the specific humidity profile closer to the surface and the mixed layer has started to recover. Furthermore, the mixed layer is growing into a region having a strong negative gradient of specific humidity. The gradient of virtual static energy above the transition layer is also increasing as long as subsidence is occurring (at least as long as Γ_{Sv} is fairly constant with height). Compare the profiles in C to those of Researcher (1902) and Quadra (1501) in Figs. 12 and 14. If subsidence continues, the mixed layer may be expected to grow into air where the gradient of specific humidity changes sign and becomes positive, see

profiles D. This could be compared to the soundings of Meteor (1811) and Quadra (1823) (see Figs. 12, 13, 14 and 15). The soundings of Dallas (1802) and Quadra (1630) (see Figs. 13 and 15) are harder to classify and could have strong negative gradients of specific humidity above the mixed layer or they could be positive. The sounding for Oceanographer (1804) (see Fig. 15) is somewhat anomalous and unfortunately, dry static energy could not be obtained for this sounding. The specific humidity profile apparently shows a lower mixed layer height than would be expected in this region and no relative maxima above the surface as do other soundings. The mixed layer is also very dry. Fig. 16 shows the soundings at Oceanographer (2115) and Quadra (2101). Since by this time the squall line was well into its decaying stage little attention has been given to them for purposes of the composite analysis. However, they are good examples of the large differences in the gradients of specific humidity at the top of the transition layer that can occur. Oceanographer (2115) has a strongly negative gradient at the top of the transition layer (unless the transition layer is some 300 metres thick which is very unlikely), whereas, Quadra (2101) seems to have a positive gradient. Further discussion of the lapse rates will be deferred until Chapter 5 where a more quantitative analysis will be attempted.

3.f Lifting Condensation Level

Fig. 21 shows the composite lifting condensation level. Comparison with Fig. 3 shows that there are no regions where the mixed layer height exceeds the lifting condensation level, as expected. Just ahead of the squall line the lifting condensation level is low and only slightly higher than the mixed layer depth whereas in the wake of the system the

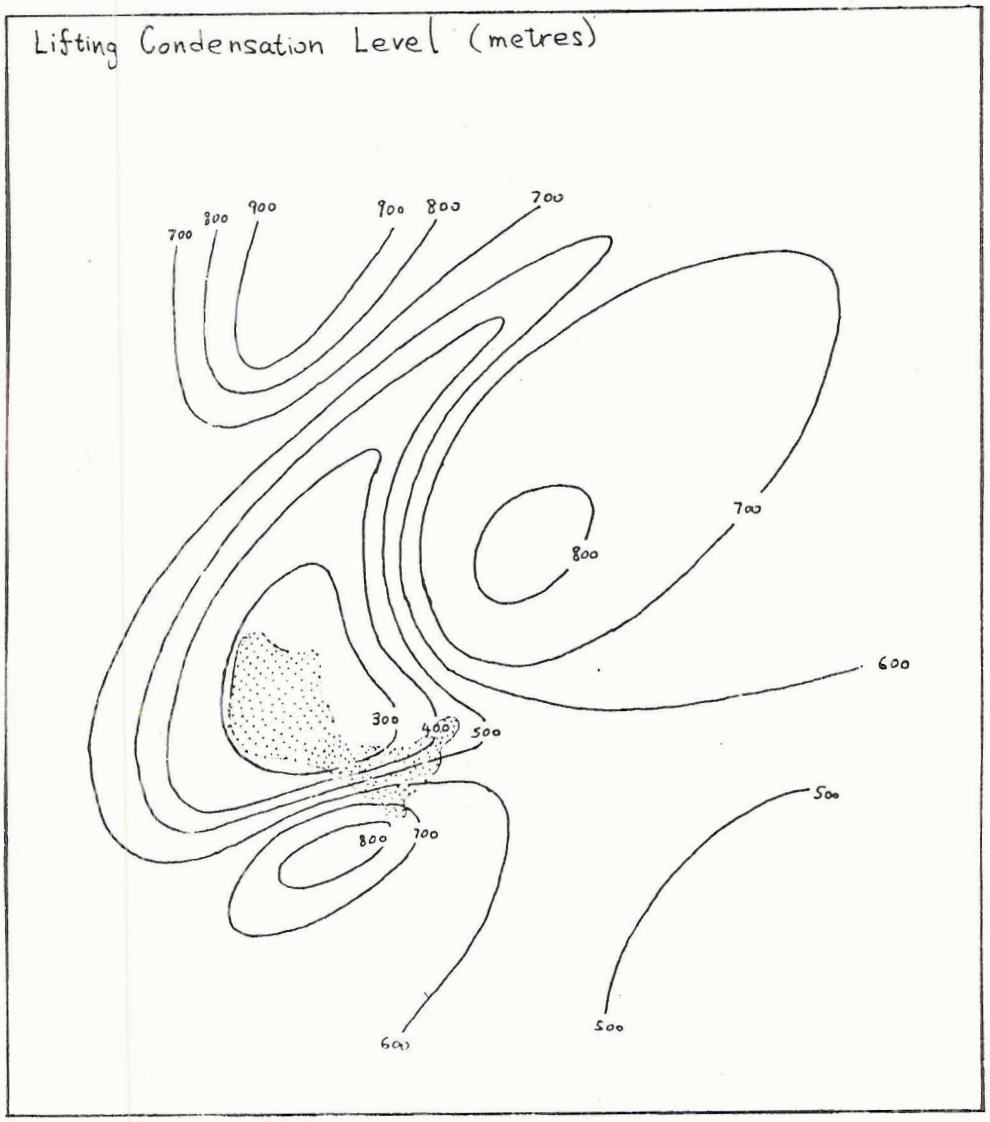

Fig. 21. Composite lifting condensation level (m).

difference is large, about 500 metres. This large difference accounts for the absence of shallow clouds atop the mixed layer in the wake region.

4. ZERO-ORDER MODEL OF THE GROWTH OF AN UNSTABLE BOUNDARY LAYER

The composite analysis provides suitable information for undertaking a detailed modeling study of the boundary layer. A simple model of the mixed layer is the zero order model developed by Ball (1960) and Lilly (1968). The version of the model used here will consider the effects of advection, variable lapse rate of virtual static energy and specific humidity, the vertical velocity at the top of the mixed layer, use the diagnosed buoyancy and latent heat fluxes, and allow inclusion of radiative and evaporative cooling.

To apply this model it is required that the Movin Obukhov length is small compared to the depth of the mixed layer, so that the production of turbulence by surface friction is negligible compared to that by buoyant convection. The Movin Obukhov length is given by

$$L = - u_*^3 \left[g s_v^{-1} K \left(\overline{w' s_v'} \right)_o \right]^{-1} \qquad (4.1)$$

where u_* is the friction velocity, s_v the virtual potential temperature, K Von Karman's constant, and $\left(\overline{w' s_v'} \right)_o$ the surface flux of virtual potential temperature. The friction velocities can be formulated in terms of a drag coefficient and wind speed, i.e. $u_* = \sqrt{c_D} u^2$. Taking the following values, $c_D = 0.0015$, $u = 5\ ms^{-1}$ $s_v = 3 \times 10^5\ J\ kg^{-1}$, $K = 0.4$, $\left(\overline{w' s_v'} \right)_o$

= 25 m K s^{-1} we obtain L = -24 m. Thus to a reasonable approximation turbulence driven by surface friction can be neglected in the squall wake.

Another important consideration is the production of turbulence due to wind shear in the transition layer. Deardorff (1978) estimated using results from the study by Moore and Long (1971) that the shear-driven entrainment becomes of equal or greater importance than convectively driven entrainment when $\Delta\bar{u} > 6\ w_*$ where $\Delta\bar{u}$ is the magnitude of the mean flow difference across the interfacial layer, and w_* the convective scale velocity given by

$$w_* = [(g/s_v)H(\overline{w's_v'})_o]^{1/3} \qquad (4.2)$$

where H is the mixed layer depth. If the transition layer depth is about 100 m and if we estimate $\Delta\bar{u}$ from wind profiles (not shown), the ratio of Δu to 6 w_* takes values between 1/12 - 4/5 with a mean of ~ 1/2 within the squall wake. The high value of this ratio for some soundings indicates that turbulent production due to wind shear could be significant. It should be pointed out that unlike the thermodynamic variables momentum did not appear to be well mixed within the mixed layer and no distinct jump in wind speed Δu was observed across the transition layer. As has already been discussed (p. 8) there is quite a bit of uncertainty in the low level wind speeds measured by rawinsonde.

The zero-order model is highly idealized and considers discontinuities in the thermodynamic fields. Idealized profiles of mean virtual static energy $\bar{s}_v$ and of mean flux $\overline{w's_v'}$ for the model are shown in Fig. 22. The capping inversion to the mixed layer is represented by Δs_v. No

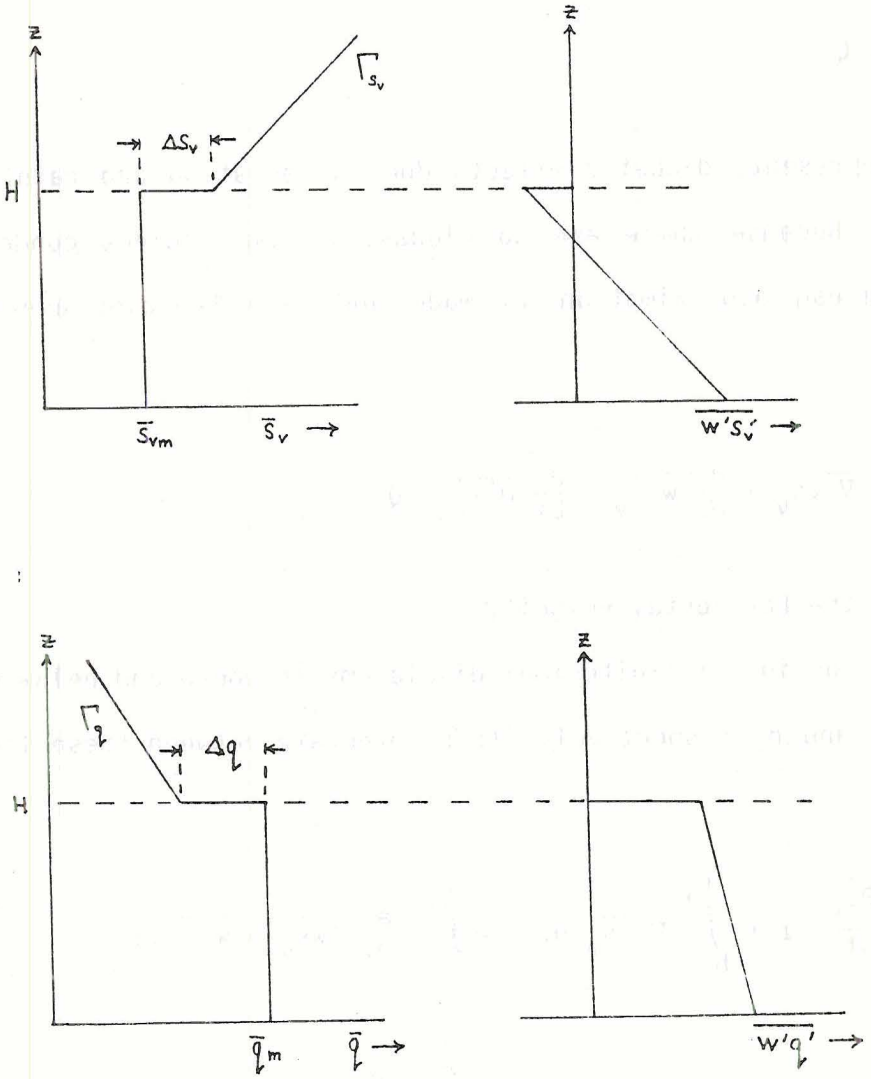

Fig. 22. Idealized profiles of mean virtual static energy $\bar{s}_v$, mean flux $\overline{w's_v'}$, mean specific humidity $\bar{q}$ and mean flux $\overline{w'q'}$ for the zero-order jump model.

clouds exist atop the mixed layer as was discussed earlier (p. 36). The equations for the growth of the mixed layer height and inversion strength are obtained in the following manner. The thermodynamic equation is

$$\frac{ds_v}{dt} = Q \tag{4.3}$$

where Q represents diabatic effects due to radiation and rainfall evaporation. Because there are no clouds, we can neglect condensation. The Boussinesq approximation is made and with Reynolds averaging we obtain

$$\frac{\partial \bar{s}_v}{\partial t} + \overline{\nabla \cdot \underset{\sim}{v} s_v} + \frac{\partial}{\partial z} \bar{w}\, \bar{s}_v + \frac{\partial}{\partial z} \overline{w' s_v'} = Q \tag{4.4}$$

where $\underset{\sim}{v}$ is the horizontal velocity.

If we consider infinitesimal displacements above and below H to the heights h_+ and h_- respectively, then integrate between these levels, we obtain

$$\int_{h_-}^{h_+} \frac{\partial \bar{s}_v}{\partial t}\, dz + \int_{h_-}^{h_+} \overline{\nabla \cdot \underset{\sim}{v} s_v}\, dz = -\int_{h_-}^{h_+} \frac{\partial}{\partial z} (\bar{\bar{w}}\bar{s}_v + \overline{w' s_v'})dz - \int_{h_-}^{h_+} \frac{\partial F_R}{\rho \partial z}\, dz \tag{4.5}$$

where we have represented the radiative or evaporative cooling term in flux form. Using Leibniz's rule and taking the limit as $h_+ - h_- \to 0$ we obtain

$$\frac{\partial H}{\partial t} + \underset{\sim}{v}\cdot\nabla H = \bar{w}_H - \frac{F_{s_v H}}{\Delta s_v} + \frac{\Delta F_R}{\rho \Delta s_v} \tag{4.6}$$

where $\bar{w}_H$ is the mean vertical velocity at H, F_{svH} the buoyancy flux, and ΔF_R is the jump in the radiative or evaporative flux at H. In the case of rainfall evaporation we envisage a flux of rain which is depleted within the transition layer by evaporation which causes a proportional amount of cooling. Of course in this model the transition layer is infinitesimal; however, in application its depth must be taken into account to estimate the evaporation of rain. At h_+ we have

$$\frac{d\bar{s}_v(h_+)}{dt} = \Gamma_{s_v} \frac{dh_+}{dt} + Q_+ \tag{4.7}$$

where Q_+ is the diabatic heating at h_+. Therefore

$$\frac{\partial \Delta s_v}{\partial t} = \Gamma_{s_v}\left(\frac{dh_+}{dt} - \bar{w}_+\right) - \left(\underset{\sim}{\bar{v}}\cdot\nabla \bar{s}_v\right)_{h_+} - \frac{\partial \bar{s}_v(h_-)}{\partial t} + Q_+ \tag{4.8}$$

where $\Delta s_v = \bar{s}_v(h_+) - \bar{s}_v(h_-)$ and $\bar{w}_+$ is the vertical velocity at h_+. Integrating (4.4) from the surface to h_- we obtain

$$\frac{\partial \bar{s}_v(h_-)}{\partial t} + \underset{\sim}{\bar{v}}_m\cdot\nabla \bar{s}_v(h_-) = \frac{F_{s_v o} - F_{s_v h_-}}{h_-} + Q_m \tag{4.9}$$

where $\underset{\sim}{\bar{v}}_m$ is the mean velocity, averaged through the depth of the mixed layer and Q_m the mean diabatic heating term. Substituting (4.9) into (4.8) we find

$$\frac{\partial \Delta s_v}{\partial t} = \Gamma_{s_v} \left(\frac{dh_+}{dt} - \bar{w}_+\right) - \left(\bar{\underset{\sim}{v}}\cdot\nabla \bar{s}_v\right)_{h_+} + \bar{\underset{\sim}{v}}_m \cdot \nabla \bar{s}_v(h_-) + \frac{F_{s_v h_-} - F_{s_v o}}{h_-} + \Delta Q \tag{4.10}$$

where $\Delta Q = Q_+ - Q_m$. Taking the limit as $h_+ - h_- \to 0$ and substituting from (4.6), we find

$$\frac{\partial \Delta s_v}{\partial t} + \bar{\underset{\sim}{v}}\cdot\nabla \Delta s_v = - \Gamma_{s_v} \left(\frac{F_{s_v H}}{\Delta s_v} - \frac{\Delta F_R}{\rho \Delta s_v}\right) + \frac{F_{s_v H} - F_{s_v o}}{H} + \Delta Q \tag{4.11}$$

where it has been assumed that horizontal velocity is independent of height. The system of equations (4.6) and (4.11) is incomplete since the buoyancy flux $F_{s_v H}$ has not been specified. The conventional closure assumption (Betts, 1973; Tennekes, 1973) is to make it proportional to the surface buoyancy flux, i.e.

$$F_{s_v H} = - k F_{s_v o} \tag{4.12}$$

where k is an entrainment parameter normally considered to have a value between 0.2 and 0.5. The buoyancy flux at the top of the mixed layer is negative. Eq. (4.6) shows that the growth of the mixed layer occurs by entrainment of potentially warmer air from above. Work is required to carry warmer air downward to be mixed into the boundary layer and so studies of this problem have normally considered the turbulent energy equation. Following Zeman and Tennekes (1977) we write

$$\left(\frac{\partial \bar{e}}{\partial t}\right)_H = \frac{g}{\bar{T}} \left(\overline{s_v' w'}\right)_H - \frac{\partial}{\partial z}\left(\overline{ew'} + \frac{\overline{p'w'}}{\rho}\right)_H - \varepsilon_H \tag{4.13}$$

where $\bar{e}$ represents the mean turbulent kinetic energy and ε the dissipation rate (other notation conforms to the usual conventions). Turbulent production due to wind shear across the transition layer has been neglected. Neglecting the term on the LHS of (4.13), i.e., assuming the turbulence is steady, and parameterizing the flux convergence term by

$$- \frac{\partial}{\partial z} \left(\overline{ew'} + \frac{\overline{p'w'}}{\rho} \right)_H = \frac{c_F \sigma_w^3}{H} \tag{4.14}$$

where σ_w is the r.m.s. turbulence velocity in the mixed layer and H an appropriate length scale (the coefficient c_F can be discounted for loss due to dissipation), we find

$$(\overline{s_v'w'})_H = - c_F \frac{\sigma_w^3}{H} \frac{T}{g} . \tag{4.15}$$

Now in convective conditions, the turbulence intensity is proportional to the convective scale w_* defined by Eq. (4.2). Substituting w_* for σ_w (letting c_f absorb the constant of proportionality) we obtain

$$(\overline{s_v'w'})_H = - c_F (\overline{s_v'w'})_o \tag{4.16}$$

which is Eq. (4.10) where $k=c_F$. This expression was first derived in this manner by Tennekes (1973). Zilitinkevich (1975) parameterized the local rate of change of turbulent kinetic energy in Eq. (4.13); however, an extensive study of this problem by Driedonks (1982) suggests it is unnecessary to take it into account. Driedonks recommends a low value for k of 0.2, whereas we have used the slightly higher value 0.25 in this study following Fitzjarrald and Garstang (1981b). The sensitivity of model results to the value of k will be examined.

Similar equations hold for the specific humidity as for the virtual static energy except the closure assumption is no longer valid. For specific humidity we have (assuming no evaporation)

$$\frac{dq_m}{dt} = \frac{F_{qo} - F_{qH}}{H} , \tag{4.17}$$

$$F_{qH} = - \Delta q \left(\frac{dH}{dt} - \bar{w}_H\right), \tag{4.18}$$

$$\frac{d\Delta q}{dt} = - \frac{F_{qH}\Gamma_q}{\Delta q} + \frac{F_{qH} - F_{qo}}{H} , \tag{4.19}$$

where q_m is the specific humidity in the mixed layer, F_{qo} and F_{qH} the fluxes of specific humidity at the surface and at the top of the mixed layer respectively, Γ_q the gradient and Δq the jump at H. Substituting (4.6) into (4.18) we find (neglecting diabatic heating)

$$F_{qH} = \frac{\Delta q}{\Delta s_v} F_{s_v H}, \tag{4.20}$$

and substituting this equation into (4.19) we obtain

$$\frac{d\Delta q}{dt} = - \frac{Fs_v H}{\Delta s_v} \left(\Gamma_q - \frac{\Delta q}{H}\right) - \frac{F_{qo}}{H} . \tag{4.21}$$

Garstang and Fitzjarrald (1981b) found that the ratio

$$R = \frac{F_{qH}}{F_{qo}} \tag{4.22}$$

is not constant in contrast to the ratio of the fluxes of virtual static energy. We can see from Eq. (4.17) that mixed layer drying requires F_{qH} to exceed F_{qo} ($R > 1$).

This model has a discontinuity in the thermodynamic variables at the top of the mixed layer, so that the transition layer is infinitesimal. In reality the transition layer has a finite depth of about 100 m. The height H when applied to the real atmosphere probably is best regarded as the distance from the surface to the middle of the transition layer rather than the mixed layer height. This view seems to be the one taken by Carson (1973) and Deardorff (1979). When the mixed layer height is large this distinction probably is not very important, however, since in the squall wake the transition layer is almost as large as the mixed layer in some regions, it could be significant. This has been the main motivation for also using the GSEM which allows for a realistic transition layer of finite depth.

5. GENERAL STRUCTURE ENTRAINMENT MODEL

Since Δs_v and Δq jumps are observed to occur over a significant vertical depth, models have been developed which attempt to include this, notably Betts (1974), and Deardorff (1978). These models are by necessity more complicated and there have not been very many comparisons of these models with observations. Due to the fact that the transition layer is a significant fraction of the depth of the mixed layer for the case being studied, Deardorff's GSEM has been used for comparison with the zero-order model.

The model is portrayed in Fig. 23. Instead of utilizing the height H where $\overline{w's'_v}$ is most negative, it utilizes the buoyancy flux crossover height h_1 where $\overline{w's'_v} = (\overline{w's'_v})_1 = 0$. In the transition layer $\bar{s}_v$ is written as

$$\bar{s}_v = s_{vm} + f(\underset{\sim}{x},t)\Delta s_v \tag{5.1}$$

where $f(\underset{\sim}{x}, t)$ is a dimensionless shape factor defined in this region with respective limits $0 \underset{\sim}{<} f \underset{\sim}{<} 1$.

The Reynolds averaged thermodynamic equation (neglecting diabatic heating)

$$\frac{d\bar{s}_v}{dt} = - \frac{\partial}{\partial z} \overline{w's'_v} \tag{5.2}$$

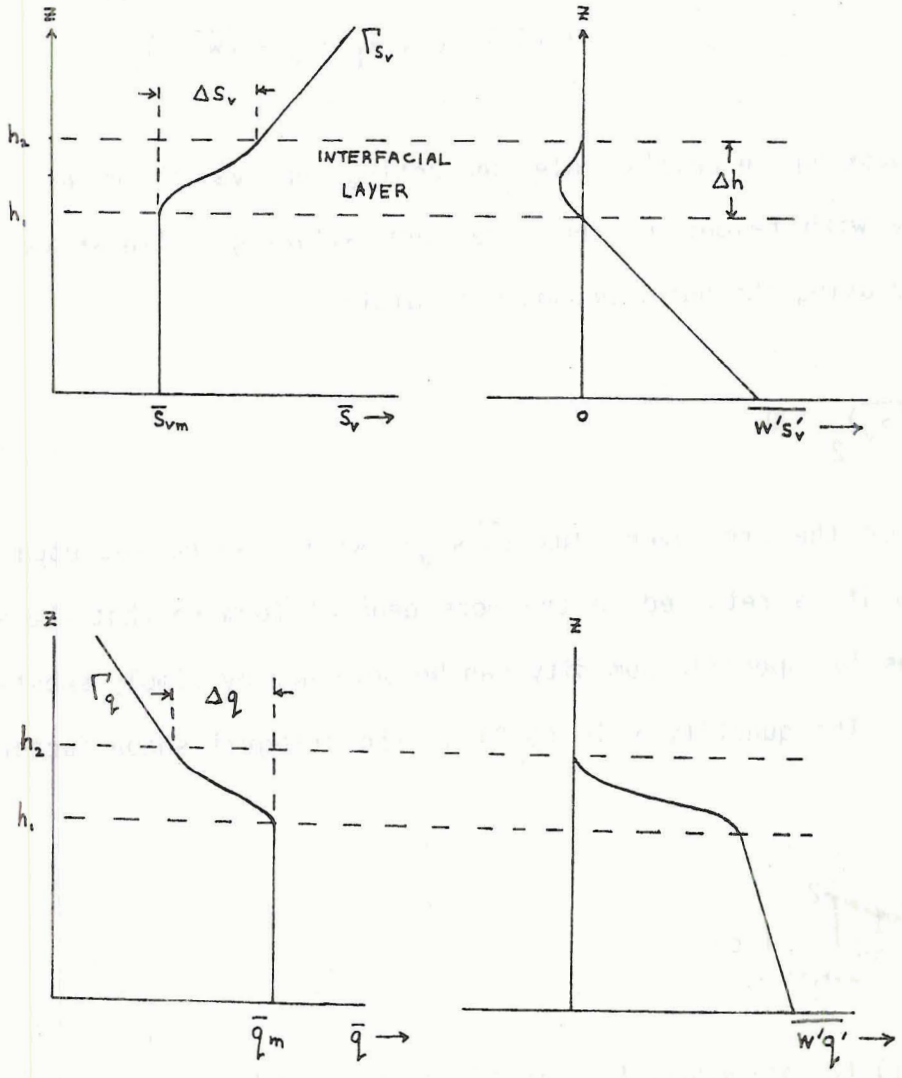

Fig. 23. Idealized profiles of mean virtual static energy $\bar{s}_v$, mean flux $\overline{w's'_v}$, mean specific humidity $\bar{q}$ and mean flux $\overline{w'q'}$ for the GSEM.

is integrated from h_1 to h_2 yielding

$$\frac{d}{dt}\int_{h_1}^{h_2} \bar{s}_v dz - \bar{s}_{v2}\frac{dh_2}{dt} + \bar{s}_{vm}\frac{dh_1}{dt} + \bar{w}_1 \Delta s_v + (1-Y)(\bar{w}_2-\bar{w}_1)\Delta s_v = (\overline{w's'_v})_1 \tag{5.3}$$

upon invoking Leibniz's rule neglecting any variation of horizontal velocity with height in the layer but allowing a linear variation of $\bar{w}(z)$ and using the outer boundary condition

$$(\overline{w's'_v})_2 = 0. \tag{5.4}$$

Later the crossover flux $(\overline{w's'_v})_1$ will also be set equal to zero (for now it is retained in the more general form so that the analogous equations for specific humidity can be obtained by simply substituting q for s_v). The quantity Y in (5.3) is the integral shape factor defined by

$$Y = \frac{1}{\Delta h}\int_{h_1}^{h_2} f\, dz. \tag{5.5}$$

From (4.1) the integral of $\bar{s}_v$ in (5.3) is given by

$$\int_{h_1}^{h_2} \bar{s}_v dz = \bar{s}_{vm}\Delta h + \Delta s_v \Delta h Y. \tag{5.6}$$

Substituting (5.6) into (5.3) performing the differentiation and re-

arranging terms we find

$$\Delta\bar{s}_v w_{el} = \alpha(\overline{w's_v'})_o - (1+\alpha)(\overline{w's_v'}) + Y\Delta h \frac{d\Delta s_v}{dt} - (1-Y)\Delta s_v \left(\frac{d\Delta h}{dt} - \Delta w\right) + \Delta s_v \Delta h \frac{dY}{dt} \tag{5.7}$$

where

$$w_{el} = \frac{dh_1}{dt} - \bar{w}_1, \tag{5.8}$$

$$\Delta w = \bar{w}_2 - \bar{w}_1, \tag{5.9}$$

$$\alpha = \left(\frac{h_2 - h_1}{h_1}\right), \tag{5.10}$$

and where the mixed-layer warming-rate equation

$$\frac{ds_{vm}}{dt} = \frac{(\overline{w's_v'})_o - (\overline{w's_v'})_1}{h_1} \tag{5.11}$$

has been used.

The equation for $d\Delta s_v/dt$ can be shown to be

$$\frac{d\Delta s_v}{dt} = \Gamma_{s_v}\left(w_{el} + \frac{d\Delta h}{dt} - \Delta w\right) - \frac{(\overline{w's_v'})_o - (\overline{w's_v'})_1}{h_1}. \tag{5.12}$$

Deardorff argues that the term dY/dt in (5.7) is negligible On substituting (5.12) into (5.7) and making this approximation, we obtain

$$(1-GY)\Delta s_v w_{el} = \alpha(1-Y)(\overline{w's_v'})_o - (1-\alpha-\alpha Y)(\overline{w's_v'})_1 - (1-Y-GY)\Delta s_v \left(\frac{d\Delta h}{dt} - \Delta w\right) \tag{5.13}$$

where

$$G = \frac{\Gamma_{s_v}(h_2-h_1)}{\Delta s_v} . \tag{5.14}$$

Invoking $(w's'_v)_1 = 0$, (5.13) becomes in dimensionless form

$$\frac{w_{el}}{w_*} = [\alpha(1-Y)R_*^{-1}-(1-Y-GY)(\frac{d\Delta h}{dt}-\Delta w)/w_*]/(1-GY) \tag{5.15}$$

where

$$w_* = [\frac{g}{s_v} h_1(\overline{w's'_v})_o]^{1/3} \tag{5.16}$$

is the convective velocity scale, and

$$R_* = \frac{g}{s_v} \frac{\Delta s_v h_1}{(w_*)^2}. \tag{5.17}$$

Deardorff suggests the following approximation for the integral shape factor

$$Y = 0.55 \exp(-0.27G). \tag{5.18}$$

He also hypothesizes the following growth equation for Δh

$$\frac{d\Delta h}{dt} = \Delta w + w_* Q \alpha R_*^{-1} \tag{5.19}$$

where

$$Q = (Q_1-Q_3)(1-GY)/Y, \tag{5.20}$$

$$Q_3 = (1 - Y)/(1 - GY), \tag{5.21}$$

$$Q_1 = Q_3^{0.4}. \tag{5.22}$$

It should be noted that in Deardorff (1979) this equation was only tested with laboratory experiments for the case of no subsidence, i.e. for $\Delta w = 0$.

To obtain the equations for specific humidity q is substituted for s_v in equations (5.11), (5.12), (5.13) and (5.14). In the case of specific himidity the flux at h_1 is in general not equal to zero as it is for the flux of virtual static energy. The same integral shape factor Y will be assumed for the specific humidity as for the virtual static energy.

6. NUMERICAL PROCEDURE

Both models have prediction equations for H, s_{vm}, Δs_v, q_m and Δq, the equations (4.6), (4.9), (4.11), (4.17) and (4.19) respectively, for the zero-order model, and the equations (5.8), (5.11), (5.12) and the appropriate equations for q_m and Δq, respectively, for the GSEM. These equations can be solved once we have specified from observations the initial values of these quantities and the fields of $\underline{v}_r$, $\bar{w}_H$, $F_{s_v o}$, Γ_{s_v}, F_{qo} and Γ_q. (Here $\underline{v}_r$ is the wind velocity relative to the squall line and is necessary to obtain the substantial derivative as will now be described).

The method used to solve these equations is similar to that used by Schubert et al. (1979), in that the equations are formulated in the natural coordinate system. However, we also transfer to a coordinate system moving with the squall line which is assumed to be in the steady state and moving at 13.5 m s^{-1} in a fixed direction. Relative to the squall line the air in the mixed layer moves towards the rear of the system (except perhaps right at the gust front). To determine the relative streamlines and isotachs the mean velocity in the mixed layer was estimated by averaging the wind speed between the surface and the top of the mixed layer. The velocity at the top of the mixed layer was estimated by linearly interpolating (or extrapolating) between the surface and 970 mb using the composite analyses of the wind fields at these levels and of the mixed layer height, i.e. for the x-component

(eastward) of velocity

$$v_x(H) = (1-\frac{H}{375\ m})\ v_x(sfc) + \frac{H}{375\ m} \cdot v_x(375\ m) \tag{6.1}$$

and similarly for the y (northerly) component. The average velocity of the squall line was then subtracted from the mean velocity field of the mixed layer to obtain the relative streamlines and isotachs shown in Fig. 24. (These are mean mixed layer streamlines). The procedure is then to numerically integrate the equations along each streamline once initial values of the variables have been specified.

For the zero-order model the equations in natural coordinates relative to the squall line are (neglecting diabatic heating):

$$v_r \frac{\partial H}{\partial x} = \bar{w}_H - \frac{F_{s_v H}}{\Delta s_v} \tag{6.2}$$

$$v_r \frac{\partial \bar{s}_{vm}}{\partial x} = \frac{F_{s_v o} - F_{s_v H}}{H}, \tag{6.3}$$

$$v_r \frac{\partial \Delta s_v}{\partial x} = - \Gamma_{s_v} \frac{F_{s_v H}}{\Delta s_v} + \frac{F_{s_v H} - F_{s_v o}}{H}, \tag{6.4}$$

$$v_r \frac{\partial \bar{q}_m}{\partial x} = \frac{F_{qo} - F_{qH}}{H}, \tag{6.5}$$

$$v_r \frac{\partial \Delta q}{\partial x} = - \frac{F_{s_v H}}{\Delta s_v} (\Gamma_q - \frac{\Delta q}{H}) - \frac{F_{qo}}{H}, \tag{6.6}$$

where

$$F_{s_v H} = - 0.25\ F_{s_v o},$$

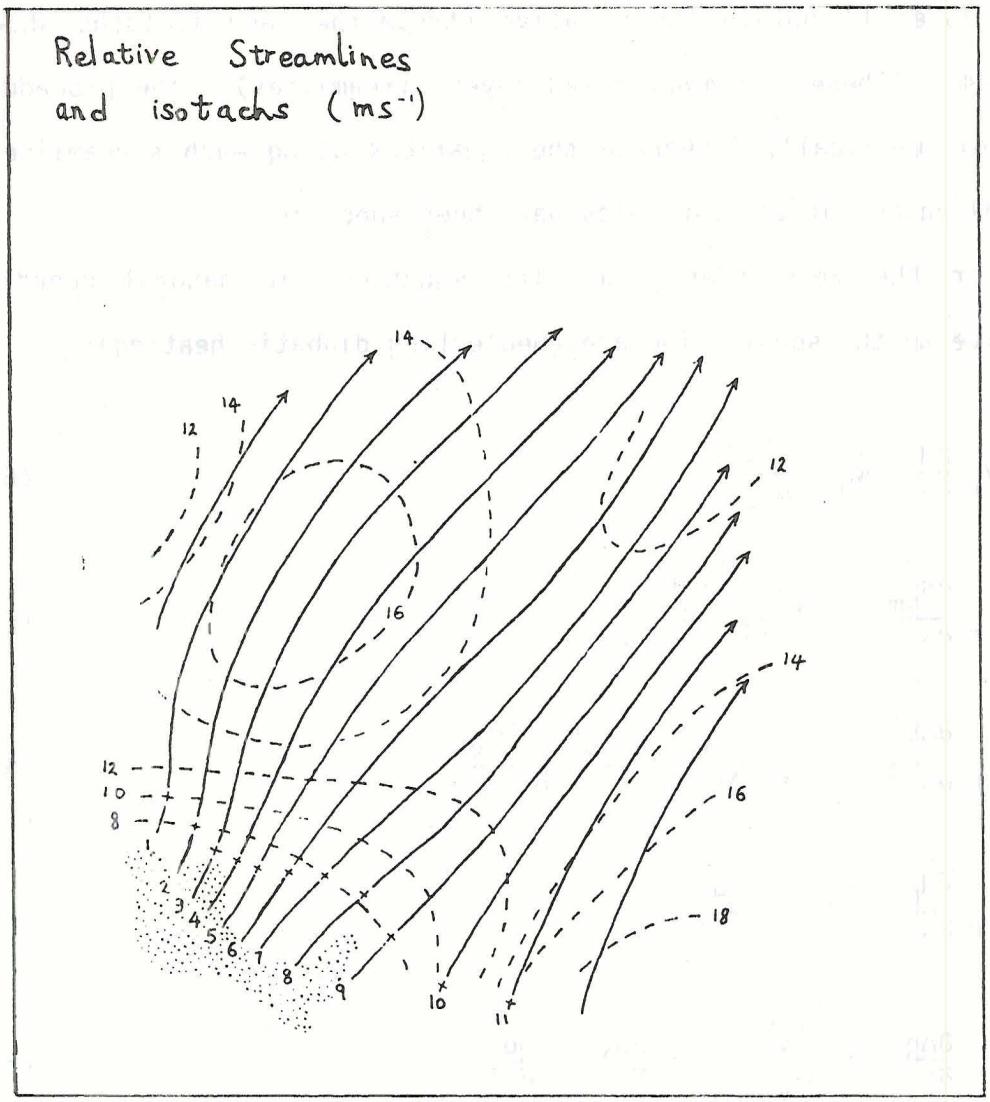

Fig. 24. Relative mixed layer streamlines (solid lines) and isotachs (dashed lines).

$$F_{qH} = \frac{\Delta q F_{qo}}{\Delta s_v},$$

v_r is the wind speed relative to the squall line and x is now the distance along a streamline. The equations for H and ΔS_v were solved using the Runge-Kutta fourth-order method. The integrations are performed along the eleven streamlines shown in Fig. 24 with the values of surface fluxes, vertical velocity, horizontal velocity and lapse rates being specified from the observed values at 30 km intervals. The space differencing used was 1 km; a cubic spline routine was used to interpolate between the 30 km increments.

Following Deardorff (1978), the GSEM equations are solved by forward differencing. The predictive equations for $\bar{S}_{vm}$, ΔS_v, h_1, Δh, q_m and Δq, written in finite difference form in natural coordinates relative to the squall line are:

$$\bar{s}_{vm}^{i+1} = \bar{s}_{vm}^{i} + \frac{\Delta x}{v_r^i} \frac{F_{s_v o}^{i}}{h_1^i}, \tag{6.7}$$

$$\Delta s_v^{i+1} = \Delta s_v^i + \frac{\Delta x}{v_r^i} \Gamma_{s_v}^i (w_{el} + \frac{d\Delta h}{dt} - \Delta w) - \frac{\Delta x}{v_r^i} \frac{F_{s_v o}^{i}}{h_1^i}, \tag{6.8}$$

$$h_1^{i+1} = h_1^i + \frac{\Delta x}{v_r^i} (w_{el}^i + \bar{w}_1^i), \tag{6.9}$$

where

$$w_{eo}^i = w_*^i \left[\alpha(1-Y)R_*^{-1} - (1-Y-GY)(v_r \frac{\partial \Delta h}{\partial x} - \Delta w)\frac{1}{w_*}\right]^i \frac{1}{(1-GY)^i}, \tag{6.10}$$

$$\Delta h^{i+1} = \Delta h^i + \frac{\Delta w}{v_r^i} (\Delta w + w_* Q \alpha R_*^{-1})^i, \tag{6.11}$$

$$q_m^{i+1} = q_m^i + \frac{\Delta x}{v_r^i} \frac{(F_{qo}^i - F_{ql}^i)}{h_1^i} , \tag{6.12}$$

where

$$F_{ql}^i = \frac{1}{(1+\alpha-\alpha Y)^i} \{ - (1-G_q Y)\Delta q w_{eo} + \alpha(1-Y)F_{qo}^i - (1-Y-G_q Y)\Delta q \left(\frac{d\Delta h}{dt} - \Delta w\right)\}, \tag{6.13}$$

$$\Delta q^{i+1} = \Delta q^i + \frac{\Delta x}{v_r^i} \Gamma_q^i \left(w_{el} + \frac{d\Delta h}{dt} - \Delta w\right)^i - \frac{\Delta x}{v_r^i} \frac{F_{qo}^i - F_{ql}^i)}{h_1^i} . \tag{6.14}$$

7. RESULTS

7.a Results of the Zero-Order and GSEM with and without Diabatic Heating

A previous study of the mixed layer recovery following the passage of the 12 September squall line has been made by Fitzgerrald and Garstang (1981b). The detailed composite analysis described in Chapter 2 has made possible a far more quantitative study, in which the fully three dimensional mixed layer structure can be examined.

The approach taken here is to specify the surface fluxes from observations allowing no feedback of predicted mixed layer temperature and specific humidities on the fluxes (see Equations 2.1, 2.2 and 2.3). The reason for not using a fully interactive model in which sea surface fluxes are predicted is that they would depend on composite fields of all the quantities that go into the model (in addition we would need a composite analysis of sea surface temperature) whereas, it seems more reasonable to use locally observed data to determine fluxes.

The vertical velocity field shown in Fig. 6 gives values at 375 m above the surface. It is necessary to interpolate (or extrapolate) from this height to the top of the mixed layer and the following formula has been used

$$w(z) = \frac{w(375\ m)}{0.6}\ (1-e^{-z/409\ m}), \qquad (7.1)$$

Fig. 25 shows the profile of vertical velocity given by this formula for the case when $w(375\ m) = -0.03\ ms^{-1}$. It gives a similar profile to that found by Gamache and Houze (1982a) for the anvil downdraft below 1 km (see their Fig. 13). As previously discussed in Chapter 3, a linear interpolation below 375 m probably underestimates slightly the magnitude of the vertical velocity and Eq. (7.1) is likely to be more realistic. Furthermore the development of the dry static energy and specific humidity profiles will be looked at in more detail, and for this a linear extrapolation between the surface and 375 metres to heights slightly above 1 km would give much larger vertical velocities than could reasonably be expected.

The initial starting points for the model integrations are shown by the crosses in Fig. 24 which lie just outside the scalloped region in Fig. 3, which is an estimate of the extent of the very cool, stable boundary layer following the squall where mixed layers are extremely small. The initial values used for the zero-order model were H = 150 m, $\Delta S_v = 0.4\ J\ g^{-1}$ and $\Delta q = -0.7\ g\ kg^{-1}$ (the jump in dry static energy for this case is $\Delta S \sim 0.52\ J\ g^{-1}$) for streamlines 1-9, H(10) = 230 m and H(11) = 360 m. Initial values of virtual static energy and specific humidity were determined from the composite analyses, Fig. 8 and Fig. 9. There is some uncertainty in the initial values of ΔS_v and Δq that should be used; however, results do not seem too sensitive to reasonable variations of these quantities (e.g., Tennekes, 1973: Johnson, 1981).

Fig. 26 shows model results for the mixed layer depth using the zero-order jump model. Fairly good agreement is found with the composite analysis shown in Fig. 3 although mixed layer recovery is slower than observed on the north side of the wake. (note that the zero-order

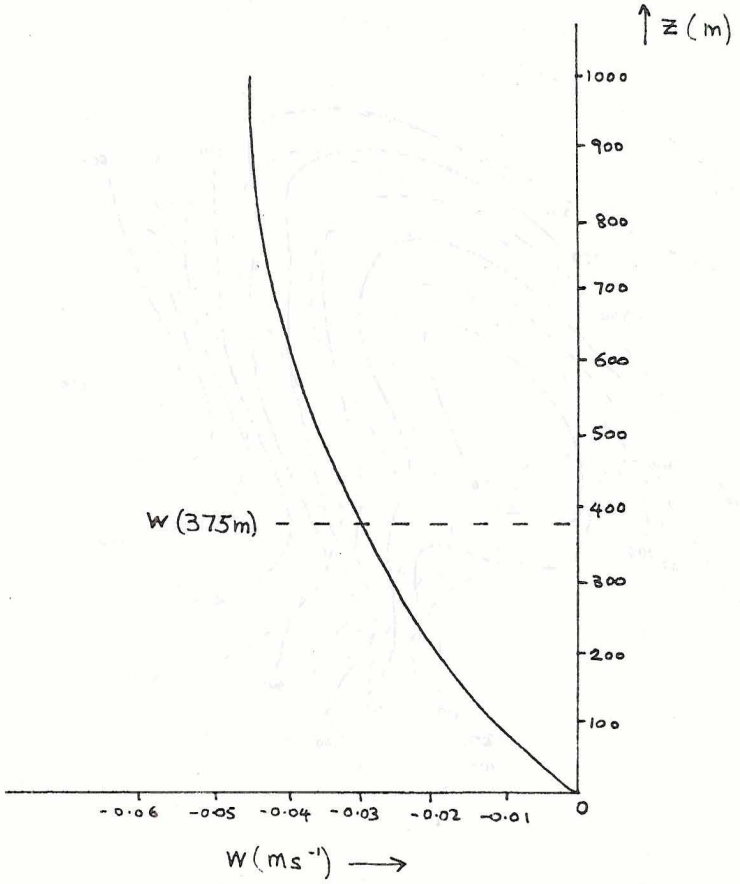

Fig. 25. Profile of vertical velocity given by Eq. (7.1) for the case $w(375\ m) = -0.03\ m\ s^{-1}$.

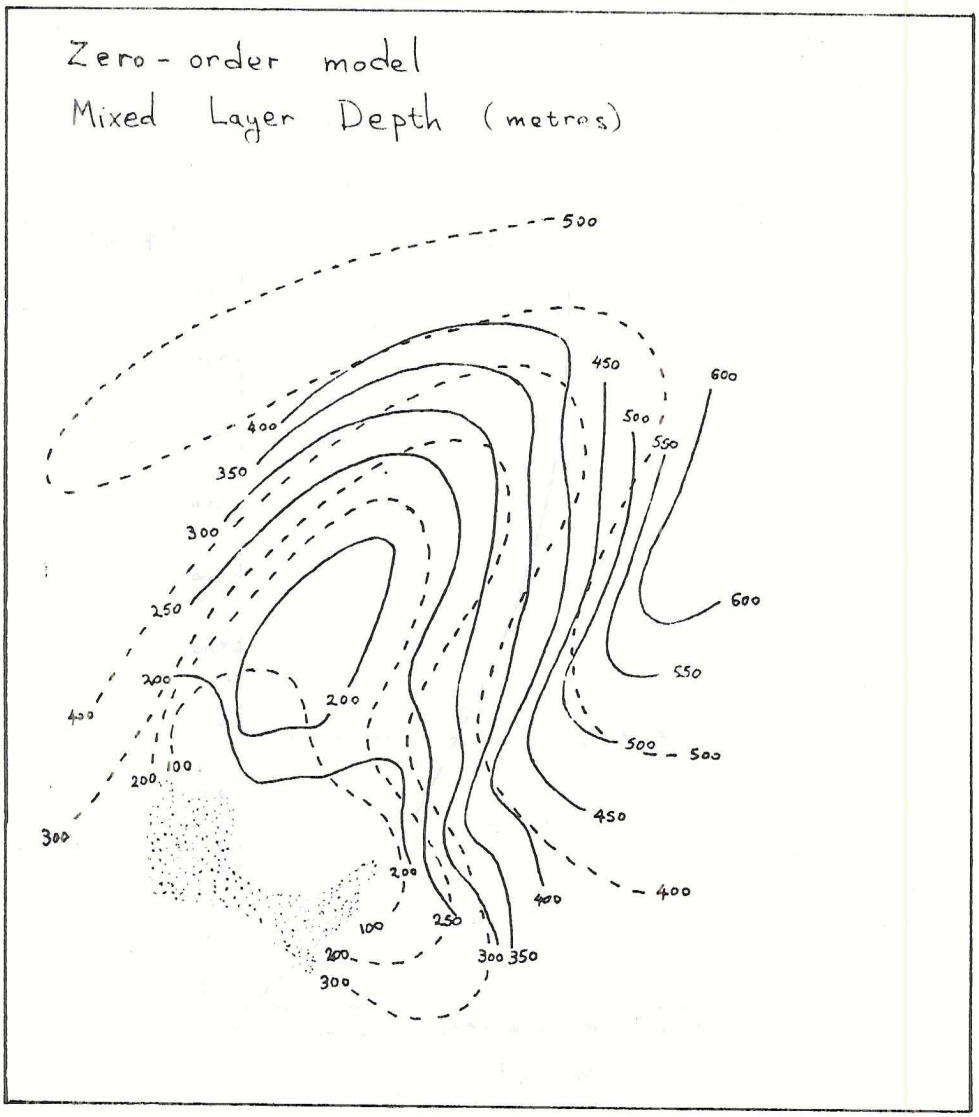

Fig. 26. Mixed layer depth (m) predicted by the zero-order jump model (solid lines). Dashed lines show observed values.

mixed layer depth should be regarded as the height of the middle of the transition layer, about 50 meters greater than the actual mixed layer depth). Figs. 27 and 28 show the model results for the mixed layer specific humidity, and surface temperature (note $T = s/C_p$ at the surface) respectively, for the case of no diabatic heating. The positioning of the minimum in q is in good agreement with observations although recovery towards the rear of the system is too slow. There is a strong gradient of q on the east side of the system, however, observations are very sparse in this region and no meaningful comparison can be made (of course the field variables used in the model are also somewhat uncertain in this part of the squall system). The model predicts rates of surface temperature increases significantly higher than observations indicate on the north side of the wake, a region where there is fairly good sounding data.

It is possible that rainfall evaporation and diabatic heating is partly responsible for the discrepancy between the observed and predicted specific humidity and surface temperatures. The predicted m.l. depth is not so sensitive to neglect of diabatic heating (later). To obtain an estimate of the importance of rainfall evaporation we use the formula developed by Manton and Cotton (1977); the rate of evaporation is given by

$$E = \{0.5R_m^{-2}\rho_w^{-1} + 124\, R_m^{-5/4}\, (\rho_o^{1/2}\, T^{-0.745})^{1/2}\}ss_l G(T,p)\bar{r}_r \qquad (7.2)$$

where $G(T,P) = \dfrac{1}{\dfrac{m_w L^2}{kR_* T^2} + \dfrac{R_* T}{e_s(T) D m_w}}$

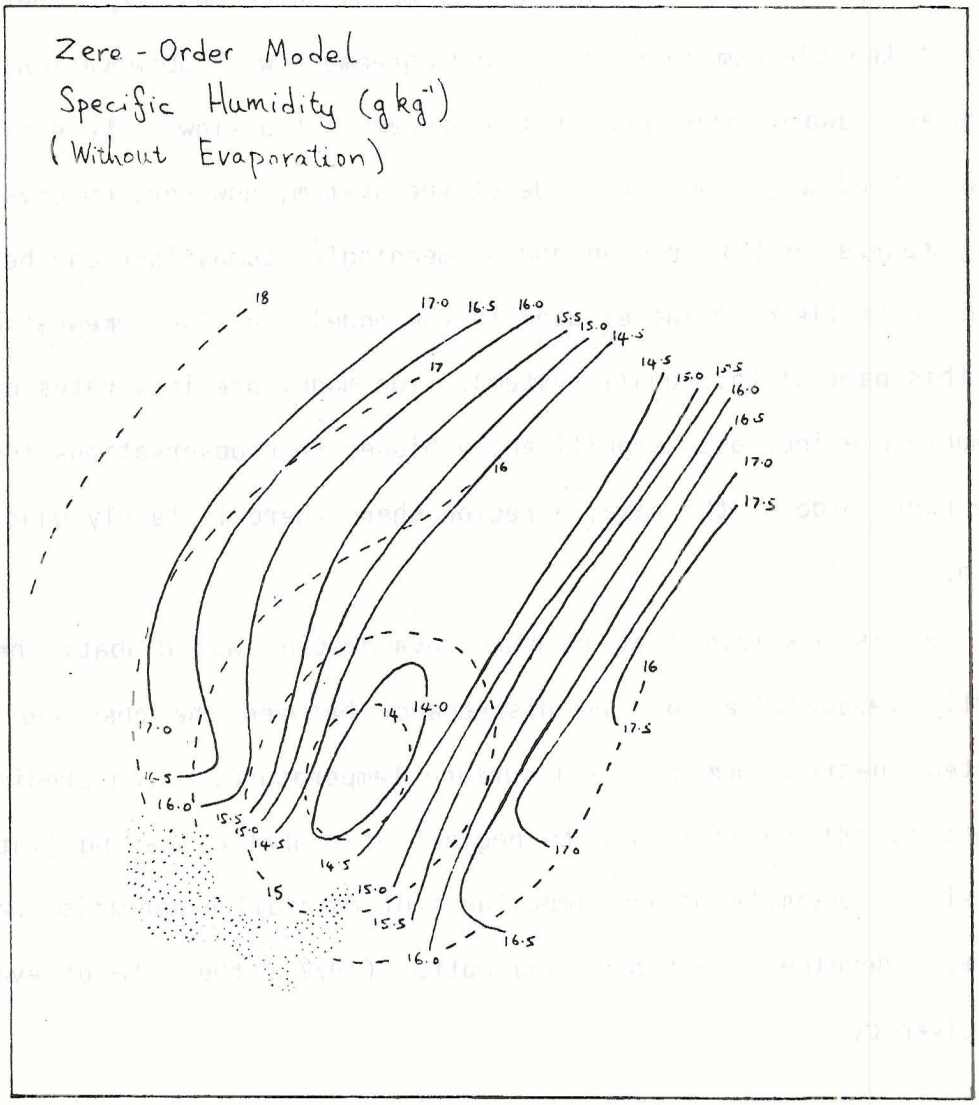

Fig. 27. Mixed layer specific humidity (g kg^{-1}) predicted by the zero-order jump model without evaporation (solid lines). Dashed lines show observed values.

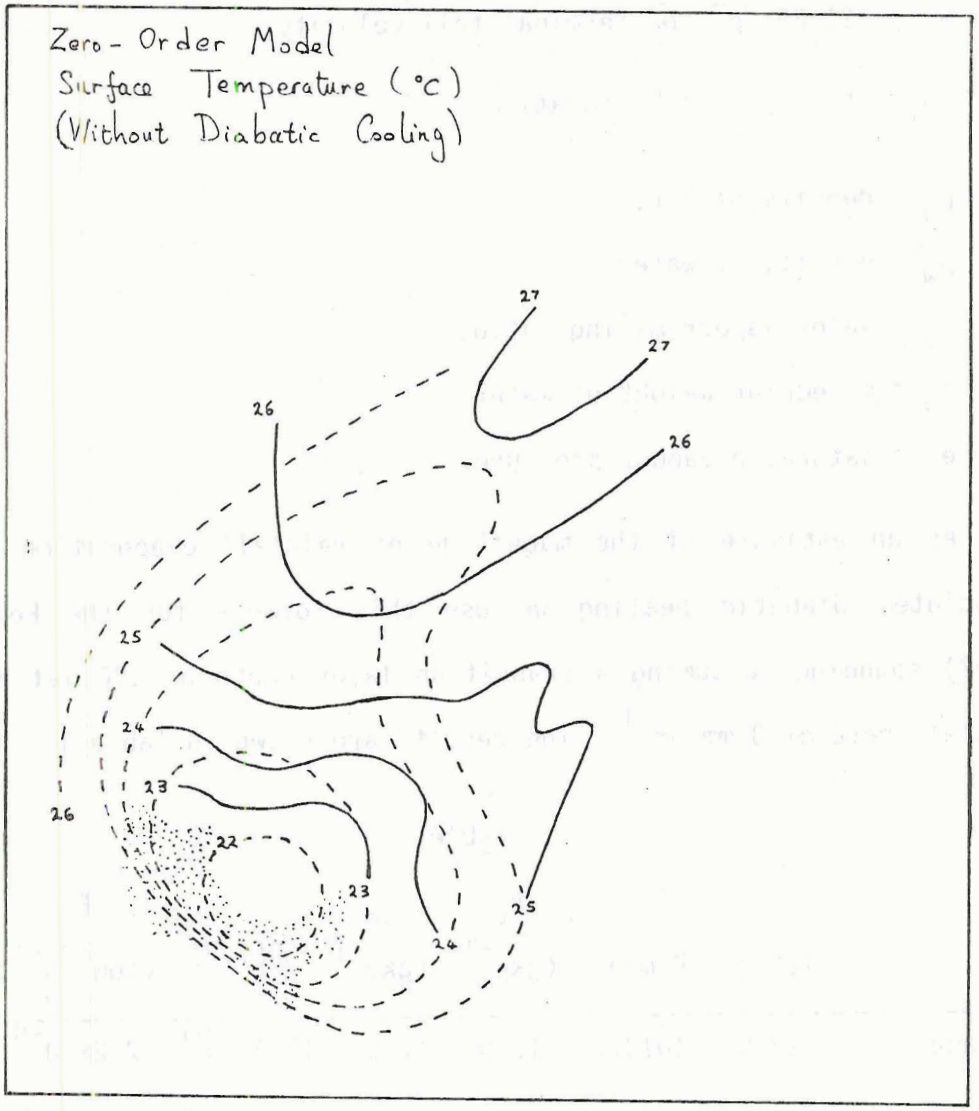

Fig. 28. Mixed layer surface temperature (°C) predicted by the zero-order jump model without diabatic heating (solid lines). Dashed lines show observed values.

$k \equiv$ molecular diffusivity of heat,

$D \equiv$ molecular diffusivity of water vapour,

$R_m \equiv$ characteristic raindrop radius, (taken to be 0.027 cm)

$r_r \equiv \rho_r/\rho_o$ mixing ratio of rain,

$r_r \rho_o v_T \equiv$ rainfall rate,

$v_T \equiv -21.26/\sqrt{\rho_o}$ the terminal fall velocity,

$ss_\iota \equiv (1 - \frac{r_v}{r_{vs}})$ subsaturation,

$\rho_o \equiv$ density of air,

$\rho_w \equiv$ density of water,

$r_v =$ water vapour mixing ratio,

$m_w =$ molecular weight of water,

$e_s =$ saturated vapour pressure.

As an estimate of the magnitude of rainfall evaporation and the associated diabatic heating we use this formula for the Researcher (1902) sounding, assuming a transition layer depth of 100 metres and a rainfall rate of 3 mm hr^{-1}. The results are shown in Table 1.

Table 1

	T(°C)	P(mb)	r_v (gkg^{-1})	r_{vs} (gkg^{-1})	$G(T_1P)$	E ($kgm^{-3}s^{-1}$)	LE (Wm^{-3})
surface	23.0	1010.7	15.0	17.8	1.23×10^{-6}	2.2×10^{-8}	0.055
mixed layer top	22.2	1000.0	15.0	17.2	1.22×10^{-6}	1.8×10^{-8}	0.045
transition layer top	22.0	989.0	14.2	17.1	1.20×10^{-6}	2.3×10^{-8}	0.059

The heating rate of about -0.05 Wm^{-3} is somewhat larger than would be expected due to radiation (for comparison a radiational heating rate of -2 K day^{-1} gives -0.03 Wm^{-3}).

Fig. 29 shows the rainfall rates from the anvil as composited by Gamache and Houze (1982). They obtained an average rainfall rate of 2.7 mm hr^{-1} over the whole anvil although in some regions it can be seen to be significantly larger. We use the observed rainfall rates from their analysis but for simplicity hold all other variables constant in Eq. (7.2). The following values have been used r_v = 15 g kg^{-1}, r_{vs} = 17.5 g kg^{-1} and T = 22.6°C, which are mean values for the Researcher (1902) sounding in the mixed layer (which is incidentally the only sounding we have in the region of significant rainfall). We shall only add a diabatic heating and moisture source term to the right hand sides of Eqs. (6.3) and (6.5), respectively, and show later in section 7.c that this is a good approximation to make. A constant radiational heating rate of -2 K day^{-1} (Johnson, 1980) is also included in the diabatic heating term. The inclusion of the moisture source and diabatic heating terms results in the specific humidity and surface temperature fields shown in Fig. 30 and Fig. 31, respectively. Fig. 30 is similar to Fig. 27 except that specific humidity increases slightly more rapidly in the region where evaporation in the mixed layer is occurring as would be expected. However, predicted specific humidities still do not increase towards the rear of the squall system as rapidly as observations indicate. Comparison of Fig. 28 and Fig. 31 shows that evaporation in the mixed layer is apparently important for sustaining the cool region in the wake of the squall line. Although quantitative agreement between the observed temperature field and predicted is by no means perfect, the results are encouraging.

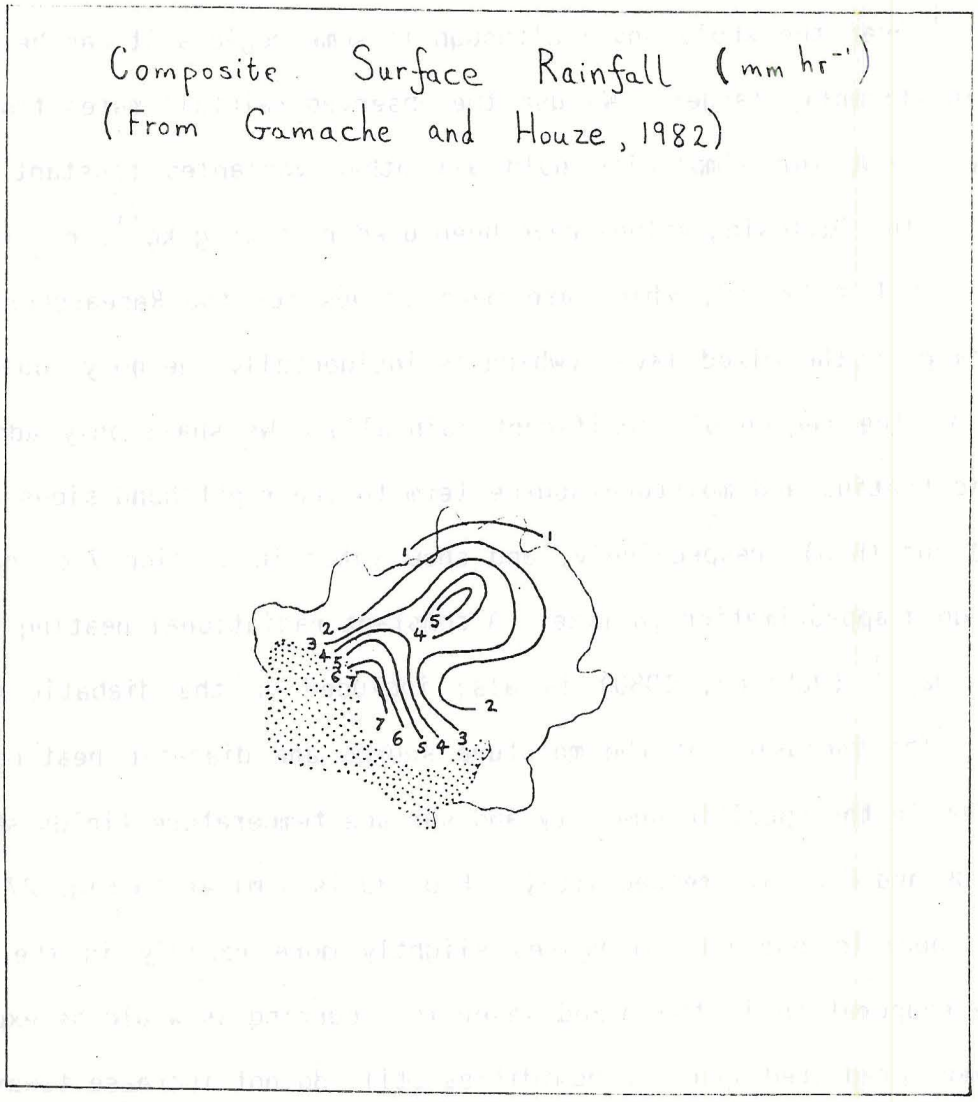

Fig. 29. Composite surface rainfall (mm hr^{-1}). (redrafted from Gamache and Houze, 1982 b).

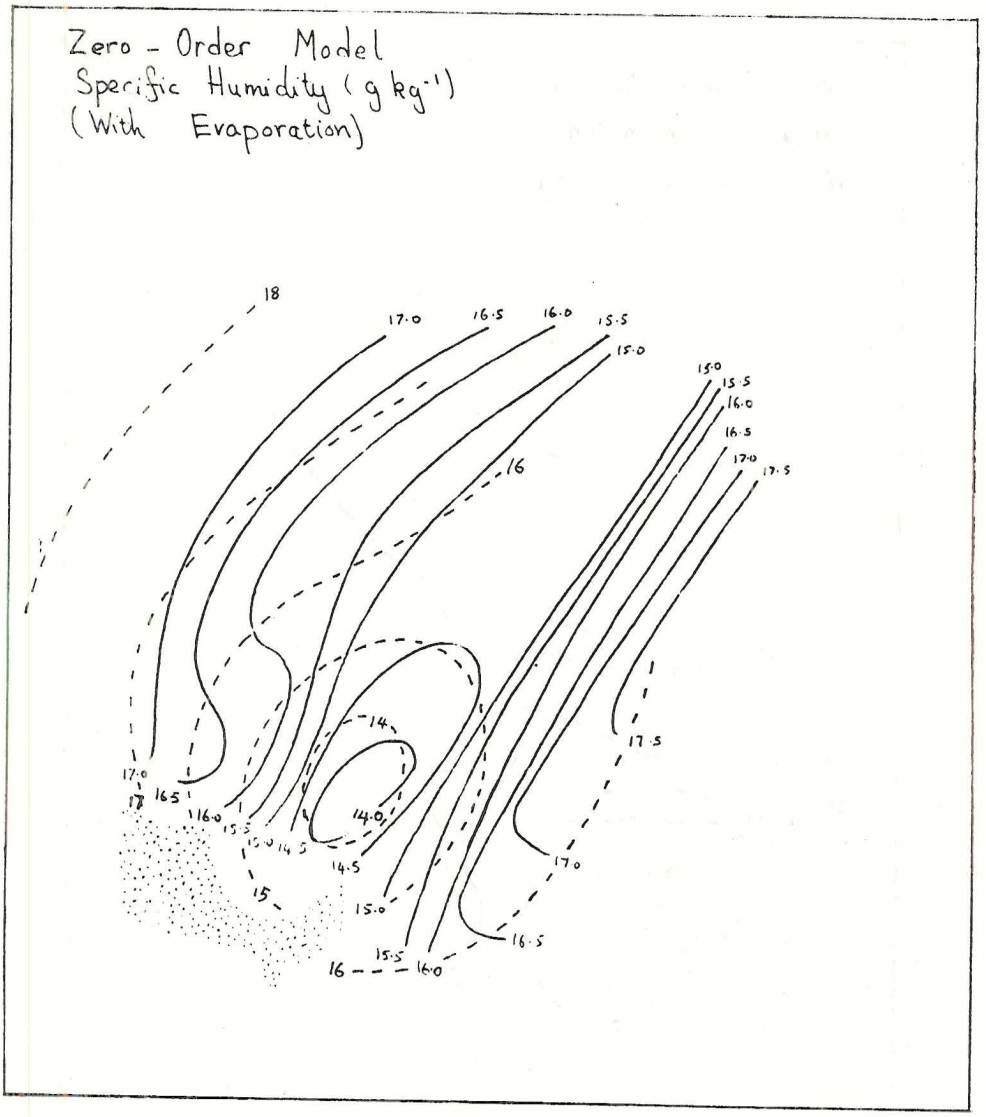

Fig. 30. Mixed layer specific humidity (g kg^{-1}) predicted by the zero-order jump model with evaporation (solid lines). Dashed lines show observed values.

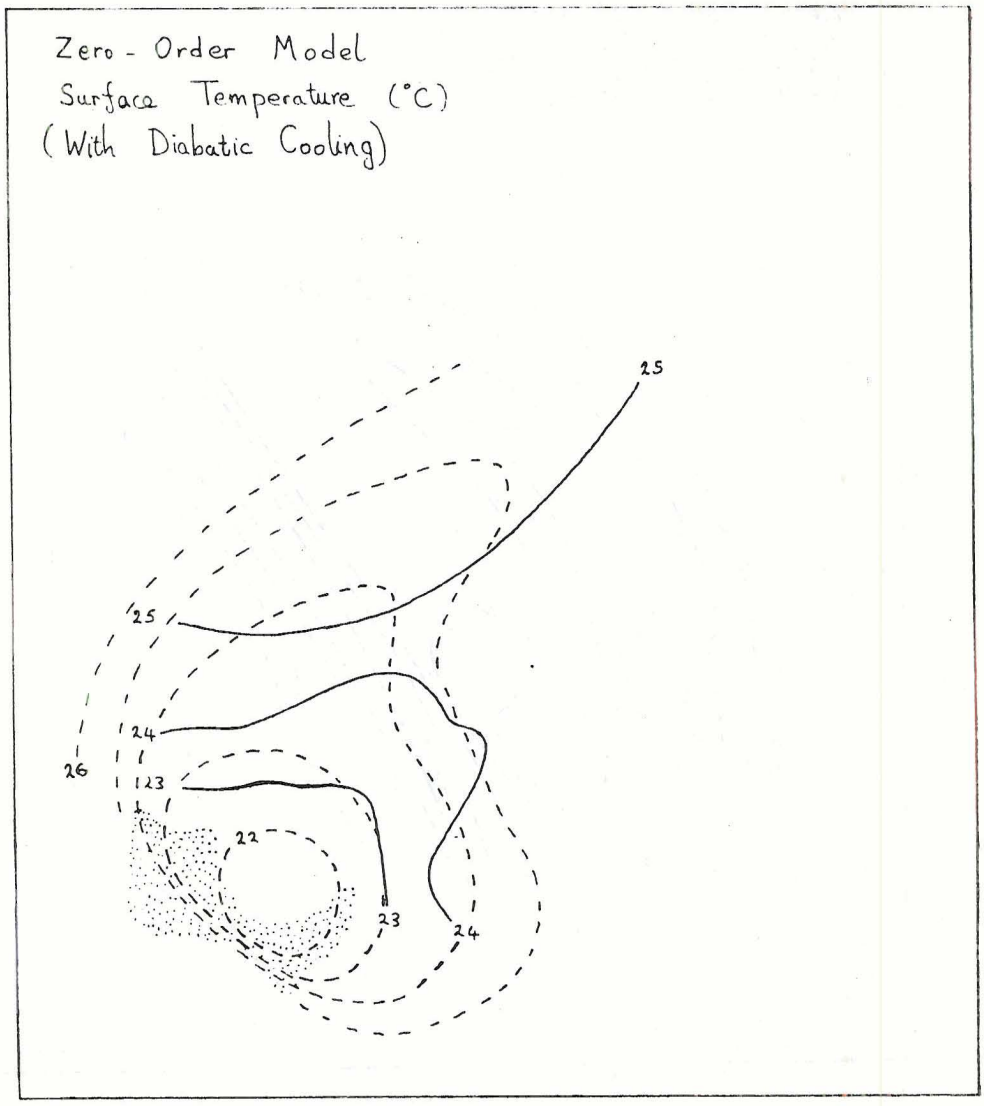

Fig. 31. Mixed layer surface temperature (°C) predicted by the zero-order jump model with diabatic heating (solid lines). Dashed lines show observed values.

Fig. 32 shows predicted quantities along streamline 5. The final value of specific humidity with evaporation occuring in the mixed layer is about 0.3 g kg^{-1} larger than that for no evaporation but still less than observed. The difference in static energy is quite large, about 1.5 J g^{-1} less when diabatic heating is included and in good agreement with observed values. Mixed layer height shows a slight increase initially and decreases to a minimum in the region of maximum downward vertical velocity; mixed layer heights to the rear of the system are slightly underpredicted. The entrainment rate, defined by

$$w_{en} = \frac{dH}{dt} - \bar{w}_H \tag{7.3}$$

is large at the beginning of the integration. It quickly reaches a relative minimum which is due to the small buoyancy flux associated with low wind speeds in the center of surface diffluence; see Fig. 4. R, the ratio of the moisture flux at H to that at the surface rapidly increases to values greater than one which is coincident with drying in the mixed layer. Values of Δq and Δs seem fairly realistic. Δq increases to values greater than -4 g kg^{-1} which compares favorably to the sounding at Q(1823), although Δs is somewhat underestimated at about 1.3 J g^{-1} compared to about 2 J g^{-1}.

A difficulty has been encountered with the GSEM. Use of the rate equation for Δh as suggested by Deardorff leads to much smaller transition layer depths (as small as 22 m) than seem feasable, see Fig. 33. (This shows an integration along streamline 4). As noted earlier, Deardorff's experiments did not include subsidence. Results obtained simply by omitting the Δw term in Eq. (5.19) are also shown. The transition layer grows from an initial value of 80 m to about 110 m. Δs is

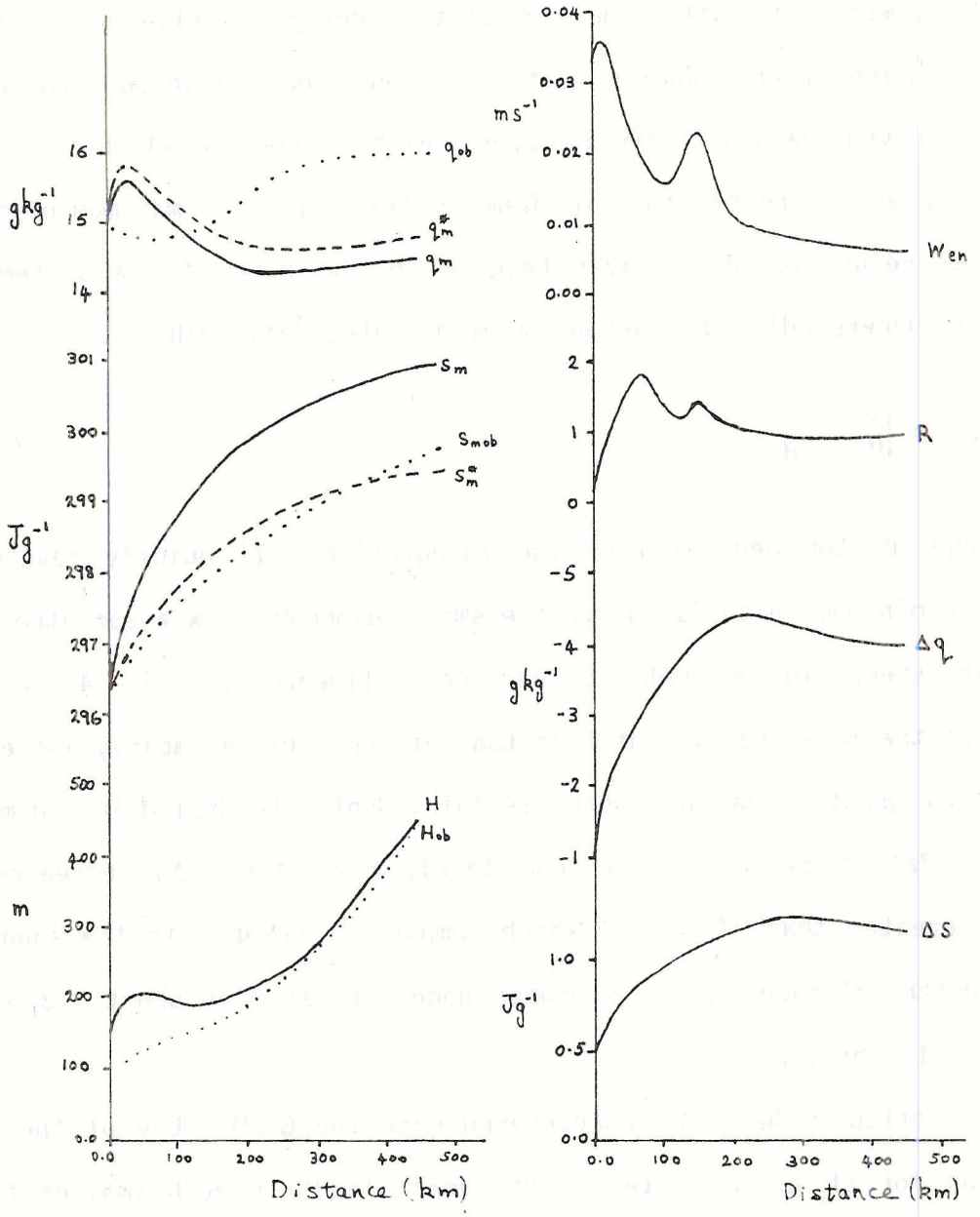

Fig. 32. Zero-order jump model predicted values for q_m, s_m, H, w_{en}, R, Δq and Δs. Solid lines are for no evaporation or diabatic heating. Dashed lines are when evaporation and diabatic heating are included (q_m^* and s_m^*). Dotted lines show observed values (q_{ob}, s_{mob}, H_{ob}).

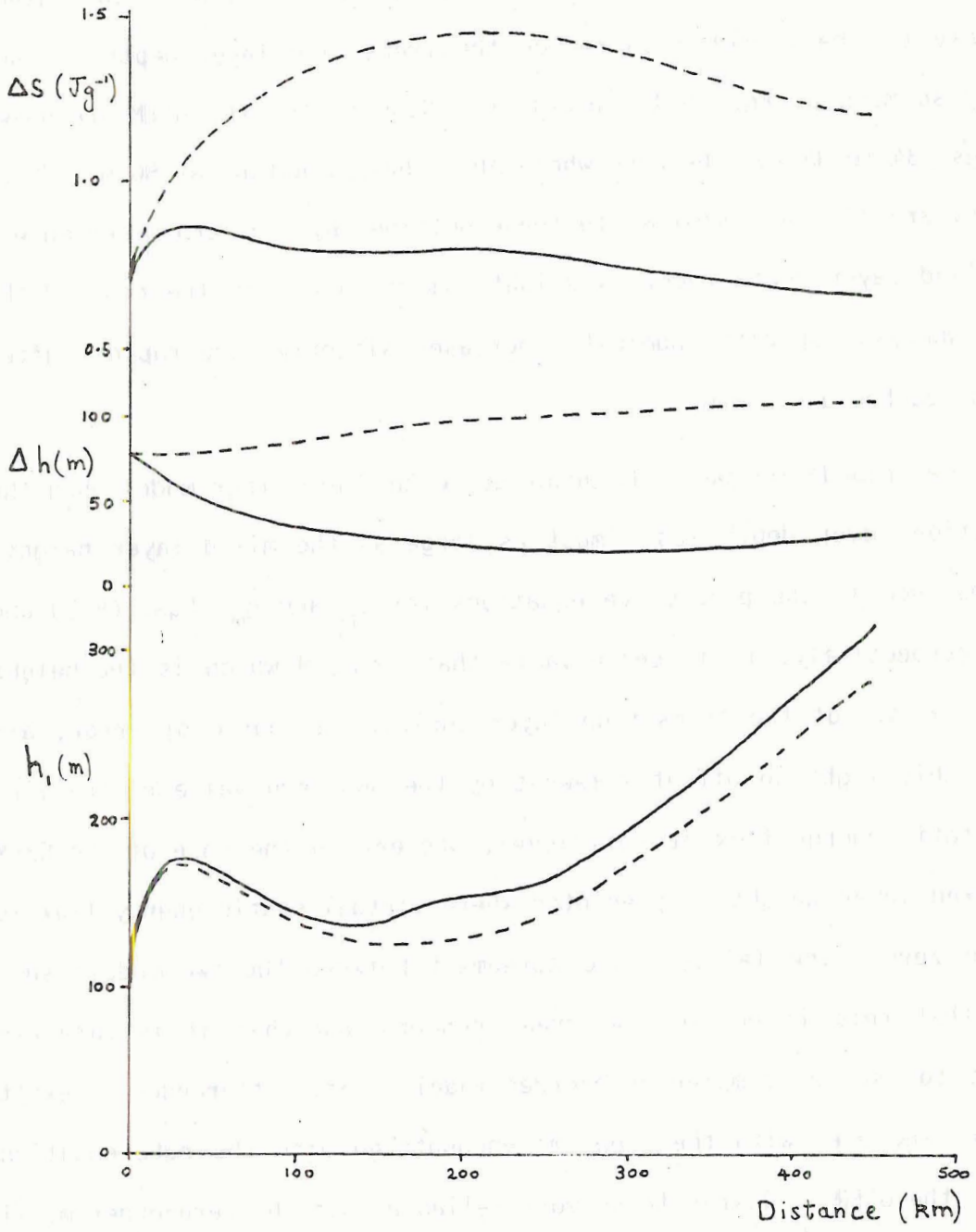

Fig. 33. Comparison of the unmodified rate equation for Δh (solid lines) with the equation when Δw is ommitted (dashed lines).

significantly different; however, it can be seen that the mixed layer depth is relatively insensitive to the variation in Δh. Subsidence probably can be expected to reduce the transition layer depth but not nearly so much as Eq. (5.19) predicts. Results for the GSEM are shown in Figs. 34 to 38 for the case where Δh is held constant at 80 m. These results are all very similar to these obtained by the zero-order model. The mixed layer depth recovers slightly more slowly in the case of the GSEM, whereas, specific humidity increases slightly more rapidly after it has reached a minimum.

Some trepadation was felt about using the zero-order model when the transition layer depth was almost as large as the mixed layer height. For instance in the predictive equations for $\bar{s}_m$ and $\bar{q}_m$, Eqs. (6.3) and (6.5) respectively, it is conceivable that using H which is the height to the middle of the transition layer could be a source of error; although this might be offset somewhat by the non-zero value of the virtual static energy flux at this level, whereas in the case of the GSEM the mixed layer height is predicted where virtual static energy flux is assumed zero. The fairly close agreement between the two models suggests that this is not of too great concern and that it is more expedient to use the simpler zero-order model. Some differences do exist however, and even with the problems encountered with the rate equation for Δh, the GSEM is likely to be more reliable than the zero-order model as long as the assumption that mixed layer turbulence is dominated by buoyant production is correct.

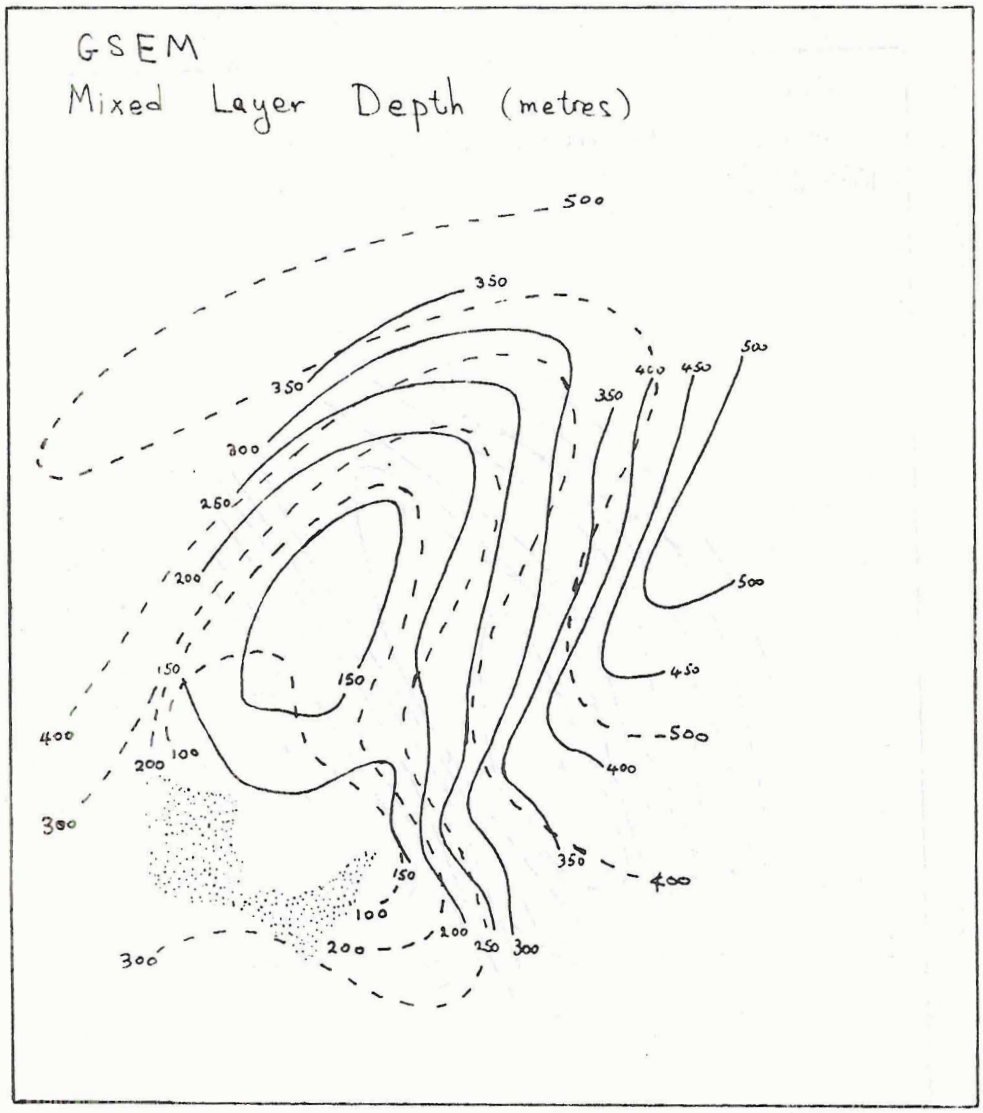

Fig. 34. Mixed layer depth (m) predicted by the GSEM (solid lines). Dashed lines show observed values.

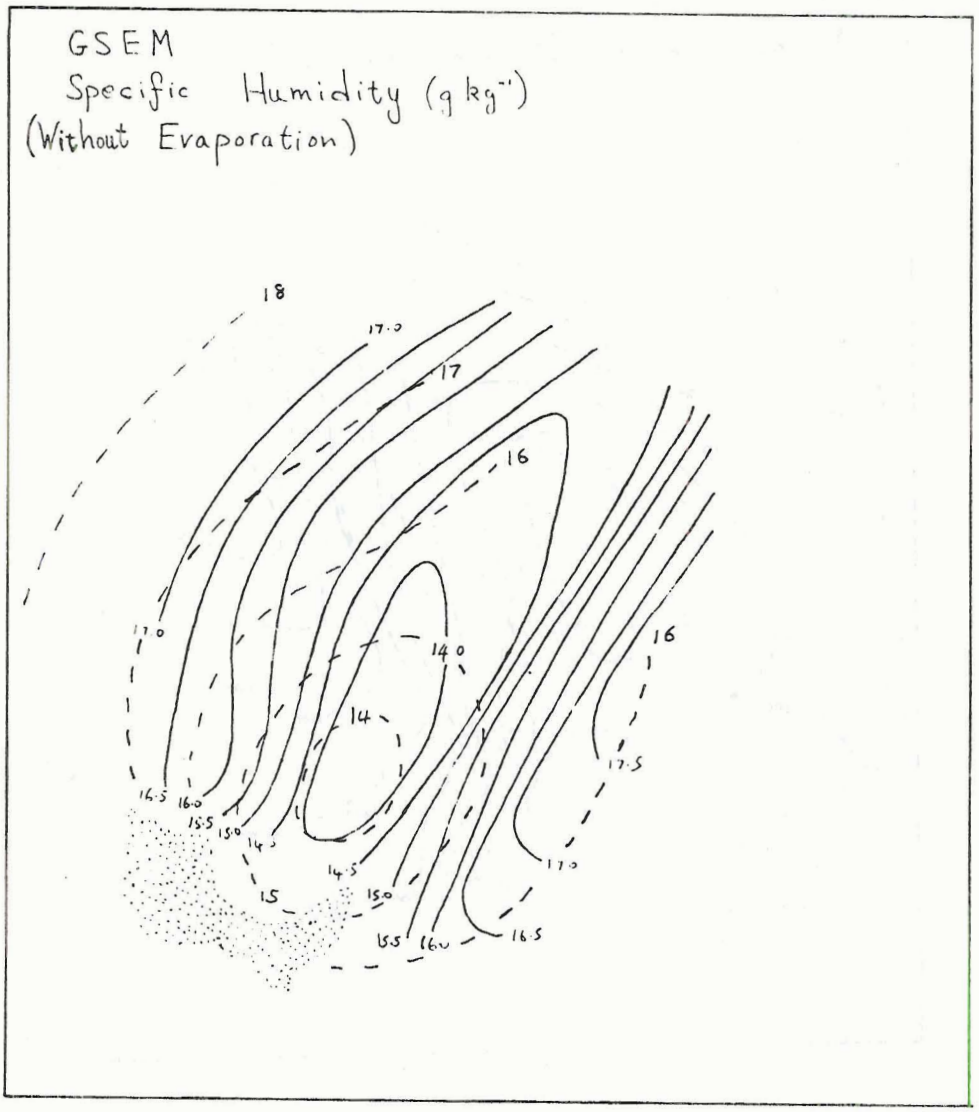

Fig. 35. Mixed layer specific humidity (g kg^{-1}) predicted by the GSEM without evaporation (solid lines). Dashed lines show observed values.

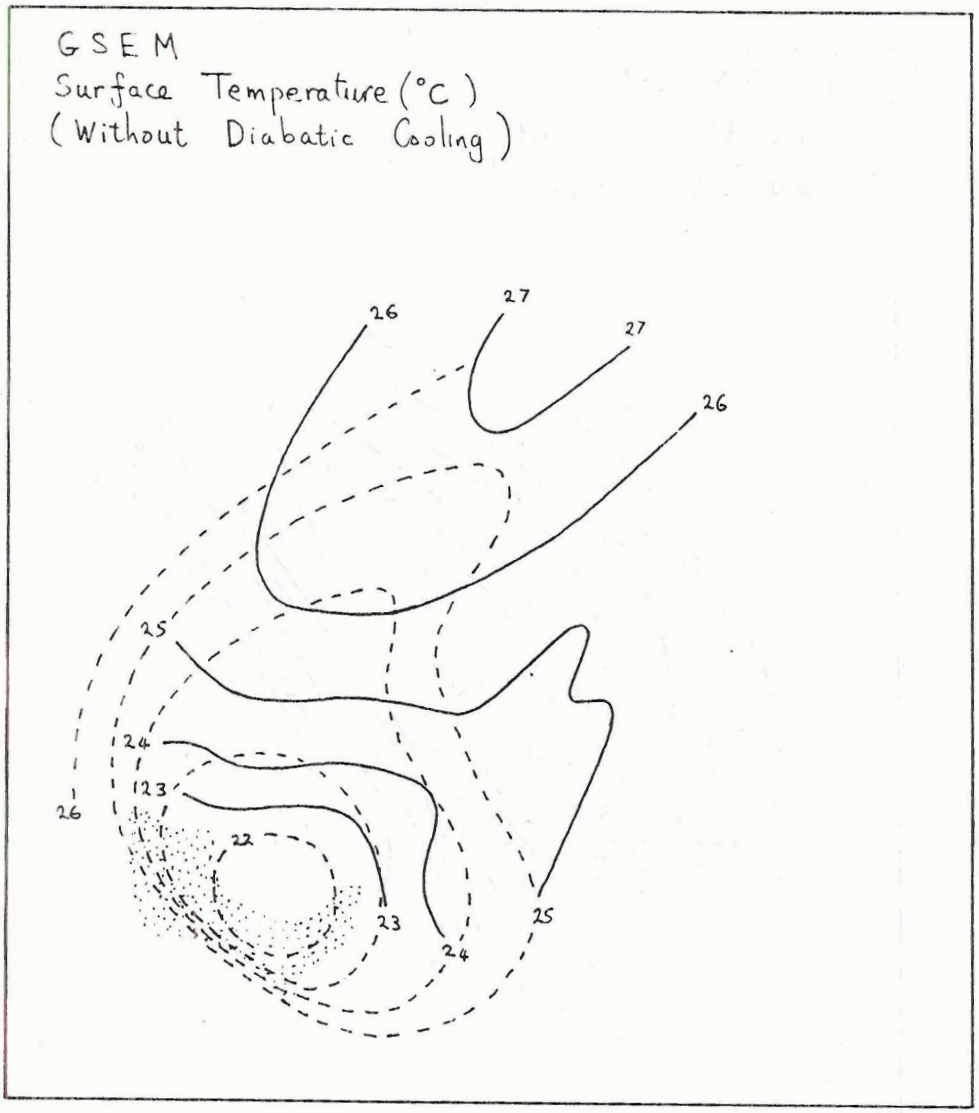

Fig. 36. Mixed layer surface temperature (°C) predicted by the GSEM without diabatic heating (solid lines). Dashed lines show observed values.

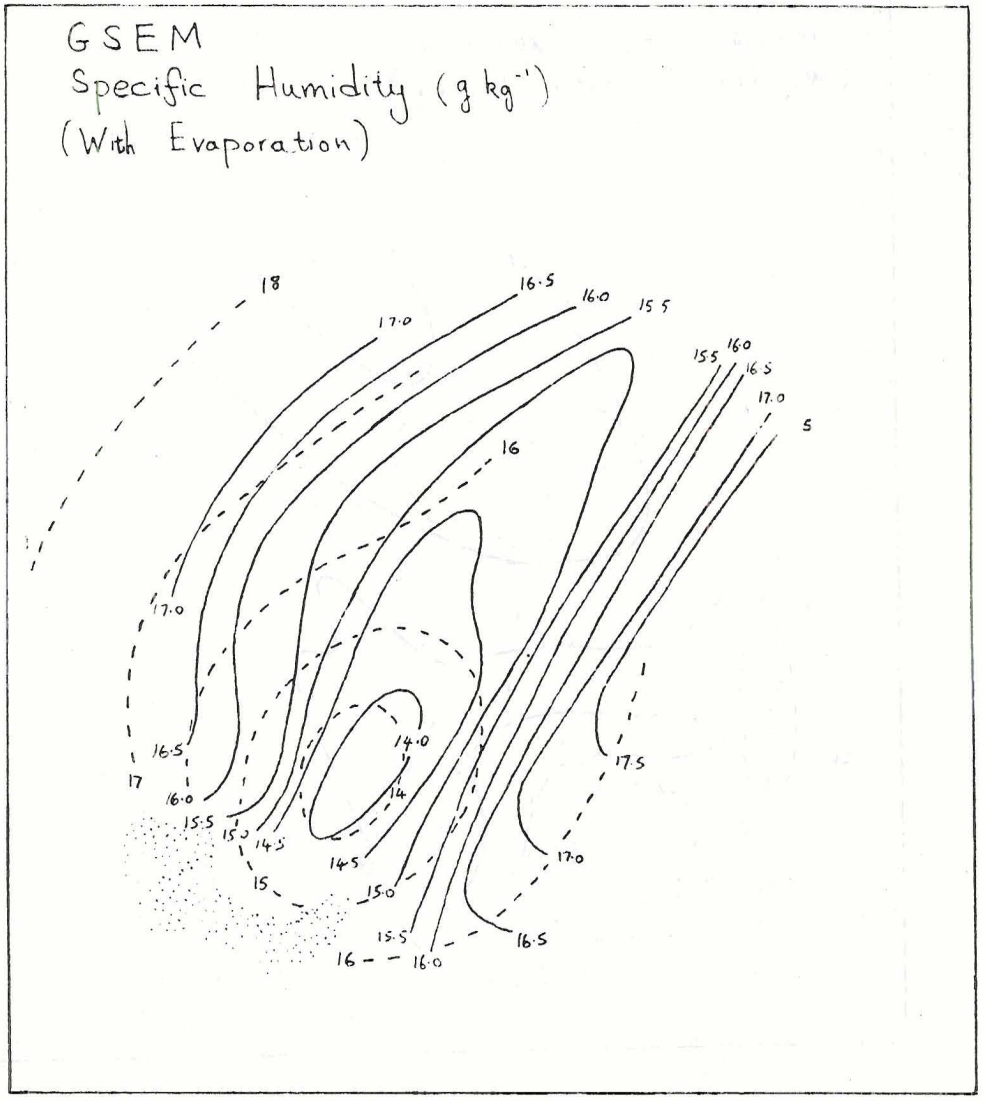

Fig. 37. Mixed layer specific humidity (g kg^{-1}) predicted by the GSEM with evaporation (solid lines). Dashed lines show observed values.

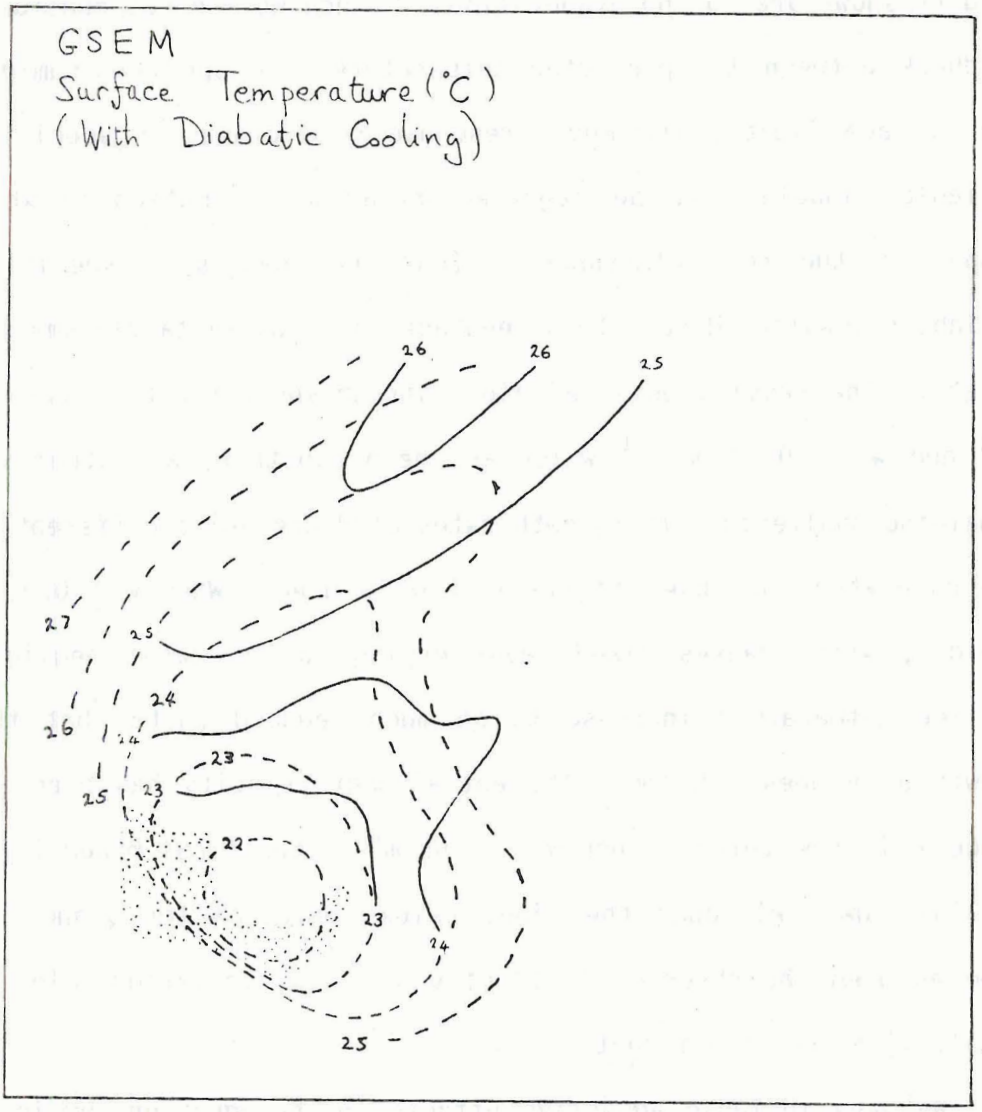

Fig. 38. Mixed layer surface temperature (°C) predicted by the GSEM with diabatic heating (solid lines). Dashed lines show observed values.

7.b Sensitivity Tests

Figs. 39 to 43 give some idea of the sensitivity of H,q and s to variations in w, v_r F_{sv}, Γ_s and Γ_q using the zero-order model (note the results shown are for no evaporation). Since we are not considering any feedback between the predicted temperatures and specific humidities on the surface fluxes, the model response to a change in specified field variables should only be regarded as an approximation to what would happen in the real atmosphere. (For the changes in specified field variables considered here this feedback is actually fairly small). Fig. 39 shows the results obtained along streamline 5 for the case where w = 0.0 and w = -0.02 m s^{-1} which are held constant, all other variables remaining unaltered. The growth rates of H are quite different than for the case when the observed field of w is used. When w = 0.0, H grows rapidly, which causes mixed layer drying to be almost negligible and surface temperature increase to be much reduced (note that the rapid growth of H does not imply the entrainment velocity has been increased since w is now zero). When w = -0.02 m s^{-1} the final mixed layer depth is very low. Although the final values obtained for q and s are the same as when the observed field of w is used, variations closer to the squall line are significant.

We have included advective effects in the equations by integrating along streamlines and using the observed wind speeds. To see the effect of neglecting advection terms we take v_r to be 13.5 m s^{-1} (the speed of the squall line). The results along streamline 5 are shown in Fig. 40. Streamline 5 runs very nearly parallel to the direction of motion of the squall line, whereas for some streamlines this is not such a good approximation and would have to be taken into consideration in estimating the error of neglecting advective terms. Fig. 40 shows that advection

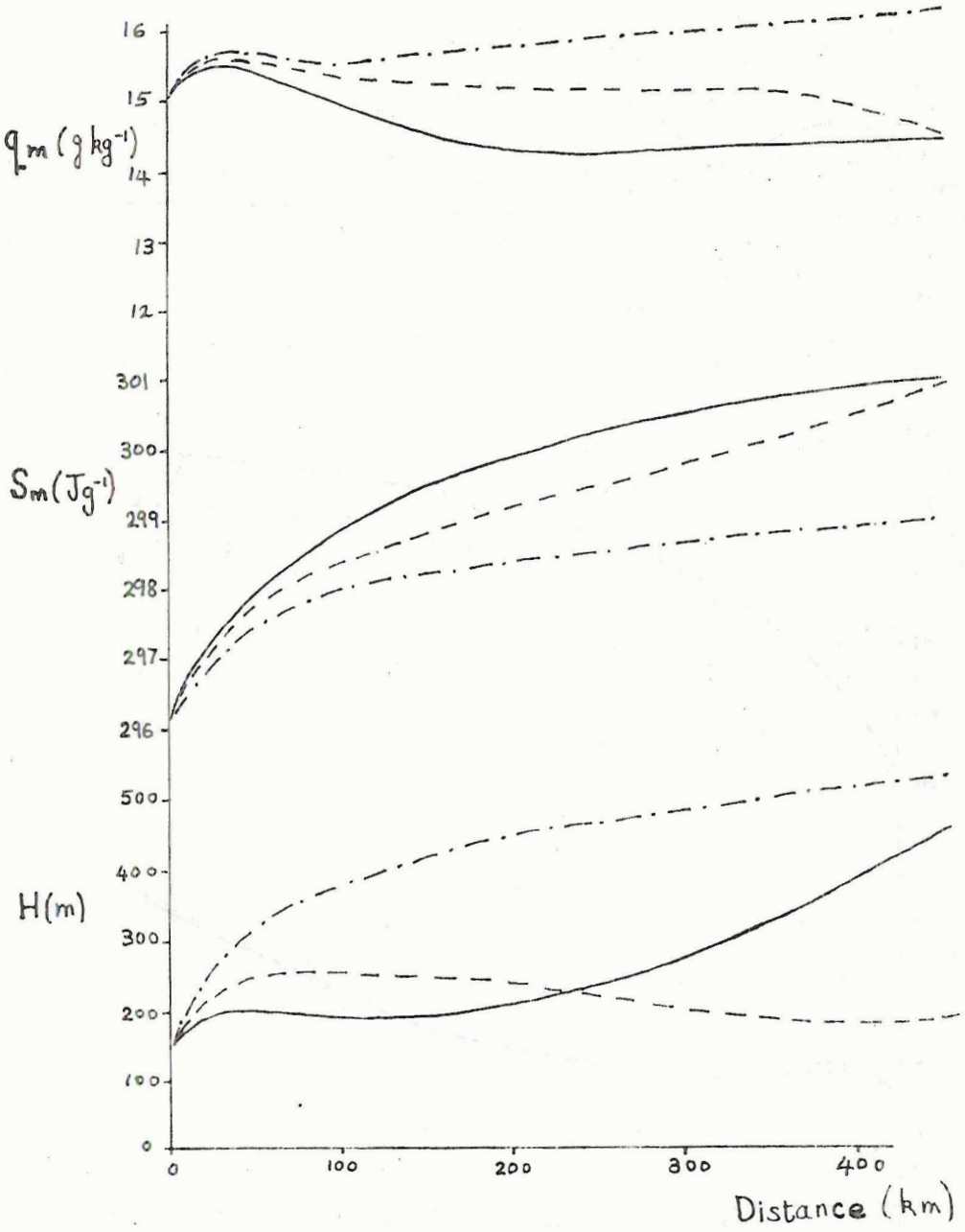

Fig. 39. Sensitivity of mixed layer height H, dry static energy s_m and specific humidity q_m to vertical velocity. Solid lines show results for observed values of vertical velocity w_H; dashed lines, results for $w_H = -0.02$ ms^{-1}; dashed dot lines results for $w_H = 0.0$ ms^{-1}.

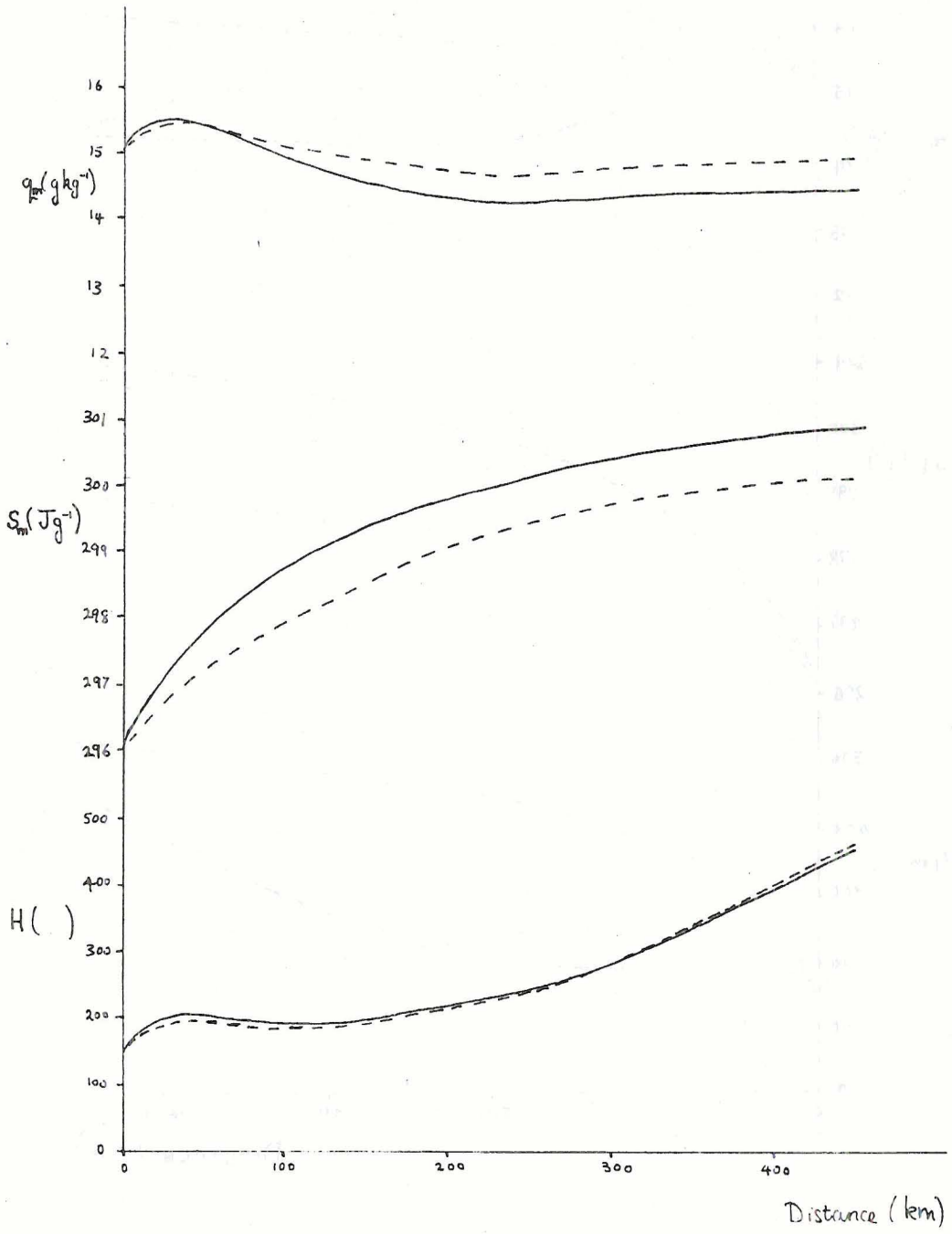

Fig. 40. Sensitivity of mixed layer height H, dry static energy s_m and specific humidity q_m to the inclusion of advective terms. Solid lines show results with advective terms; dashed lines, results without advective terms.

has very little effect on the mixed layer height, however, it does have a noticeable effect on the specific humidity and dry static energy. Neglecting advection changes specific humidity by as much as 0.4 g kg^{-1} and dry static energy by as much as 0.8 J g^{-1}. It is concluded that errors due to uncertaintly in observed wind speeds are probably small, but that advection terms should be included if accurate values of specific humidity and dry static energy are to be predicted.

As can be seen in Fig. 41 the differences between having constant buoyancy fluxes (15 Wm^{-2} and 30 Wm^{-2}) and using the actual fluxes are large. When the buoyancy flux is 30 W m^{-2} quite a rapid growth of H occurs. Very strong mixed layer drying is predicted which must be due to a large entrainment rate at the top of the mixed layer. Conversely for the case when the buoyancy flux is held at 15 W m^{-2}, mixed layer growth is slower and the entrainment rate is less leading to reduced drying. Dry static energy increase is substantially reduced when the buoyancy flux is small.

Fig. 42 shows the sensitivity to variations in Γ_s. For the case when Γ_s is held constant at 6 J kg^{-1} m^{-1} (which is considerably less than the observed gradient of dry static energy in the wake of the squall line) rapid growth of the mixed layer and strong drying occurs. Dry static energy increase is not as fast as when the observed gradients are used since the mixed layer depth is larger. When Γ_s is held at 14 J kg^{-1} m^{-1} the greater stability leads to lower mixed layer heights and thus higher temperatures, whereas surface drying is less.

Variations of the gradient of specific humidity have a small effect on the mixed layer depth as can be seen in Fig. 43 where Γ_q is held at -3 g kg^{-1} km^{-1} and -12 g kg^{-1} km^{-1}. Corresponding to these small

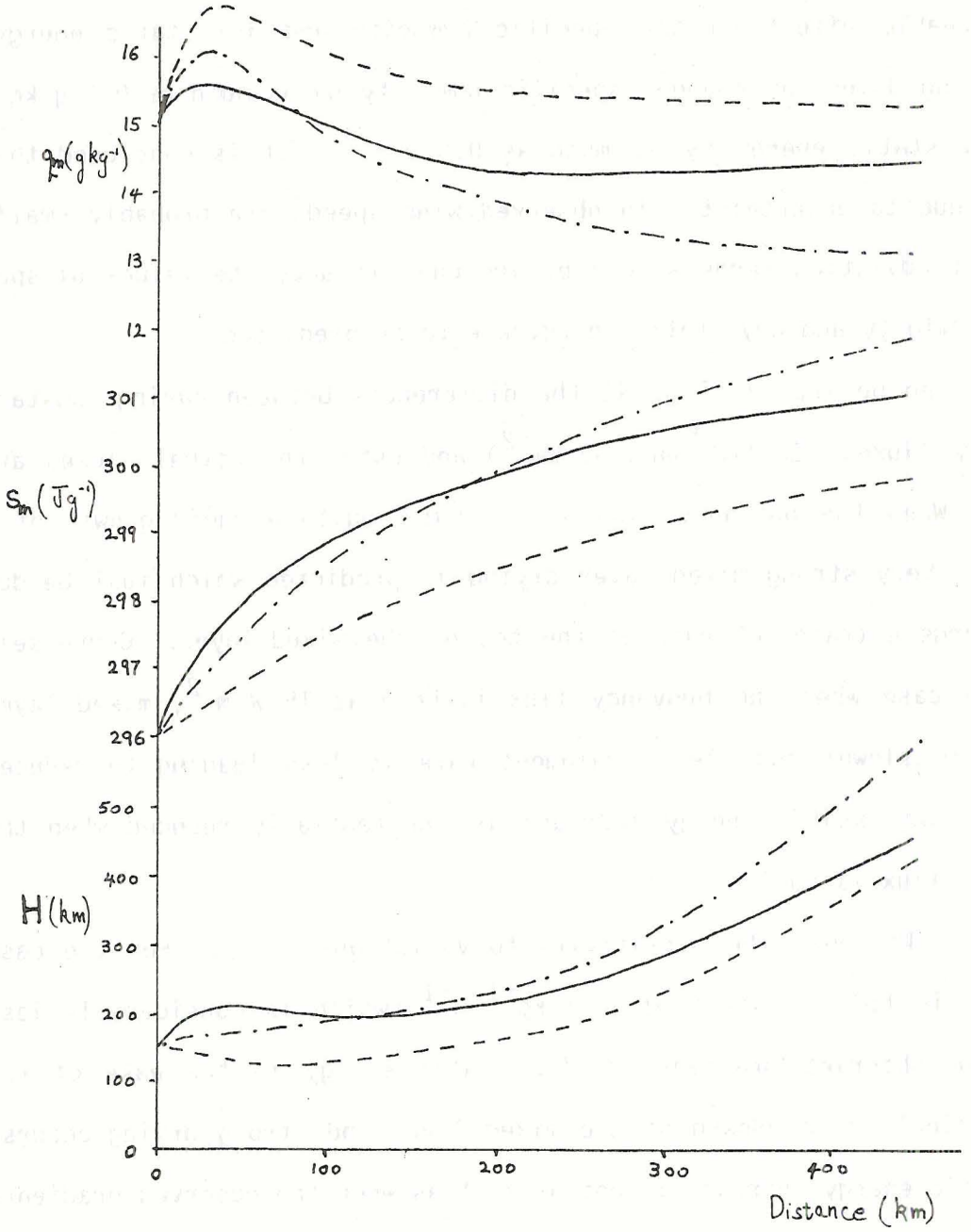

Fig. 41. Sensitivity of mixed layer height H, dry static energy s_m and specific humidity q_m to virtual static energy flux. Solid lines show results for observed values of virtual static energy flux F_{sv}; dashed lines, results for F_{sv} = 15 Wm^{-2}; dashed dot lines results for F_{sv} = 30 Wm^{-2}.

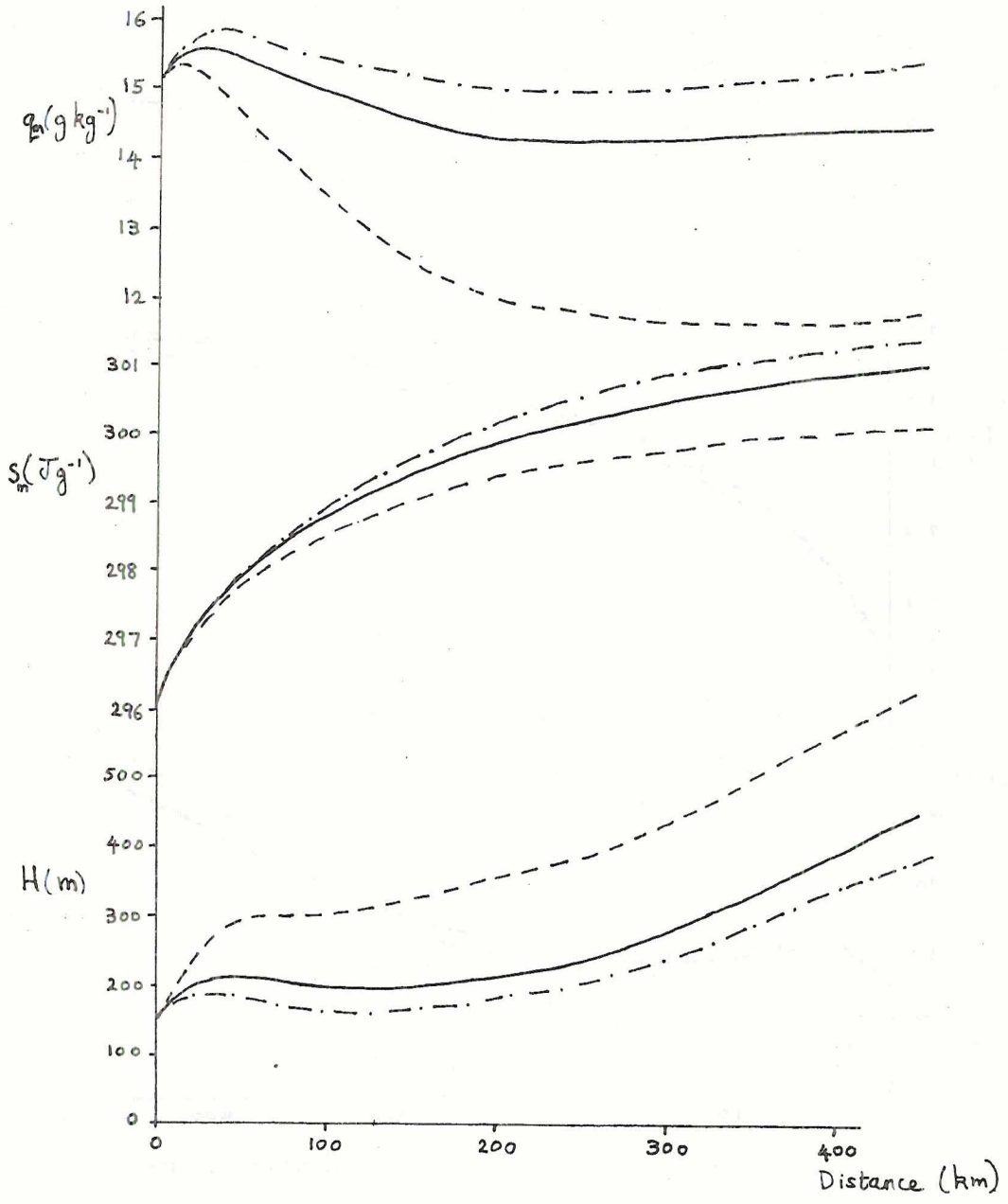

Fig. 42. Sensitivity of mixed layer height H, dry static energy s_m and specific humidity q_m to the gradient of dry static energy. Solid lines show results for observed values of the gradient of dry static energy Γ_s; dashed lines, results for Γ_s = 6 J kg^{-1} m^{-1}; dashed dot lines results for Γ_s = 14 J kg^{-1} m^{-1}.

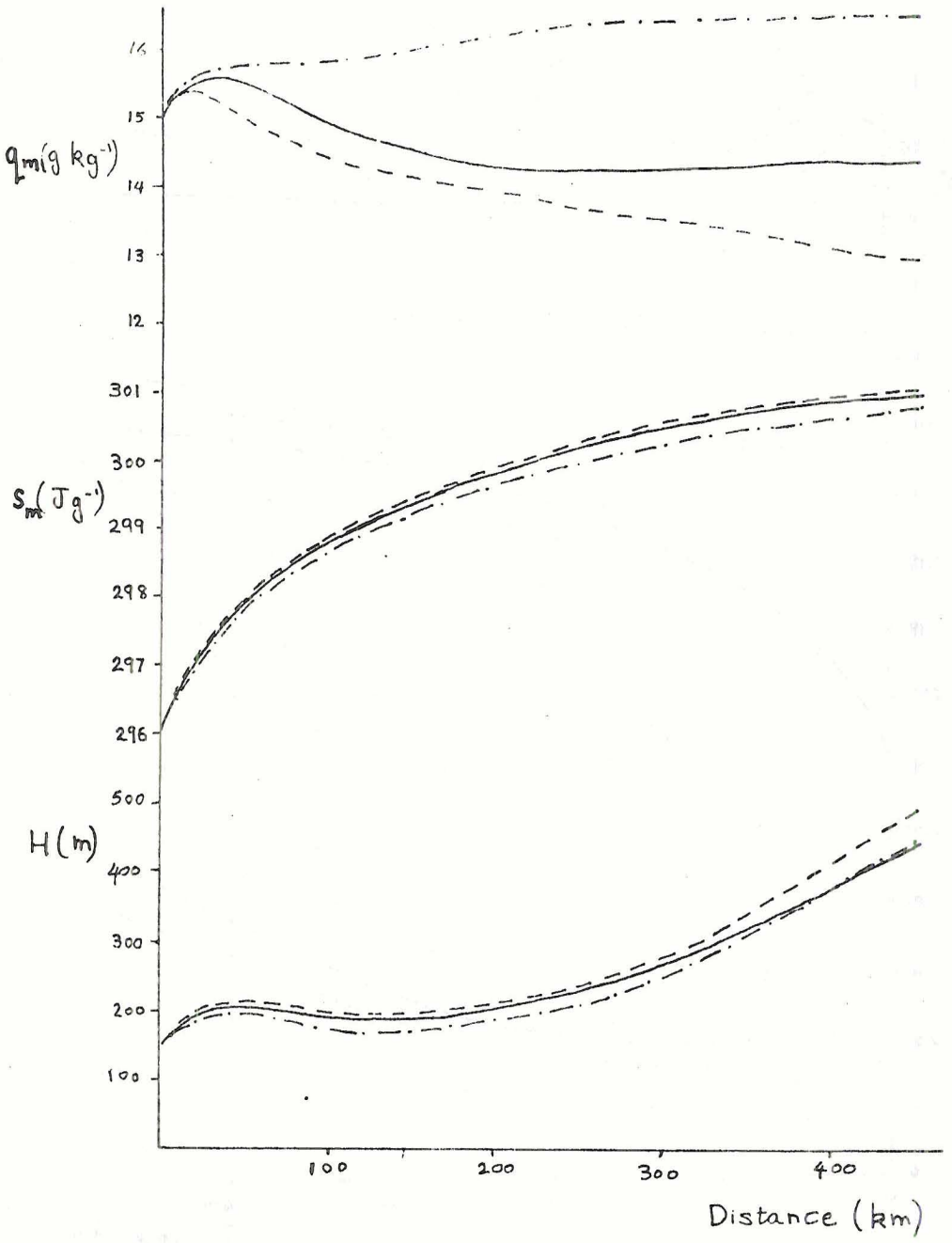

Fig. 43. Sensitivity of mixed layer height H, dry static energy s_m and specific humidity q_m to the gradient of specific humidity. Solid lines show results for observed values of the gradient of specific humidity Γ_q = -12 g kg^{-1} kg^{-1}; dashed dot lines results for Γ_q = -3 g kg^{-1} km^{-1}.

changes in H only slight differences in dry static energy are observed. However, the predicted mixed layer specific humidity is very sensitive to changes in the lapse rate.

When feedback of predicted temperatures and specific humidities on surface fluxes are considered in a fully interactive model (where the approximation of constant sea surface temperature was made) the results of the sensitivity tests remain qualitatively the same (not shown). What emerges from these sensitivity tests is that choosing constant values for these field variables can lead to large differences in predicted values of H, q and s, and that the time variation of these quantities (relative to the ground) needs to be considered. Fitzjarrald and Garstang (1981) for instance chose constant values for the lapse rates of virtual static energy, specific humidity, and surface fluxes, did not include horizontal advective terms and did not have as reliable a vertical field as was used here. Another important point is that for the purpose of the sensitivity test we have chosen large variations (more or less extreme values) and held them constant, far larger variations than can be expected due to errors in the observations. Probably reasonable estimates of the errors in the input variables at any point are w(± 0.005 ms^{-1}) at 375 m, v_r($\pm$ 1 ms^{-1}), F_{sv}(± 5 Wm^{-2}), Γ_s(± 2 J kg^{-1} m^{-1}), Γ_q(± 3 g kg^{-1} km^{-1}). Although errors are cumulative, reasonable agreement between predicted mixed layer depth and observed could be expected as long as results are not too sensitive to the initial conditions and the entrainment parameter k. This conclusion would also extend to prediction of the dry static energy except this is apparently strongly dependent on rainfall evaporation. Model results for mixed layer specific humidity are very sensitive to lapse rates of specific humidity which

has turned out to be one of the hardest observational quantities to accurately determine (it is also very sensitive to the lapse rate of dry static energy; however, the range of variation for this quantity is not so large).

We now consider the sensitivity to the initial conditions, the entrainment parameter, and F_{qo}. F_{qo} is known to about the same accuracy as F_{Sv} and only has an effect on the specific humidity. Fig. 44(a) shows results obtained choosing initial values of H = 100 m and 200 m compared to the original choice of 150 m. It can be seen the mixed layer depth quickly adjusts so that after only 50 km differences become very small. The effect on the specific humidity and dry static energy are more noticeable. Fig. 44(b) shows the results of using initial values of ΔS_v of 0.2 and 0.6 Jg^{-1} rather than 0.4 Jg^{-1}. The differences obtained for all predicted quantities are virtually negligible. The sensitivity of specific humidity to the initial choice of Δq (not shown) is fairly small. The effect of changing the initial value of s or q is to shift the predicted curves for these quantities without changing their shape. Fig. 45 shows results obtained for choosing values for the entrainment parameter of 0.2 and 0.3, compared to the original choice of 0.25. Predicted quantities are quite insensitive to this parameter.

It can be concluded that the sensitivity to the initial conditions and the value of the entrainment parameter is fairly small, and that to obtain accurate results using this type of model (assuming of course the model assumptions are reasonable for this study) it is just as important if not more so to know with some confidence the fields of vertical velocity, horizontal velocity, surface fluxes and lapse rates.

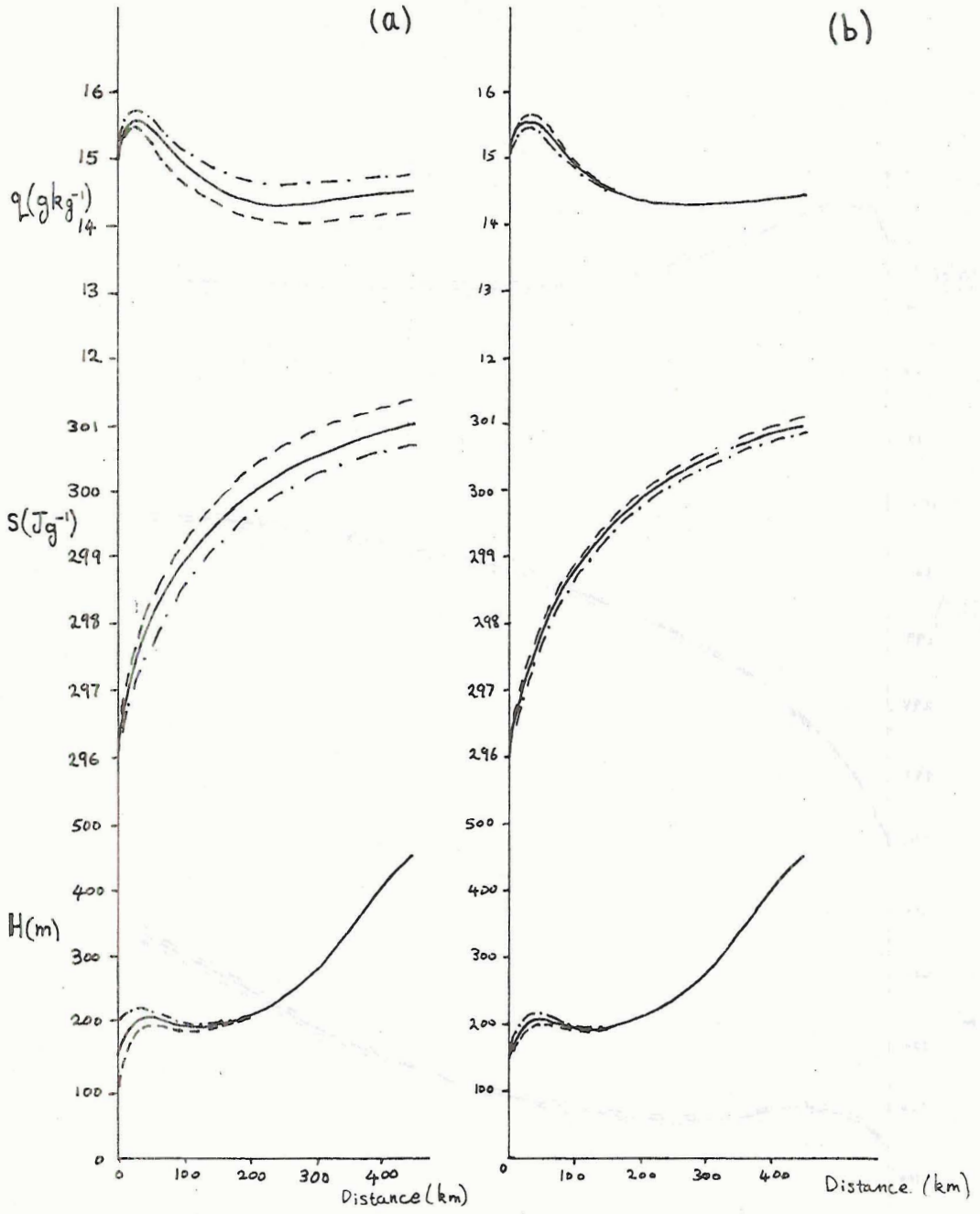

Fig. 44. Sensitivity of mixed layer height H, dry static energy s_m and specific humidity q_m to (a) initial value of H; solid lines show results for observed value H = 150 m; dashed lines for initial H = 100 m; dashed dot lines for initial H = 200 m; (b) initial value of the jump in virtual static energy Δs_v; solid lines show results for observed value Δs_v = 0.4 J g^{-1}; dashed lines for initial Δs_v = 0.2 J g^{-1}; dashed dot line for initial Δs_v = 0.6 J g^{-1}.

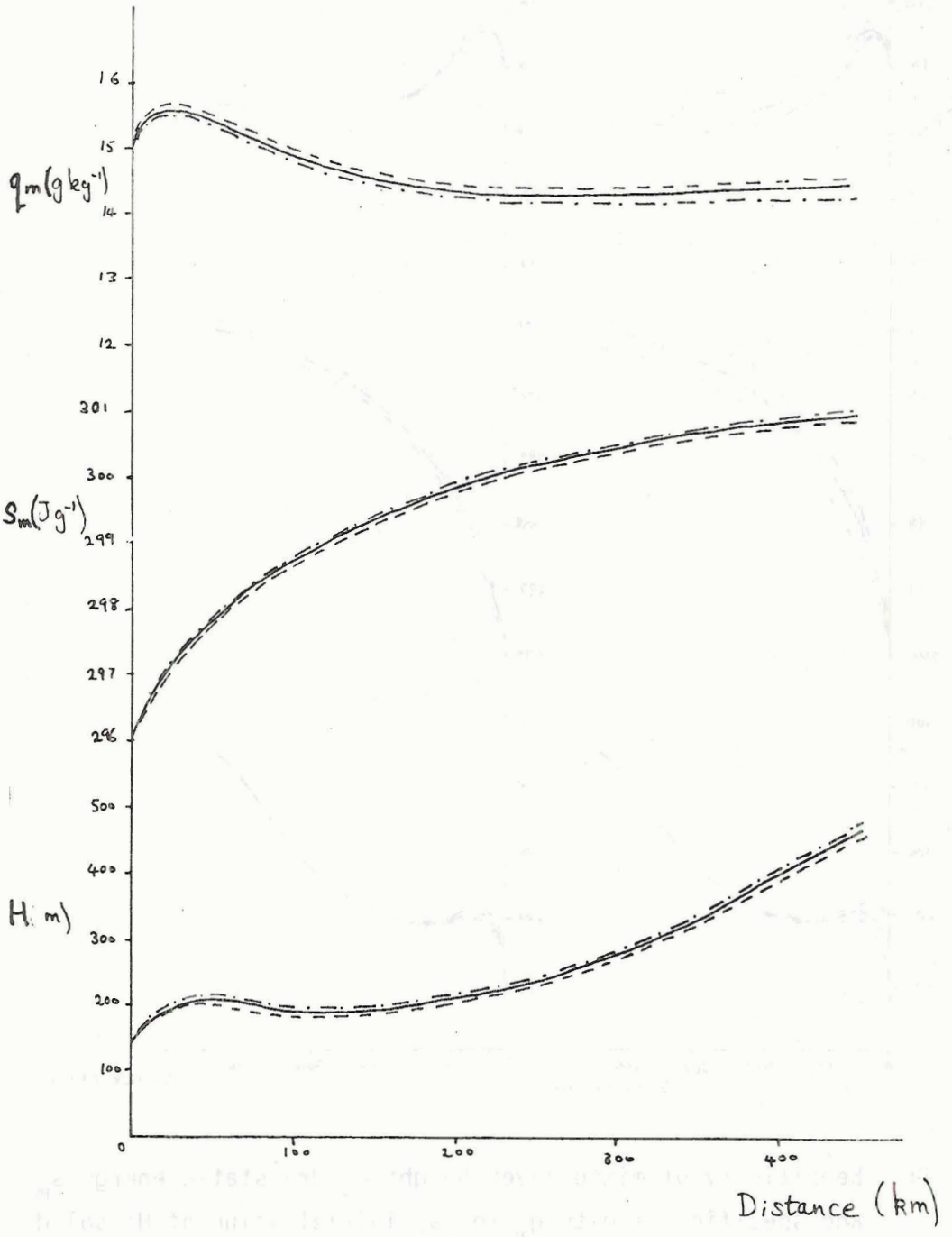

Fig. 45. Sensitivity of mixed layer height H, dry static energy s_m and specific humidity q_m to the entrainment parameter k. Solid lines show results for k = 0.25, dashed lines for k = 0.2 and dash dot lines for k = 0.3.

7.c A More Detailed Investigation of the Role of Rainfall Evaporation and Diabatic Heating

Up to now a number of diabatic heating and moisture source terms have been neglected in the governing equations. Diabatic heating terms were included in the zero-order model, e.g. Eqs. (4.6) and (4.11), but have not been utilized in the calculations so far. Since we are going to consider the flux divergence of heat and moisture across the transition layer, it seems more appropriate to use the GSEM rather than the zero-order model. The equations including diabatic heating and moisture source terms are given in Appendix B. We shall neglect diabatic heating due to radiation and only consider that due to rainfall evaporation. We need to determine the magnitude of the terms Q_{R2}, Q_{RM}, E_2, E_m, F_{R2}, F_{R1} and F_{E1}, where Q_R is the diabatic heating rate, E the evaporation rate, F_R the flux of heat and F_E the flux of rain; the subscripts 1, 2 and m refer to the values of these quantities at h_1, h_2 and the mean value in the mixed layer, respectively. We note from Eq. (B3) that

$$\Delta F_R = - L\Delta F_E \tag{7.4}$$

where $\Delta F_R = F_{R2} - F_{R1}$ and $\Delta F_E = F_{E2} - F_{E1}$. Now

$$\Delta F_R = - \int_{h_1}^{h_2} \rho Q_R(z)dz \tag{7.5}$$

$$\cong - \rho Q_{Rmt}\Delta h$$

where Q_{Rmt} is the mean heating rate in the transition layer.

We can estimate ΔF_R using the composite analysis of rainfall rates and Eq. (7.2) once we have specified Δh. Furthermore, we can show that the ΔQ term in Eqs. (B4) and (B6) is small compared to other terms. From Table 1, we estimate

$$\Delta Q = Q_{R2} - Q_{Rm} \cong (-0.059 + 0.050) = -0.009 \text{ W m}^{-3},$$

and

$$\Delta F_R \cong -Q_{Rm} t^{\Delta h} \simeq -(-0.059 - 0.045)\times 80 = 4.2 \text{ W m}^{-2}.$$

Comparing the magnitude of the terms involving ΔQ_R and ΔF_R in Eq. (B6), we find

$$Y\Delta h \Delta Q_R : \Delta F_R$$

is about 0.36 : 4.0, where we have estimated Y as ½. (Deardorff (1979) shows from observations that Y usually has a value somewhat less than ½). Comparing the last two terms in Eq. (B4) we find

$$\frac{F_{S_v 1} - F_{S_v o}}{h_1} : \Delta Q_R$$

is about 0.16 : 0.009, where we have taken F_{Svo} to be 25Wm^{-2} and h_1 to be 200 m. Hence it seems reasonable to neglect ΔQ_R. Similarly in Eq. (B7) we can neglect the term involving F_E. In Eq. (B5) we compare the terms

$$\Gamma_q \Delta W : \Delta E$$

which is about 5×10^{-8} : 0.30×10^{-8} where we have taken $\Delta W = 0.005 \text{ ms}^{-1}$ and $\Gamma_q = 0.00001 \text{ m}^{-1}$ showing that ΔE can be neglected in this equation. Hence, the equations are modified only by the terms involving ΔF_R and

ΔF_E which are estimated using the Researcher (1902) sounding. All variables in Eq. (7.2) are held constant except the rainfall rate. This sounding was taken slightly after the time for which the squall system was considered to be in the steady state, however, it is the only one situated in the region where significant rainfall occurred.

Results obtained when these terms are included are shown in Fig. 46 for streamline 5. Also shown are the results obtained when ΔF_R and ΔF_E are omitted but Q_{Rm} and E_m are still included in Eqs. (B9) and (B10), which can be compared to the case when all diabatic heating and moisture source terms are neglected. The effect on the mixed layer height is fairly small. The rate of increase of dry static energy is slightly reduced when the term involving ΔF_R is included since the mixed layer height is somewhat larger in the first part of the integration. The inclusion of ΔF_R and ΔF_E slightly increases the mixed layer specific humidity. The inversion strength ΔS is noticeably increased, whereas, Δq is virtually unaffected. The conclusion that can be drawn is that the main effect of including diabatic heating is in reducing the rate of increase of mixed layer dry static energy (by permitting evaporative cooling) and that this is mostly due to the inclusion of the Q_{Rm} term in Eq. (6.7) (which gives Eq. (B9)). The addition of diabatic heating and moisture source terms produces slightly higher values of mixed layer specific humidity.

7.d Development of Specific Humidity and Dry Static Energy Profiles

As described in Chapter 3 the specific humidity profile has an unusual structure, the development of which has important consequences for the lapse rate at the top of the transition layer. The moisture budget equation in the stable air above the transition layer, neglecting

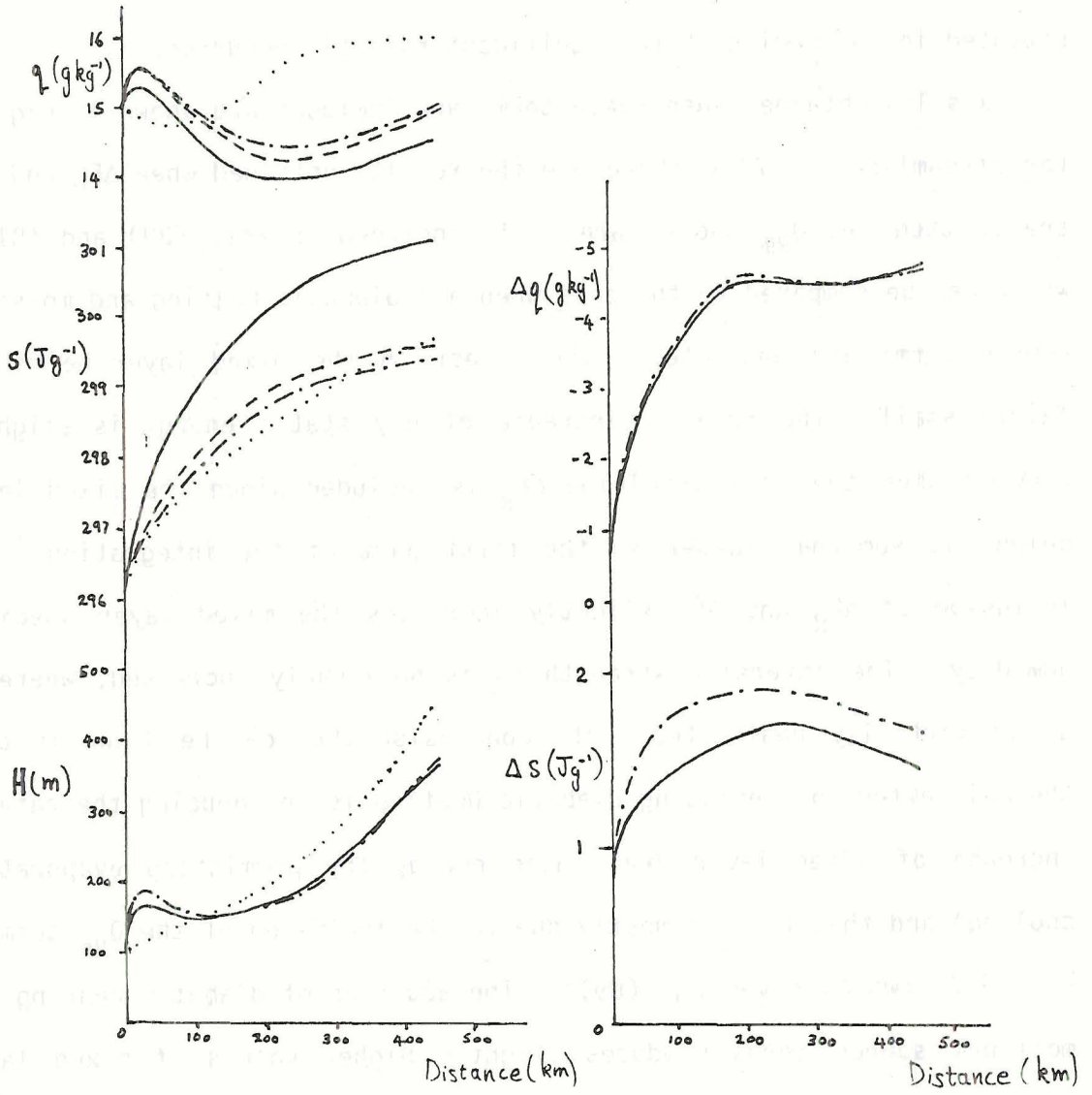

Fig. 46. Effect of inclusion of diabatic heating terms on mixed layer height H, dry static energy s, specific humidity q, Δs and Δq. Solid lines show results without diabatic heating and moisture source terms; dashed lines are results when diabatic heating and moisture source terms are included but ΔF_R and ΔF_E neglected; dash-dot lines results when ΔF_R and ΔF_E are also included; dotted lines show observed values (see text for details).

sources and sinks is

$$\frac{d_H q}{dt} + \bar{w}\Gamma_q = 0 \tag{7.6}$$

where

$$\frac{d_H}{dt} = \frac{\partial}{\partial t} + \underset{\sim}{v}\cdot\nabla$$

If we demand $\underset{\sim}{v}$ and Γ_q to be constant with height, then differentiating Eq. (7.6) with respect to z we obtain

$$\frac{d_H}{dt}\Gamma_q + \frac{\partial \bar{w}}{\partial z}\Gamma_q = 0 \tag{7.7}$$

Differentiating again with respect to z we find vertical velocity has to be a linear function of height, and Eq. (7.7) becomes

$$\frac{d_H \Gamma_q}{dt} = -\frac{w}{z}\Gamma_q \tag{7.8}$$

Unfortunately the conditions under which this equation was derived are highly restrictive; the wind field analyses at the surface and at 970 mb, and the specific humidity profiles clearly show that neither $\underset{\sim}{v}$ or Γ_q are well approximated by being held constant with respect to z. The streamline analysis at 850 mb by Gamache and Houze (1981a) show there is considerable wind shear between the surface and this level. Eq. (7.8) is thus only of qualitative importance in that we would expect the effect of subsidence would be to tend to increase the gradient at the top of the transition layer as long as the gradient was approximately constant with height. In the case of the dry static energy profiles this condition is fairly well met and would seem to account for the increase in stability of the air within the wake of the squall system. However, the problem of determining the thermodynamic structure of the

air above the mixed layer is a complicated one, and to solve it properly we would need to trace the trajectories of air parcels from the region of convective scale downdrafts to well behind the line. The streamlines are not constant with height and so the air in a column at any point behind the squall line could have originated from very different regions. Furthermore, the effect of rainfall evaporation and diabatic heating could be significant.

It is fairly simple to determine the effect of subsidence on a lapse rate which is a function of height as long as we still consider horizontal velocity to be independent of height. In this case as we follow the motion, the change in lapse rate of specific humidity at a particular level is due to vertical advection of moisture. The vertical displacement of a parcel along a streamline can be determined from

$$v_r(x) \frac{dz}{dx} = w(x,z) \qquad (7.9)$$

If the incompressible continuity equation is approximately satisfied then the vertical velocity is required to be constant with height. Forward differencing Eq. (7.9), and linearly extrapolating from 375 m to obtain the vertical velocity field gives the results shown in Fig. 47 where the initial profile used was based on the Researcher (1902) sounding. The integration was started 50 km along streamline 5 to approximately correspond to the position of the Researcher (1902) sounding. It can be seen that the relative maxima in specific humidity approaches the surface considerably faster than observations indicate. The lowest height the relative maxima reaches is about 330 m some 250 km along streamline 5.

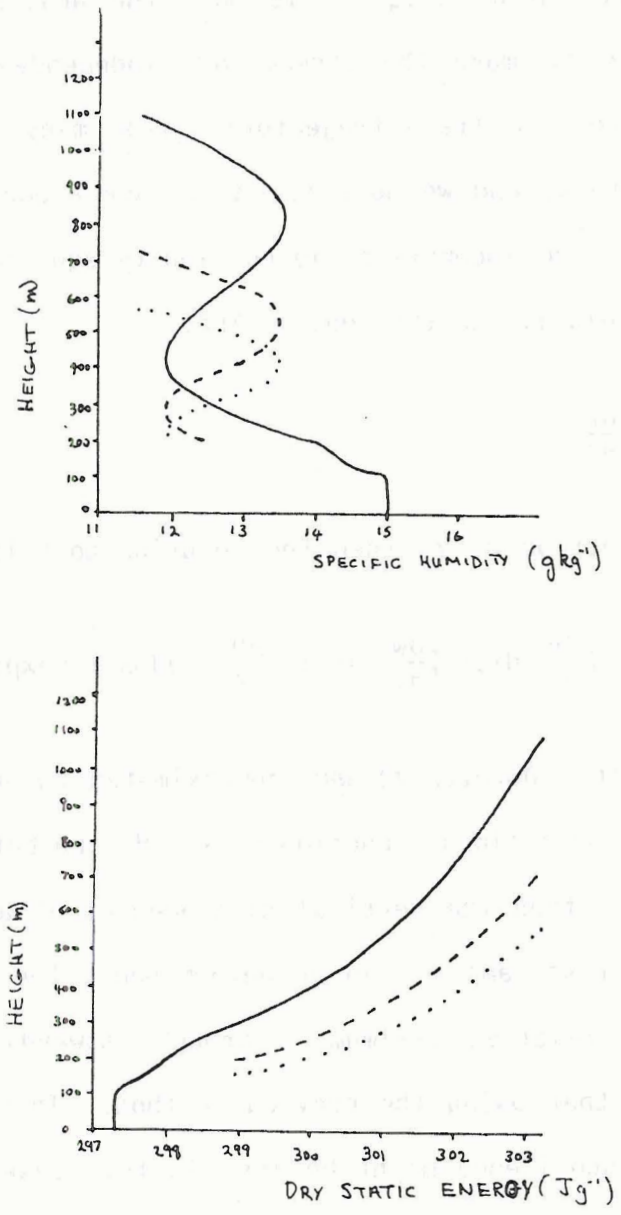

Fig. 47. The effect of subsidence (linear with height) on profiles of specific humidity and dry static energy. Results are shown for integrations along streamline 5. The initial profiles (solid lines) are 50 km along streamline 5; the dashed lines show results at 100 km; the dotted lines at 150 km.

The discrepancy could be due to the fact that the vertical velocity is not linear with height but is probably more like that shown in Fig. 25. It is possible to include a nonlinear variation of w with height by letting v_r be a function of height. To make the analysis tractable though we still have to make the streamlines independent of height; otherwise we would have to trace trajectories from many different regions, a formidable task, and we do not really have a good enough data set to attempt this. The incompressible continuity equation written in natural coordinates relative to the squall line, is

$$\frac{\partial v_r}{\partial x} + v_r \frac{\partial \theta}{\partial n} = - \frac{\partial w}{\partial z}$$

If $\partial\theta/\partial n$ is not a function of z, then the solution to this equation is

$$v_r(x,z) = - \exp(-\int \frac{\partial \theta}{\partial n}\, dx) \cdot \int [\frac{\partial w}{\partial z} \exp (\int \frac{\partial \theta}{\partial n}\, dx)]dx + C\exp(-\int \frac{\partial \theta}{\partial n}\, dx)$$

where C is a constant. $\partial w/\partial z(x,z)$ was approximated by an analytical function and $\partial\theta/\partial n(x)$ by a linear function of x. Having both the fields of $v_r(x,z)$ and $w(x,z)$ then the vertical displacement of an air parcel with distance along a streamline can be determined. The results (not shown) are that the relative maximum is brought towards the surface slightly faster than that using the previous method. This is probably not too surprising; subsidence might be less in this case than it was for the previous one, however v_r is also less at higher levels so an air parcel remains within the mesoscale downdraft region for longer.

The poor agreement with observations suggests either the vertical velocity field being used is significantly in error or that the

approximation that streamlines are independent of height is not a good one. We do have evidence that the latter approximation is not a good one since there is significant vertical wind shear.

8. SUMMARY AND DISCUSSION

In this study a procedure has been developed for obtaining the fully three dimensional mixed layer structure in the boundary layer wake of a GATE tropical squall line by formulating the model equations relative to the squall system in natural coordinates. The results of the modeling study are in fairly good agreement with observations.

The asymmetry of the mixed layer height found in a composite analysis by Johnson and Nicholls (1983) seems to be well simulated by both models. Mixed layer growth is inhibited by mesoscale subsidence and to a lesser extent (but still significantly) by the large gradient of virtual static energy, above the transition layer. The very stable lapse rate in the wake of the squall is probably mainly due to the mesoscale subsidence, although it could be partly produced within the convective region. The rapid mixed layer growth on the south east side of the wake (Johnson and Nicholls, 1983) can be attributed to the stronger buoyancy flux, and weaker subsidence.

Data show that downdraft air within the convective cores that reaches the surface is drier (in an absolute sense) than the air preceding the squall line. The depth of this downdraft outflow is about 500-1000 m, within which the gradient of specific humidity above the transition layer is negative. As the mixed layer starts to grow it entrains drier air from above, which can lead to further reduction of the specific humidity. The mesoscale subsidence leads to a decrease in

the depth of the convective downdraft outflow layer so that in some regions the mixed layer depth exceeds it and starts to grow into the air above, which is of different character having a larger moisture content.

Fitzjarrald and Garstang (1981b) hypothesized that mixed layer drying was a result of rapid mixed layer growth as well as of subsidence as proposed by Zipser (1977). Both of these factors can lead to large entrainment rates. Obviously the rate of drying will also depend on the difference in moisture content of the entrained air and that of the mixed layer which is very sensitive to the gradient of specific humidity above the transition layer. The largest drying in the squall wake seems to occur in regions of strongly negative gradients of specific humidity which tend to be coincident with strong subsidence. Fairly rapid growth of the mixed layer is predicted in regions where low level specific humidity is increasing, for example to the east side of the squall wake (Figs. 26 and 27), so at least for this system this would not seem to be the significant factor associated with drying. However, it should be emphasized that the composite analysis of the gradients of specific humidity above the transition layer, particularly in the region where they are apparently very large, is based on fairly sparse sounding data, and so the importance of large negative gradients of specific humidity, while suggestive, cannot yet be regarded as conclusive. The situation is further complicated by the fact that mixed layer specific humidity also depends on the surface moisture flux.

Model results suggest rainfall evaporation is important for sustaining the cool region within the squall wake. The effect of rainfall evaporation can be included fairly accurately in the model by adding a single term to the system of equations. Predicted mixed layer depth (H)

is not sensitive to diabatic effects in this model since the prediction equation for H contains only terms involving jumps in diabatic heating across the inversion (which are small) and buoyancy flux is determined using observed fields of temperature and specific humidity. In a fully interactive model where surface fluxes are predicted, say, using bulk aerodynamic expressions, rather than taken as observed, then diabatic effects might, in principal, modify the predictions of the mixed layer depth. For instance, if precipitation evaporation were neglected in a fully interactive model then the predicted mixed layer temperature would be higher leading to reduced surface fluxes and hence shallower predicted mixed layer depths. Fortunately, however, for the realistic rainfall evaporation estimates used here, the predicted and observed surface fluxes have been found to be in relatively good agreement, thus justifying and making internally consistent the approach adopted in this study.

In principle it is possible to do a budget study in which the diabatic heating and rainfall evaporation within the mixed layer can be estimated using the observed fields of mixed layer height surface temperature, specific humidity and surface fluxes. This was attempted but the results were very "noisy". The evaporation rate even had the wrong sign within the squall wake. This is not too surprising when we consider that the increase in model predicted mixed layer specific humidity when we included rainfall evaporation using Eq. (7.2) was only 0.3 g kg^{-1} (see Fig. 32). Presumably we would have to know the specific humidity field to better accuracy than this to separate out the increase due to rainfall evaporation. The magnitude of the diabatic heating (estimated from Eq. B9) had the right sign close to the squall, although

it was about twice as large as that predicted by Eq. (7.2) and the assumed radiational heating rate; but it had the wrong sign (warming instead of cooling) to the rear of the squall system.

A number of approximations have been made which make it a somewhat tentative conclusion that the model is correctly simulating the real atmosphere. These approximations are (1) the assumption of steady state; (2) the neglect of shear produced turbulence within the transition layer and at the sea surface; (3) the assumption that the horizontal velocity is constant with height up to the top of the transition layer; (4) the specification of the entrainment parameter k in the case of the zero-order model or the transition layer depth Δh in the case of the GSEM; (5) the determination of the fields of vertical wind speed, horizontal velocity, sea surface fluxes, lapse rates and rainfall rates; (6) the assumptions made in the diabatic heating computation; (7) the determination of the initial values of mixed layer height, dry static energy and specific humidity; (8) the determination of the initial values of the jumps in dry static energy and specific humidity across the transition layer; (9) that the idealized model profiles are good representations of the actual ones.

Despite the above limitations, this modeling study represents a considerable improvement over previous works of this kind. Among the improvements are: better observational data to compare with model predictions, modeling of the fully three dimensional mixed layer structure, inclusion of advective terms, the effects of diabatic heating and a finite transition layer depth. The observations indicate that in the squall wake the gradients atop the mixed layer of dry static energy and

specific humidity are considerably larger than have been used in previous studies. The large stability has a significant effect on mixed layer growth; the large specific humidity gradient is apparently important for mixed layer drying. Advective terms and diabatic effects should be included for accurate prediction of surface temperature. The zero-order model seems to work quite well giving results that differ little from those of the GSEM which has a finite transition layer depth. It is hypothesized that the air reaching the surface in downdraft cores is drier (in absolute sense) than the air preceding the squall line and that this air spreads out beneath moister air in between downdraft cores leading to the unusual specific humidity profiles observed in most of the squall wake soundings.

It is hoped that this study in making more explicit the factors influencing mixed layer recovery following the passage of a squall line will lead to an improved basis for the parameterization of convective effects in large scale numerical weather prediction models.

LIST OF REFERENCES

Arakawa, A. and W.H. Schubert, 1974: Interaction of a cumulus cloud ensemble with the large-scale environment. Part I. J. Atmos. Sci., 31, 674-701.

Aspliden, G.A., Y. Tourre, and J.B. Sabine, 1976: Some climatological aspects of West African disturbance lines during GATE. Mon. Wea. Rev., 104, 1029-1035.

Ball, F.K., 1960: Control of inversion height by surface heating. Quart. J. R. Met. Soc., 86, 483-494.

Betts, A.K., 1973: Non-precipitating cumulus convection and its parameterization. Quart. J. R. Met. Soc., 99, 178-196.

Betts, A.K., 1974: Reply to comment on the paper "Non-precipitating cumulus convection and its parameterization." Quart. J. R. Met. Soc., 100, 469-471.

Betts, A.K., 1976: The thermodynamic transformation of the tropical subcloud layer by precipitation and downdrafts. J. Atmos. Sci., 33, 1008-1020.

Businger, J.A., 1982: The fluxes of specific enthalpy, sensible heat and latent heat near the earth's surface. J. Atmos. Sci., 39, 1889-1892.

Carson, D.J., 1973: The development of a dry inversion-capped convectively unstable boundary layer. Quart. J. R. Met. Soc., 99, 450-467.

Deardorff, J.W., 1979: Prediction of convective mixed-layer entrainment for realistic capping inversion structure. J. Atmos. Sci., 36, 424-436.

Driedonks, A.J.M., 1982: Models and observations of the growth of the atmospheric boundary layer. Boundary-Layer Meteorol. 23, 283-306.

Fitzjarrald, D.R. and Garstang, M., 1981a: Vertical structure of the tropical boundary layer. Mon. Wea. Rev., 109, 1512-1526.

Fitzjarrald, D.R. and Garstang, M. 1981b: Boundary layer growth over the tropical ocean. Mon. Wea. Rev., 109, 1762-1772.

Frank, W.M., and G.D. Emmitt, 1981: Computation of vertical total energy fluxes in a moist atmosphere. Boundary-Layer Meteor., 21, 223-230.

Gamache, J.F. and R.A. Houze, Jr., 1982a: Mesoscale air motions associated with a tropical squall line. Mon. Wea. Rev., 110, 118-135.

Gamache, J.F. and R.A. Houze, Jr., 1982b: Water budget of a mesoscale convective system in the tropics. Submitted to J. Atmos. Sci.

Gaynor, J.E., and P.A. Mandics, 1978: Analysis of the tropical marine boundary layer during GATE using acoustic sounder data. Mon. Wea. Rev., 106, 223-232.

Houze, R.A., Jr., 1977: Structure and dynamics of a tropical squall-line system observed during GATE. Mon. Wea. Rev., 105, 1540-1567.

Johnson, R.H., 1980: Diagnosis of convective and mesoscale motions during Phase III of GATE. J. Atmos. Sci., 37, 733-753.

Johnson, R.H., 1981: Large-scale effects of deep convection on the GATE tropical boundary layer. J. Atmos. Sci., 38, 2399-2413.

Johnson, R.H., and M.E. Nicholls, 1982: A composite analysis of the boundary layer accompanying a tropical squall line. Submitted to Mon. Wea. Rev.

Lilly, D.K., 1968: Models of cloud-topped mixed layers under a strong inversion. Quart. J. R. Met. Soc., 94, 292-309.

Manton, M.J. and W.R. Cotton, 1977: Parameterization of the atmospheric surface layer. J. Atmos. Sci., 34, 331-334.

Moore, M.J., and R.R. Long, 1971: An experimental investigation of turbulent stratified shearing flow. J. Fluid. Mech., 49, 635-655.

Payne, S.W., and M.M. McGarry, 1977: The relationship of satellite inferred convective activity to easterly waves over West Africa and the adjacent ocean during Phase III of GATE. Mon. Wea. Rev., 105, 413-420.

Reinking, R.F., and G. Barnes, 1981: A comparison of tropical oceanic heat fluxes determined by airborne eddy correlation and shipboard bulk aerodynamic techniques. Boundary-Layer Meteor., 20, 353-370.

Schubert, W.H., J.S. Wakefield, E.J. Steiner and S.K. Cox, 1977: Marine stratocumulus convection. Part I: Governing equations and horizontally homogeneous solutions. J. Atmos. Sci., 36, 1286-1307.

Schubert, W.H., J.S. Wakefield, E.J. Steiner and S.K. Cox, 1977: Marine stratocumulus convection. Part II: Horizontally inhomogeneous solutions. J. Atmos. Sci., 36, 1308-1324.

Tennekes, H., 1973: A model for the dynamics of the inversion above a convective layer. J. Atmos. Sci., 30, 558-567.

Zilitinkevich, S.S., 1975: Comments on the paper by H. Tennekes. J. Atmos. Sci., 32, 991-992.

Zipser, E.J., 1977: Mesoscale and convective-scale downdrafts as distinct components of squall line structure. Mon. Wea. Rev., 105, 1568-1589.

APPENDIX A

LIST OF SYMBOLS

C_e	bulk transfer coefficient for water vapor
C_h	bulk transfer coefficient for sensible heat
C_p	specific heat
D	molecular diffusivity of water vapor
E_o	surface evaporation
F_E	flux of rain
F_R	heat flux
F_{s_v}	flux of virtual static energy
H	mixed layer height for zero-order model
K	Von Karman's constant
L	Monin Obukhov length or latent heat of vaporization
Q	diabatic heating
Q_m	vertically averaged diabatic heating in mixed layer
R	ratio of specific humidity flux at H to that at the surface
R_m	characteristic raindrop radius
S_o	surface sensible heat flux
Y	integral shape factor
c_D	drag coefficient
c_F	flux convergence coefficient
$\bar{e}$	mean turbulent kinetic energy
e_s	saturated vapor pressure

f	dimensionless shape factor
g	acceleration of gravity
h_1	height of mixed layer for GSEM
h_2	distance to top of transition layer for GSEM
h_+, h_-	incremental displacements above and below H
k	entrainment parameter
m_w	molecular weight of water
p'	perturbation pressure
q, $\bar{q}$, q'	specific humidity: total, mean, perturbation
r_r	mixing ratio of rain
r_v	mixing ratio of water vapor
s	dry static energy
s_v, $\bar{s}_v$, s'_v	virtual static energy: total, mean, perturbation
ss_ι	subsaturation
$\bar{u}_o$	mean wind speed at 10 m
u_*	friction velocity
$\underset{\sim}{v}$	horizontal velocity vector
$\bar{\underset{\sim}{v}}_m$	mean horizontal velocity averaged through depth of mixed layer
v_r	velocity relative to squall line
v_T	terminal fall velocity
w, $\bar{w}$, w'	vertical velocity: total, mean, perturbation
w_{en}	entrainment velocity
$\bar{w}_H$	mean vertical velocity at H
w_*	convective scale velocity
Γ_q	gradient of specific humidity above the transition layer
Γ_s	gradient of dry static energy above the transition layer

Γ_{s_v}	gradient of virtual static energy above the transition layer
ε	dissipation rate
σ_w	r.m.s. turbulence velocity
ω	vertical velocity in p-coordinates
Δh	transition layer depth
Δq	jump in specific humidity across transition layer
Δs_v	jump in virtual static energy across transition layer

APPENDIX B

GSEM WITH DIABATIC HEATING

Here we wish to include all terms due to rainfall evaporation and diabatic heating. The thermodynamic equation and moisture budget equation become

$$\frac{d\bar{S}_v}{dt} = - \frac{\partial}{\partial z} \overline{w' S_v'} - \frac{1}{\rho} \frac{\partial F_R}{\partial z} \tag{B1}$$

$$\frac{d\bar{q}}{dt} = - \frac{\partial}{\partial z} \overline{w' q'} - \frac{1}{\rho} \frac{\partial F_E}{\partial z} \tag{B2}$$

where F_R is the heat flux and F_E is the flux of rain. We note that if the heat flux is due to rainfall evaporation that

$$- \frac{1}{\rho} \frac{\partial F_R}{\partial z} = \frac{L}{\rho} \frac{\partial F_E}{\partial z} \tag{B3}$$

i.e. if we have rain falling through a layer within which evaporation is occurring then $\partial F_E / \partial z < 0$ so that according to Eq. (B3) cooling of the layer is taking place.

If we go through the same steps as is in Chapter 4 we obtain the following set of equations

$$\frac{d}{dt} \Delta S_v = \Gamma_{S_v} \left(W_{e1} + \frac{d}{dt} \Delta h - \Delta W \right) + \frac{F_{S_v 1} - F_{S_v o}}{h_1} + \Delta Q_R \tag{B4}$$

where $\Delta Q_R = Q_{R2} - Q_{Rm}$,

Γ_{R2} is the heating rate at h_2,

Q_{Rm} is the mean heating rate in the mixed layer;

$$\frac{d}{dt}\Delta q = \Gamma_q \left(W_{e1} + \frac{d}{dt}\Delta h - \Delta W\right) + \frac{F_{q1} - F_{qo}}{h_1} + \Delta E \tag{B5}$$

where $\Delta E = E_2 - E_m$,

E_2 is the evaporation rate at h_2,

E_m is the mean evaporation rate in the mixed layer;

$$\frac{W_{e1}}{W_*} = \frac{1}{(1-GY)} \left\{ \alpha(1-Y)R_*^{-1} - \frac{(1-Y-GY)}{W_*}\left(\frac{d\Delta h}{dt} - \Delta W\right) + \frac{Y\Delta h \Delta Q_R}{\Delta S_v W_*} + \frac{\Delta F_R}{\rho \Delta S_v W_*} \right\} \tag{B6}$$

where $\Delta F_R = F_{R2} - F_{R1}$,

F_{R2} is the heat flux at h_2,

F_{R1} is the heat flux at h_1;

$$F_{q_1} = \frac{1}{(1+\alpha-\alpha Y)} \left\{ -(1-G_q Y)\Delta q W_{e1} + \alpha(1-Y)F_{q_o} - (1-Y-G_q Y)\Delta q \left(\frac{d\Delta h}{dt} - \Delta W\right) + Y\Delta h \Delta E + \frac{\Delta F_E}{\rho} \right\} \tag{B7}$$

where $\Delta F_E = F_{E2} - F_{E1}$,

F_{E2} is the flux of rain at h_2,

F_{E1} is the flux of rain at h_1;

$$\frac{dh_1}{dt} = W_{e1} + \bar{W}_1 \tag{B8}$$

$$\frac{d\bar{S}_{vm}}{dt} = \frac{\overline{W'S'_v}_o}{h_1} + Q_{Rm} \qquad \text{(B9)}$$

$$\frac{d\bar{q}_m}{dt} = \frac{\overline{W'q'}_o - \overline{W'q'}_1}{h_1} + E_m. \qquad \text{(B10)}$$

We also need an equation for Δh or as we have done here specify it as a constant.